EVALUATION AND INTER-COMPARISON OF SATELLITE PRECIPITATION ESTIMATIONS FOR EXTREME FLOOD EVENTS IN PENINSULAR MALAYSIA

EUGENE SOO ZHEN XIANG

FACULTY OF ENGINEERING
UNIVERSITY OF MALAYA
KUALA LUMPUR

2020

EVALUATION AND INTER-COMPARISON OF SATELLITE PRECIPITATION ESTIMATIONS FOR EXTREME FLOOD EVENTS IN PENINSULAR MALAYSIA

EUGENE SOO ZHEN XIANG

THESIS SUBMITTED IN FULFILMENT OF THE REQUIREMENTS FOR THE DEGREE OF DOCTOR OF PHILOSOPHY

FACULTY OF ENGINEERING
UNIVERSITY OF MALAYA
KUALA LUMPUR

2020

UNIVERSITY OF MALAYA

ORIGINAL LITERARY WORK DECLARATION

Name of Candidate: **EUGENE SOO ZHEN XIANG**

Registration/Matric No: **KHA 140088**

Name of Degree: **DOCTOR OF PHILOSOPHY**

Title of Thesis: **EVALUATION AND INTER-COMPARISON OF SATELLITE PRECIPITATION ESTIMATIONS FOR EXTREME FLOOD EVENTS IN PENINSULAR MALAYSIA**

Field of Study: **WATER RESOURCES ENGINEERING**

I do solemnly and sincerely declare that:

(1) I am the sole author/writer of this Work;
(2) This Work is original;
(3) Any use of any work in which copyright exists was done by way of fair dealing and for permitted purposes and any excerpt or extract from, or reference to or reproduction of any copyright work has been disclosed expressly and sufficiently and the title of the Work and its authorship have been acknowledged in this Work;
(4) I do not have any actual knowledge nor do I ought reasonably to know that the making of this work constitutes an infringement of any copyright work;
(5) I hereby assign all and every rights in the copyright to this Work to the University of Malaya ("UM"), who henceforth shall be owner of the copyright in this Work and that any reproduction or use in any form or by any means whatsoever is prohibited without the written consent of UM having been first had and obtained;
(6) I am fully aware that if in the course of making this Work I have infringed any copyright whether intentionally or otherwise, I may be subject to legal action or any other action as may be determined by UM.

Candidate's Signature Date:

Subscribed and solemnly declared before,

Witness's Signature Date:

Name:

Designation:

EVALUATION AND INTER-COMPARISON OF SATELLITE PRECIPITATION ESTIMATIONS FOR EXTREME FLOOD EVENTS IN PENINSULAR MALAYSIA

ABSTRACT

Satellite precipitation products (SPP) have been useful in any hydrological applications as their extensive spatial coverage and finer space and time resolutions. However, these satellite estimations exhibit large systematic and random errors which may cause large uncertainties in any hydrological applications. In this study, three advanced satellite precipitation products, i.e. CMORPH, TRMM 3B42V7, and PERSIANN are utilized in conjunction with the ground observation to investigate their performance in detecting rain, capturing storms and rainfall pattern during extreme flood events. This study evaluates and compares the capability of the SPP by focusing on the 2014-2015 northeast monsoon extreme flood events. Three affected river basins, i.e. Kelantan (13,100 km^2), Johor (1,652 km^2) and Langat river basin (2,350 km^2) are chosen as study areas. Firstly, to compare with the grid-based satellite estimations, a validation between five spatial interpolation methods (Arithmetic Mean (AM), Thiessen Polygon (TP), Inverse Distance Weighting (IDW), Ordinary Kriging (OK), and Spline (SP)) with ground observations is done whereby the result shows that none of the spatial interpolation methods is superior to the others. Furthermore, the result shows that all three SPP have performed reasonably well for the Kelantan river basin whereas for the other two river basins, only TRMM and CMORPH perform better. As these SPP exhibit biases, the three widely used approaches of bias correction, namely Linear Scaling (LS), Local Intensity Scaling (LOCI) and Power Transformation (PT) are applied on the daily SPP to improve the estimations. Bias correction analysis is performed using the aforementioned methods to the Langat river basin only. Findings indicate that the LS scheme is able to match the mean precipitation of every SPP but does not correct the standard deviation (*SD*) and coefficient of variation

(*CV*) of the estimations regardless of extreme floods selected. For the LOCI scheme, TRMM and CMORPH estimations in certain floods show a significant improvement in the result but not for PERSIANN. PT scheme is found to be the best method as it improves most of the statistical performances as well as the rainfall distribution of the floods. In addition, this study also evaluates the sensitivity of the parameters used in the BC process where the result indicates that the PT scheme is found to be the least sensitive in correcting the daily SPP compared to the other two schemes. Finally, this study performs rainfall-runoff simulation by employing the Hydrological Modelling System (HEC-HMS) to validate the performance of the raw and bias-adjusted SPP for the 2014-2015 flood events in the Langat river basin. Generally, corrected precipitations exhibit a significant improvement during the high rainfall event especially LOCI-adjusted TRMM and CMORPH. For PERSIANN-simulated flow, the BC schemes are able to improve the discharge simulation. However, further calibration is suggested in order to enhance its accuracy.

Keywords: Satellite precipitation, Extreme flood, Malaysia, Bias correction, Hydrological modeling

PENILAIAN DAN PERBANDINGAN ANTARA SATELIT HUJAN TERHADAP BANJIR EKSTRIM DI SEMENANJUNG MALAYSIA

ABSTRAK

Produk hujan satelit (SPP) telah berguna dalam mana-mana aplikasi hidrologi disebabkan oleh liputan spatial yang luas dan resolusi ruang dan masa yang lebih baik. Walaubagaimanapun, anggaran satelit ini menunjukkan ralat sistematik dan rawak besar yang boleh menyebabkan ketidakpastian besar dalam sebarang aplikasi hidrologi. Dalam kajian ini, tiga produk terkini hujan satelit, iaitu CMORPH, TRMM 3B42V7 dan PERSIANN digunakan bersama dengan stesen pemerhatian di padang untuk menyiasat prestasi mereka dalam mengesan hujan, menyukat ribut dan corak hujan semasa peristiwa banjir ekstrim. Kajian ini menilai dan membandingkan kebolehan SPP dengan memfokuskan pada banjir ekstrim monsun timur laut 2014-2015. Tiga lembangan sungai yang terkesan iaitu Lembangan Sungai Kelantan (13,100 km^2), Johor (1,652 km^2) dan Langat (2,350 km^2) telah dipilih sebagai kawasan kajian. Pertamanya, untuk membandingkan dengan anggaran satelit berasaskan grid, pengesahan antara lima kaedah interpolasi spatial (Min aritmetik (AM), Poligon *Thiessen* (TP), Pengimbang Jarak Songsang (IDW), *Kriging* Biasa (OK), dan *Spline* (SP)) dengan stesen pemerhatian di padang telah dilakukan dimana keputusan menunjukkan bahawa tiada kaedah interpolasi spatial yang lebih baik daripada kaedah yang lain. Tambahan lagi, hasil kajian ini menunjukkan bahawa ketiga-tiga SPP telah dapat menganggarkan hujan dengan baik untuk Lembangan sungai Kelantan manakala bagi dua lagi lembangan sungai, hanya TRMM dan CMORPH yang menunjukkan keputusan lebih baik. Memandangkan SPP ini mempamerkan ralat, tiga kaedah pembetulan ralat (BC) yang paling meluas digunakan iaitu Penskalaan linear (LS), Skala Keamatan Setempat (LOCI) dan Transformasi kuasa (PT) telah digunakan pada data harian SPP untuk meningkatkan anggaran. Analisa pembetulan ralat dilakukan menggunakan kaedah yang dinyatakan pada Lembangan

Sungai Langat sahaja. Keputusan menunjukkan yang skim LS mampu selaraskan purata hujan bagi setiap SPP tetapi tidak membetulkan sisihan piawai (*SD*) dan pekali variasi (*CV*) anggaran satelit tanpa mengira banjir ekstrim yang dipilih. Bagi skim LOCI, anggaran TRMM dan CMORPH dalam banjir-banjir tertentu menunjukkan peningkatan penting dalam keputusan tetapi tidak pada anggaran PERSIANN. Skim PT didapati sebagai kaedah terbaik kerana ia meningkatkan prestasi kebanyakan statistik dan juga taburan hujan banjir. Tambahan juga, kajian ini juga menilai sensitiviti parameter yang digunakan dalam proses BC dimana keputusan menunjukkan yang skim PT didapati menjadi paling kurang sensitif dalam membetulkan SPP harian berbanding dengan dua skim lain. Akhir sekali, kajian ini melaksanakan simulasi hujan air larian dengan menggunakan Sistem Pemodelan Hidrologi (HEC-HMS) untuk mengesahkan prestasi SPP asal dan pembetulan-ralat SPP untuk peristiwa banjir 2014-2015 di Lembangan Sungai Langat. Secara umumnya, pembetulan hujan mempamerkan peningkatan ketara semasa peristiwa hujan lebat terutamanya pembetulan-LOCI TRMM dan CMORPH. Bagi aliran simulasi PERSIANN, skim BC mampu meningkatkan simulasi aliran sungai. Walau bagaimanapun, penentukuran lanjut adalah dicadangkan untuk meningkatkan ketepatannya.

Kata-kata kunci: Hujan satelit, Banjir ekstrim, Malaysia, Pembetulan ralat, Pemodelan hidrologi

ACKNOWLEDGEMENTS

First and foremost, I would like to express my heartfelt gratitude to my principal supervisor, Dr. Wan Zurina Wan Jaafar. Her guidance, support, and continuous encouragement have enabled me to complete my research. She has shown great patience, kindness and provided excellent motivation throughout the course of my doctoral degree. Without her understanding and guidance, the completion of my doctoral degree would have remained a farfetched dream.

Next, I would also like to express my gratitude to my co-supervisor Assoc. Prof. Dr. Lai Sai Hin who has also provided support and shared his immense knowledge during my doctoral study. I am also thankful to all my colleagues in the Department of Civil Engineering who were truly understanding, supportive and always encouraged me to have patience and hard work as well as to those who contributed directly and indirectly in bringing the project to completion.

This work was supported by the Malaysia Ministry of Higher Education (MOHE) for their FRGS research grant (Project No. FP039-2014B) and the University of Malaya for PPP grant (Project No. PG194-2015B). I also would like to acknowledge the Department of Irrigation and Drainage Malaysia for providing the daily precipitation rain gauge and streamflow data as well as the developers of all SPP for providing the downloadable rainfall data.

Finally, and most importantly, I would like to thank my family who offers never-ending support and continuous encouragement throughout my years of study and through the process of researching and writing this thesis. Thank you very much.

“Thank you everyone for being an important part of my story…”

Eugene Soo Zhen Xiang

TABLE OF CONTENTS

Abstract iii

Abstrak v

Acknowledgements vii

Table of Contents viii

List of Figures xiii

List of Tables xvi

List of Symbols and Abbreviations xvii

List of Appendices xxi

CHAPTER 1: INTRODUCTION 1

1.1 Background of Study 1

1.2 Identification of Problem 3

1.2.1 Recent floods in Malaysia 3

1.2.2 Rainfall measurement 3

1.2.3 Studies of SPP in Malaysia 6

1.3 Research Questions 7

1.4 Objectives of the Study 8

1.5 Scope of the Study 8

1.6 Significance of the Study 11

1.7 Organization of the Thesis 12

CHAPTER 2: LITERATURE REVIEW 14

2.1 Introduction 14

2.2 Monsoon weather systems in Southeast Asia 14

2.3 Weather of Malaysia 17

2.4 Ground-based rainfall measurement 18
2.4.1 Rain gauge measurement 18
2.4.2 Automatic Weather Stations (AWS) 22
2.4.3 Weather radar 23
2.5 Remote Sensing Applications in Weather and Climate 23
2.5.1 Weather Radar 25
2.5.2 Weather Satellites 28
2.6 Satellite Precipitation Products (SPP) 29
2.7 Errors of Satellite Precipitation Estimations 31
2.7.1 The density of ground-based rainfall measurement 31
2.7.2 Rain detection, systematic, and random errors of SPP 33
2.7.3 Seasonality, storm type, and topography 33
2.8 Hydrological modeling studies in Malaysia 35
2.9 SPP forced hydrological models 36
2.10 Summary 36

CHAPTER 3: EVALUATION OF RAW SATELLITE PRECIPITATION PRODUCTS FOR EXTREME FLOOD EVENTS IN MALAYSIA 38
3.1 Introduction 38
3.2 Review on Previous SPP Studies 38
3.3 Description of the study area 40
3.3.1 Langat river basin 41
3.3.2 Kelantan river basin 42
3.3.3 Johor river basin 43
3.4 Data Acquisition 44
3.4.1 Rain gauge network 44
3.4.2 Satellite rainfall estimations 46

3.5 Methods 48
3.5.1 Interpolation of rain gauge precipitation 48
3.5.1.1 Arithmetic Mean (AM) 49
3.5.1.2 Thiessen Polygon (TP) 49
3.5.1.3 Inverse Distance Weighting (IDW) 50
3.5.1.4 Kriging 51
3.5.1.5 Spline… 51
3.5.2 Evaluation indexes 52
3.5.2.1 Quantitative evaluation indexes 53
3.5.2.2 Categorical evaluation indexes 54
3.6 Results and Discussions 55
3.6.1 Evaluation of various interpolation methods for rain gauge observations…. 55
3.6.2 Evaluation of SPP against interpolated rain gauge observations 59
3.6.3 Rain Detection Ability Assessment of SPP 69
3.6.4 Capturing Storm Performance of SPP 71
3.7 Summary 73

CHAPTER 4: BIAS ADJUSTMENT OF SATELLITE PRECIPITATION ESTIMATIONS.. 76
4.1 Introduction 76
4.2 Review on Bias Correction 76
4.3 Description of the study area and selected flood events 80
4.4 Data Acquisition 83
4.5 Bias correction methods 83
4.5.1 Linear Scaling (LS) 84
4.5.2 Local intensity scaling (LOCI) 85

4.5.3 Power transformation (PT) 85
4.6 Results and Discussions 86
4.6.1 Evaluation of raw satellite estimates over selected extreme flood events 86
4.6.2 Performance evaluation of bias-corrected satellite estimates 87
4.6.2.1 Rainfall pattern and distribution 87
4.6.2.2 Statistical performance 91
4.6.3 Variation and sensitivity of parameters 94
4.7 Summary 97

CHAPTER 5: PRECISION OF RAW AND BIAS-ADJUSTED SATELLITE PRECIPITATION ESTIMATIONS IN RAINFALL-RUNOFF MODELLING.... 99
5.1 Introduction 99
5.2 Review on Hydrological Modelling with SPP Estimations 99
5.3 Methods 101
5.3.1 Hydrologic Modelling System (HEC-HMS) 101
5.3.2 Soil Conservation Service Curve Number (SCS-CN) method 103
5.3.3 SCS unit hydrograph method 104
5.3.4 Muskingum method 104
5.3.5 Hydrologic simulation process 104
5.3.6 Model Performance Indicators 106
5.4 Results and Discussions 108
5.4.1 Comparison of SPP rainfall estimates with rain gauge (RG) observations…… 108
5.4.2 Model calibration 110
5.4.3 Model Validation using Raw and Bias-adjusted SPP Rainfall Datasets 112
5.4.3.1 Simulation of streamflow with raw SPP estimations 113

5.4.3.2 Simulation of streamflow with Bias-adjusted SPP estimations…… 114

5.5 Summary 118

CHAPTER 6: CONCLUSIONS AND RECOMMENDATIONS 120

6.1 Introduction 120

6.2 Verification of Spatial Interpolation Methods of Rain Gauge Network 120

6.3 Validation of SPP at Different Geographic Location of Peninsular Malaysia 121

6.4 Evaluation of Bias-Adjusted SPP Estimations 121

6.5 Rainfall-runoff using Raw and Bias-Adjusted SPP Estimations 122

6.6 Recommendations and Future Perspectives 123

References 124

List of Publications and Papers Presented 141

Appendix 142

LIST OF FIGURES

Figure 1.1: Conceptual framework of research 10

Figure 2.1: Southeast Asia 15

Figure 2.2: Rain Gauge 19

Figure 2.3: Meteorological Station in Mersing 22

Figure 2.4: The Electromagnetic Spectrum 24

Figure 2.5: Passive and active remote sensing 25

Figure 2.6: Weather radar in Miri, Sarawak, Malaysia 26

Figure 2.7: Sample of radar observation in Malaysia 26

Figure 2.8: The global satellite observation system 28

Figure 2.9: Number of stations used by the GPCC 32

Figure 3.1: Location of the study areas. 41

Figure 3.2: Distribution of rain gauge stations in (a) Langat, (b)Kelantan and (c) Johor river basin. 44

Figure 3.3: Results of interpolation methods for daily mean precipitation of the Kelantan river basin on 17th December 2014. (a) TP; (b) IDW (c) OK; (d) SP 57

Figure 3.4: Results of interpolation methods for daily mean precipitation of the Langat river basin on 22nd December 2014. (a) TP; (b) IDW (c) OK; (d) SP 58

Figure 3.5: Results of interpolation methods for daily mean precipitation of the Johor river basin on 25th December 2014. (a) TP; (b) IDW (c) OK; (d) SP 58

Figure 3.6: Comparison of daily mean precipitation series between interpolated ground observations and (a) CMORPH, (b) TRMM and (c) PERSIANN satellite observations for the 2014-2015 flood events at Kelantan river basin. 60

Figure 3.7: Comparison of daily mean precipitation series between interpolated ground observations and (a) CMORPH, (b) TRMM and (c) PERSIANN satellite observations for the 2014-2015 flood events at Langat river basin. 61

Figure 3.8: Comparison of daily mean precipitation series between interpolated ground observations and (a) CMORPH, (b) TRMM and (c) PERSIANN satellite observations for the 2014-2015 flood events at Johor river basin. 62

Figure 3.9: Scatter plots comparisons of daily mean precipitation for satellite precipitation products versus rain gauge observation for Kelantan, Langat and Johor river basins. 65

Figure 3.10: Comparison of the (a) coefficient of determination (R^2), (b) coefficient of Pearson Correlation (*CC*), (c) percentage bias (*PBias*), (d) mean absolute error (*MAE*), (e) root mean square error (*RMSE*) and (f) normalized root mean square error (*NRMSE*) for three SPP versus rain gauge observations over Kelantan, Langat and Johor river basins during 2014-2015 flood events. 67

Figure 3.11: Rain Detection Capability of SPP in (a) Kelantan, (b) Langat and (c) Johor river basins 69

Figure 3.12: The Heidke Skill Score (*HSS*) of three satellite precipitation products (CMORPH, TRMM and PERSIANN) for storm thresholds ranging from 10 mm to 100 mm in Kelantan river basin 71

Figure 3.13: The Heidke Skill Score (*HSS*) of three satellite precipitation products (CMORPH, TRMM, and PERSIANN) for storm thresholds ranging from 1 mm to 20 mm in Langat river basin........ 72

Figure 3.14: The Heidke Skill Score (*HSS*) of three satellite precipitation products (CMORPH, TRMM, and PERSIANN) for storm thresholds ranging from 1 mm to 30 mm in Johor river basin 73

Figure 4.1: (a) Location of study area. (b) Distribution of gauge stations and DEM of the Langat river basin. 81

Figure 4.2: Daily mean precipitation series of selected flood events in Langat river basin 82

Figure 4.3: Frequency distribution of daily precipitation of selected flood events in Langat river basin. 82

Figure 4.4: Time series of daily rainfall data (mm/day) and daily accumulated rainfall data (mm) of gauge observations, raw and bias-corrected satellite estimations for selected flood events in Langat river basin. 88

Figure 4.5: Quantile-Quantile plots of raw and corrected satellite estimations versus gauged observations for every flood event in Langat river basin. 90

Figure 4.6: Scatter plots of statistics of the rain gauge (RG) precipitation versus raw and corrected satellite precipitation estimations. 92

Figure 4.7: Boxplot of the parameters used in BC for every satellite estimation. [(a) Parameter *s* for LS scheme, (b) Parameter *c* for LOCI scheme, (c) Parameters *a* and (d) *b* for PT scheme] 96

Figure 4.8: Sample histogram of bootstrap values for 1000 random samples. 96

Figure 5.1: Schematic diagram for the setup of HEC-HMS hydrological modeling system. 102

Figure 5.2: Overall hydrologic simulation process 106

Figure 5.3: Comparison of daily mean precipitation series between interpolated RG observations and selected SPP estimations for 2014-2015 flood events at Langat river basin. 109

Figure 5.4: Comparison of runoff hydrograph for 2014-2015 flood events 111

Figure 5.5: Comparison of raw and bias-adjusted (a) TRMM, (b) CMORPH and (c) PERSIANN simulated flow and RG calibrated flow for 2014-2015 flood events at Langat river basin. 115

Figure 5.6: Flow duration curves of raw and bias-adjusted SPP simulated flows. 117

LIST OF TABLES

Table 2.1: Recommended minimum densities of rain gauge stations............................21

Table 3.1: Information about satellite precipitation products (SPP)..............................46

Table 3.2: Contingency table for comparing gauge and satellite precipitation estimate 55

Table 3.3: Highest areal rainfall of each interpolation method during 2014-2015 flood events...56

Table 3.4: Statistical analysis of SPP versus rainfall interpolation methods for the 2014-2015 flood events. 66

Table 3.5: Overall rain detection capability of each precipitation product.....................70

Table 4.1: Overview of some BC schemes. 77

Table 4.2: Selected flood events for this study 81

Table 4.3: Inter-correlation of rain gauge observations between selected flood events in Langat river basin...82

Table 4.4: Statistical Results of Raw Satellite Estimations for the overall Langat river basin 87

Table 4.5: Nash-Sutcliffe Efficiency..89

Table 4.6: Statistical analysis of original and corrected satellite estimations versus gauged observations at Langat river basin..93

Table 4.7: The mean, resampled mean and 95% confidence interval (95% CI) for every parameter applied on the SPP. 97

Table 5.1: Classification of performance of *NSE* of models..107

Table 5.2: Statistical analysis of raw and bias-adjusted SPP versus IDW-interpolated RG observations for the 2014-2015 flood events at Langat river basin 109

Table 5.3: Optimized model parameter sets of HEC-HMS model 111

Table 5.4: Calibration result for every sub-event...112

Table 5.5: Statistical result for raw and bias-corrected TRMM streamflow................116

Table 5.6: Statistical result for raw and bias-corrected CMORPH streamflow...........116

Table 5.7: Statistical result for raw and bias-corrected PERSIANN streamflow 116

LIST OF SYMBOLS AND ABBREVIATIONS

ACC	:	Accuracy
AM	:	Arithmetic Mean
AMSR-E	:	Advanced Microwave Scanning Radiometer for Earth Observing System
AMSU	:	Advanced Microwave Sounding Unit
ANNs	:	Artificial Neural Networks
AO	:	Arctic Oscillation
APHRODITE	:	Asian Precipitation – Highly – Resolved Observational Data Integration Towards Evaluation
ARIMA	:	Auto-Regressive Integrated Moving Average
AWS	:	Automatic Weather Stations
BC	:	Bias Correction
CC	:	Coefficient of Pearson Correlation
CERES	:	Clouds and the Earth's Radiant Energy System
CI	:	Confidence Interval
CMORPH	:	Climate Prediction Center (CPC) morphing technique
CN	:	Curve Number
CONUS	:	Continental United States
CSI	:	Critical Success Index
CV	:	Coefficient of Variation
DEM	:	Digital Elevation Model
DID	:	Drainage and Irrigation Department
DT	:	Decision Tree
EASM	:	East Asian Summer Monsoon
EAWM	:	East Asian Winter Monsoon
EM	:	East Malaysia
EMS	:	Electromagnetic Spectrum

FAR	:	False Alarm Ratio
FR	:	Frequency Ratio
GBHM	:	Geomorphology-Based Hydrological Model
GEO	:	Geostationary
GES-DISC	:	Goddard Earth Sciences Data and Information Services Center
GIS	:	Geographical Information System
GOES-IR	:	Geosynchronous Satellite Longwave Infared Imagery
GPCC	:	Global Precipitation Climatology Center
GPCP	:	Global Precipitation Climatology Project
GPM	:	Global Precipitation Measurement Mission
GSMaP	:	Global Satellite Mapping of Precipitation
HBV	:	Hydrologiska Byråns Vattenbalansavdelning
HEC-HMS	:	Hydrologic Engineering Center's Hydrologic Modelling System
HIMS	:	Hydro Informatic Modelling System
HSS	:	Heidke Skill Score
IDW	:	Inverse Distance Weighting
IM	:	Inter-monsoon
IMERG	:	Integrated Multi-satellitE Retrievals for GPM
IOP	:	Indian Ocean–western Pacific
IR	:	Infrared
JAXA	:	Japan Aerospace Exploration Agency
LEO	:	Low Earth Orbiting
LOCI	:	Local Intensity Scaling
LR	:	Logistic Regression
LS	:	Linear Scaling
LSM	:	Land Surface Model
MAE	:	Mean Absolute Error

MMD	:	Malaysian Meteorology Department
NASA	:	National Aeronautics and Space Administration
NEM	:	Northeast Monsoon
NOAA	:	National Oceanic and Atmospheric Administration
NRMSE	:	Normalized Root Mean Square Error
NSE	:	Nash-Sutcliffe Efficiency
NWP	:	Numerical Weather Prediction
OK	:	Ordinary Kriging
PBias	:	Percent Bias
PED	:	Parameter Efficient Distributed
PERSIANN	:	Precipitation Estimation from Remotely Sensed Information using Artificial Neural Networks
PERSIANN-CCS	:	PERSIANN-Cloud Classification System
PM	:	Peninsular Malaysia
PMW	:	Passive Microwave
POD	:	Probability of detection/ Hit rate
PT	:	Power Transformation
QME	:	Quantile mapping based on an Empirical distribution
QMG	:	Quantile Mapping based on a Gamma distribution
QQ plots	:	Quantile-Quantile plots
R^2	:	Coefficient of Determination
RCM	:	Regional Climate Models
RG	:	Rain Gauge
RMSE	:	Root Mean Square Error
SAC-SMA	:	SACramento Soil Moisture Accounting
SCS-CN	:	Soil Conservation Service Curve Number
SD	:	Standard Deviation
SH	:	Siberian High

SP	:	Spline
SPP	:	Satellite Precipitation Products
SWAT	:	Soil Water Assessment Tool
SWM	:	Southwest Monsoon
TMI	:	TRMM Microwave Imager
TMPA	:	TRMM Multi-satellite Precipitation Analysis
TP	:	Thiessen Polygon
TRMM	:	Tropical Rainfall Measuring Mission
USACE	:	United State Army Corps of Engineers
VIC	:	Variable Infiltration Capacity
VIS	:	Visible
VPR	:	Vertical Profile of Reflectivity
WCN	:	Weighted Curve Number
WMO	:	World Meteorological Organization
WoE	:	Weight of Evidence
WPSH	:	Western Pacific Subtropical High

LIST OF APPENDICES

Appendix A: List of Selected Rain Gauge Stations ………………………... 142

Table A1: Rain Gauge Stations in Langat River Basin…………………….. 142

Table A2: Rain Gauge Stations in Kelantan River Basin…………………... 143

Table A3: Rain Gauge Stations in Johor River Basin………………………. 144

CHAPTER 1: INTRODUCTION

1.1 Background of Study

Climate change is the most significant threat to living beings in this world. Recent seasons have shown the effects of climate change in the form of extreme temperature and precipitation regimes, increasing global sea level and so on. In most of the regions in this world, extremities in weather condition cause flooding, which is one of the most widespread of hydro-meteorological hazards that can be particularly disruptive, leading to widespread collapse of infrastructure (Khan *et al.*, 2011; Scofield & Kuligowski, 2003; Seyyedi *et al.*, 2014).

In order to identify the trends in the statistics of historical streamflow, reliable climatic information is critical for climate analyses and for verification of climate model simulations (Easterling *et al.*, 1999; Moazami *et al.*, 2013). Rainfall data or precipitation is an important input required for water resource management, hydrologic and ecologic modeling, recharge assessment, and irrigation scheduling (Behrangi *et al.*, 2011; Jiang *et al.*, 2012; Mair & Fares, 2010; Su *et al.*, 2008). Unfortunately, the extreme transience and spatial inhomogeneity of rainfall make it one of the most challenging variables to quantify as an input to hydrological models, particularly in regions for which surface gauge and radar observations are sparse (Gu *et al.*, 2010).

Satellite precipitation products (SPP) have been emerging as one of the most important precipitation data sources in hydrology, climatology and meteorology studies for the last few decades. These products have been successfully applied in studying the precipitation patterns at global scale as well as regional scale. These remotely sensed data have several advantages over the traditional measurements including higher spatial resolution and uninterrupted coverage and hence beneficial over the ungauged catchments, especially mountainous and oceanic regions (Behrangi *et al.*, 2011; Collischonn *et al.*, 2008; de

Coning, 2013; Gado *et al.*, 2017; Moazami *et al.*, 2013; Tian *et al.*, 2009). Various new global high-resolution SPP have been operationally available, including the National Oceanic and Atmospheric Administration (NOAA) Climate Prediction Center morphing technique product (CMORPH) (Joyce *et al.*, 2004), the Tropical Rainfall Measuring Mission (TRMM) Multi-satellite Precipitation Analysis products (TMPA) (Huffman *et al.*, 2007), the Precipitation Estimation from Remotely Sensed Information using Artificial Neural Networks (PERSIANN) (Hsu *et al.*, 1997; Sorooshian *et al.*, 2000), the Global Satellite Mapping of Precipitation (GSMaP) (Kubota *et al.*, 2007), and so on. These SPP have provided quasi-global high-temporal (≤3 h) and spatial (≤0.25°) resolution precipitation maps.

Although SPP have been widely used in various meteorological models, these satellite estimations are still imperfect and prone to systematic and random errors associated with observations, sampling, and retrieval algorithms. (Dinku *et al.*, 2009; Jiang *et al.*, 2018; Pereira Filho *et al.*, 2010; Piani *et al.*, 2010; Teutschbein & Seibert, 2013; Villarini *et al.*, 2009; Vu *et al.*, 2018). The models could augment or suppress rainfall biases to the streamflow based on the response mode of the model (Fang *et al.*, 2015; Habib *et al.*, 2014; Segond *et al.*, 2007).

In this study, three advanced SPP, including TRMM 3B42 Version 7 (V7), CMORPH and PERSIANN were utilized in conjunction with the rain gauge ground observations to investigate the rainfall pattern specifically during extreme flood events due to Northeast Monsoon (NEM). The three selected river basins, i.e. Langat, Kelantan and Johor river basin are located at the west, north and south parts of Peninsular Malaysia, respectively. Later, this study attempts to improve these selected SPP with different approaches of bias correction schemes followed by assessing their suitability and performance in predicting runoff through the hydrological simulation.

1.2 Identification of Problem

1.2.1 Recent floods in Malaysia

Malaysia, of which the weather is hot and humid all year round, receives an average rainfall of about 2500 mm annually and this country is susceptible to extreme flooding events especially in the East Coast of Peninsular Malaysia. In recent years, flooding events are increasing in terms of frequency and impact. For example, the 2014-2015 floods in Malaysia have been described as the worst flood in decades. The damages caused by this flood has affected badly the people causing them great devastation, especially when it comes to the loss of homes and other infrastructures. Theoretically, this flood happened due to NEM and suppose only the East Coast of Peninsular Malaysia will be affected. However, during this event, more than half of the Peninsular Malaysia, including those regions at the central part and west side, were affected and most of the rivers had reached dangerous levels. More than 200,000 people were affected and 21 people were killed due to this natural disaster (Akasah & Doraisamy, 2015). According to the senior meteorological officer from the Malaysian Meteorological Department, Mohd Hisham Mohd Anip, a full moon became the cause for the high tide in addition to the presence of the northeast monsoon winds that blowing consistently across the South China Sea from November until March 2015. He added, incessant rainfall caused water from the upstream to not reach the confluence and resulted in an overflowing river.

1.2.2 Rainfall measurement

Precipitation or rainfall is the key input for hydrometeorological modeling and applications. The accuracy and reliability of hydrologic studies heavily depend on the availability of good quality precipitation estimates. Precipitation measurements can be conducted as ground-based precipitation measurements (such as rain gauge and radar networks) and satellite-based precipitation measurements. Rain gauges provide a direct physical measurement of the surface precipitation; however, they are susceptible to certain errors such as the size of collectors, evaporative loss, out-splash, leveling, siting of gauges, the effect of wind, etc. (Strangeways, 2004). Moreover, establishing and maintaining the infrastructure of the rain gauge and radar network is costly. These networks are also either sparse or non-existent in remote parts of the world and in developing countries. This situation is further exacerbated in regions with complex topography where precipitation is characterized by high spatio-temporal variability. In these regions, rain gauges are generally located in lowland due to accessibility considerations, thus underrepresenting the precipitation occurring in highland. SPP are perhaps the only source to fill this important gap. SPP retrieval algorithms enable the representation of high space-time variability of precipitation field with quasi-global coverage hence they are potentially attractive for hydrologic modeling studies in data-sparse regions.

In order to identify the trends in the statistics of historical streamflow, reliable climatic information is critical for climate analyses and for verification of climate model simulations (Easterling *et al.*, 1999; Moazami *et al.*, 2013). Rainfall data or precipitation is an important input required for water resource management, hydrologic and ecologic modeling, recharge assessment, and irrigation scheduling (Behrangi *et al.*, 2011; Jiang *et al.*, 2012; Mair & Fares, 2010; Su *et al.*, 2008). However, it is difficult to determine the amount of rain that falls across the world as the temporal and spatial distribution of rainfall is not even (Gu *et al.*, 2010).

Rain gauge was the most common instrument used to measure how much rain has fallen. There are several types of rain gauge that are usually used to collect rainfall depth such as tipping-bucket rain gauge, weighing precipitation gauge, and telemetering rain gauge. According to Suhaila *et al.* (2010), since year 1975 to 2004, the Malaysian Meteorology Department (MMD) and Drainage and Irrigation Department (DID) had collected the daily rainfall data from 30 rain gauge stations from four regions, i.e. northwest, west, southwest, and east over Peninsular Malaysia. This instrument was cheap and easy to install and calibrate and had been used for decades, and thus the only available information from which to derive long records of reference precipitation (Tapiador *et al.*, 2012). However, these precipitation measuring stations sometimes fail in providing a continuous record of precipitation.

Precipitation can also be estimated using weather radar due to its continuous spatial coverage (Habib *et al.*, 2012) but it has difficulties in hardware calibration (Yilmaz *et al.*, 2005). The area covered by weather radar is still limited; the precipitation can be undetected, or the rate can be underestimated as the distance from the radar increases. (Diederich *et al.*, 2015; Gu *et al.*, 2010; Scofield & Kuligowski, 2003). Moreover, the accuracy of the reflectivity values can be influenced by fixed targets such as ground clutter, beam block or anomalous propagation (de Coning, 2013; Diederich *et al.*, 2015).

Although SPP have been widely used in various meteorological models, these satellite estimations are still imperfect and prone to systematic and random errors associated with observations, sampling, and retrieval algorithms. (Dinku *et al.*, 2009; Pereira Filho *et al.*, 2010; Piani *et al.*, 2010; Teutschbein & Seibert, 2013; Villarini *et al.*, 2009). Also, the models could augment or suppress rainfall biases to the streamflow based on the response mode of the model (Fang *et al.*, 2015; Habib *et al.*, 2014; Segond *et al.*, 2007).

In February 2014, the Global Precipitation Mission (GPM) (Hou *et al.*, 2014) was launched as a follow-on to TRMM and the objective was to observe global precipitation more frequently and more accurately than TRMM. The GPM design is based on the improvement of the shortcomings of TRMM and hence an in-depth study of the performance of TRMM could provide the basis for a study on GPM improvements. Yet, despite having a significant period of rainfall records, extensive studies of TRMM accuracy in measuring rainfall in South East Asia, specifically in Malaysia, are sparse.

1.2.3 Studies of SPP in Malaysia

In the past, studies about the evaluation of SPP in Malaysia appear to be limited. Varikoden *et al.* (2010) evaluated the performance of TRMM 3B42V6 rainfall data in Peninsular Malaysia which covers only about 40% of the total area of Malaysia and this study using only four precipitation gauges for the purpose of validation. Semire *et al.* (2012) validated the various version of TRMM Microwave Imager (TMI) such as 2A12, 3B42V6, 3B43V6, and Global Precipitation Climatology Center (GPCC) with the monthly precipitation data collected over 10 years (2001–2010) from 22 precipitation gauges distributed over Malaysia. Both studies showed that 3B43V6 performs well over Malaysia, with a ±15% error bias at monthly scale. However, these studies were conducted at monthly scale and compared only few SPP, thus limiting their conclusions.

Later, Tan *et al.* (2015) compares daily, monthly, seasonal, and annual rainfall amount at 342 rain gauges over Malaysia using the five SPP (3B42RT, 3B42V7, GPCP (Global Precipitation Climatology Project) 1DD, PERSIANN, and CMORPH) and a ground-based precipitation product (APHRODITE - Asian Precipitation – Highly – Resolved Observational Data Integration Towards Evaluation). In their study, they assessed the accuracy and spatial variations of each SPP by regions and found that the SPP performed better in the northeast monsoon (NEM) than in the southwest monsoon (SWM). Also, the SPP's performance was the best in the regions receiving higher annual precipitation such as eastern and southern Peninsular Malaysia and northern East Malaysia. By contrast, poor SPP performance occurred over western Peninsular Malaysia which is characterized by low rainfall amounts since it is sheltered by the Titiwangsa Range and Sumatra. They also concluded that the TRMM products outperformed the PERSIANN product for this country particularly in estimating precipitation during the 2006–2007 flood event. Generally, this study was just focused on the comparison between the original SPP estimations and the capability of SPP in recent years remains unclear as the assessment period of this study is only from 2003 to 2007. More comprehensive comparisons of various SPP can not only provide guidance on the selection of better products over Malaysia for local application but also offer insight into the strengths and weaknesses of different satellite products over this typical tropical climatic zone, enabling further improvement of the satellite products.

1.3 Research Questions

Based on the problem statements described in Section 1.2, the following research questions were addressed.

i. Which rainfall interpolation methods is suitable to convert the point-based rain gauge network to a gridded surface at the same resolution of the satellite data?

ii. How do the latest SPP perform during recent extreme floods in various river basins of Peninsular Malaysia?

iii. How to improve the available SPP estimations so that more accurate prediction of extreme events can be achieved?

iv. After improvement, are these improved SPP able to replace the rain gauge observations and driven in hydrological modeling?

1.4 Objectives of the Study

The main goal of this study is to assess the suitability and performance of the selected SPP in predicting runoff through hydrological simulation during the 2014-2015 flood event. In order to achieve the goal, the main objectives of this research are as follows.

i. To validate various spatial interpolation methods to be adopted on the rain gauge network before comparing with the grid-based satellite estimations.
ii. To evaluate the performance of satellite precipitation products (SPP) during extreme floods at three different geographic locations of Peninsular Malaysia.
iii. To infer the improvement that can be made using SPP so that more accurate predictions of extreme events can be achieved.
iv. To simulate rainfall-runoff during selected events based on raw and improved SPP estimations.

1.5 Scope of the Study

The present study attempts to evaluate three advanced SPP including TRMM 3B42 Version 7 (V7), CMORPH and PERSIANN during a huge tragedy of flood that happened at the end of 2014 in the three different river basins, i.e. Langat, Kelantan and Johor river basin located at the west, north and south parts of Peninsular Malaysia, respectively. The study was divided into four sections. Firstly, before comparing the rain gauge observations with the selected SPP estimations, a comparative evaluation of a set of interpolation methods including the Arithmetic Mean (AM) (Anctil *et al.*, 2006; Creutin & Obled, 1982; Shaw & Lynn, 1972), Thiessen Polygon (TP) (Thiessen, 1911), Inverse Distance Weighting (IDW) (Di Piazza *et al.*, 2011; Ly *et al.*, 2011; Ly *et al.*, 2013; Wagner *et al.*, 2012), Ordinary Kriging (OK) (Buytaert *et al.*, 2006; Zhang & Srinivasan, 2009) and Spline (SP) (Franke, 1982; Hutchinson, 1995; Mitáš & Mitášová, 1988; Tait *et* *al.*, 2006) was performed on the rain gauge network for all river basins using the Geographical Information System (GIS) platform, to identify the most suitable spatial interpolation methods to be compared with the gridded surface SPP estimations. Next, the gridded surface rain gauge observations will be compared with the selected SPP estimations and the performance in terms of rainfall pattern, detection and capturing storm ability were assessed.

Later, this study attempts to improve the SPP estimations by adopting bias correction (BC) schemes including the Linear Scaling (LS) (Lenderink *et al.*, 2007), Local Intensity Scaling (LOCI) (Schmidli *et al.*, 2006) and Power Transformation (PT) (Leander & Buishand, 2007) methods to produce more accurate prediction before the data are ready to be input in the hydrologic modeling. It is found that studies regarding the BC on SPP estimations in Malaysia appear to be limited. Finally, the simulation process was carried out to simulate the rainfall-runoff during the 2014-2015 flood events based on the raw and improved (LS, LOCI and PT) SPP estimations (TRMM, CMORPH, and PERSIANN) that had been performed previously. The Hydrological Modelling System (HEC-HMS) was employed to validate the performance of the raw and bias-adjusted SPP simulated flows with rain gauge model parameters. Figure 1.1 shows the design framework for this research where it illustrates the overall process and the flow of work.

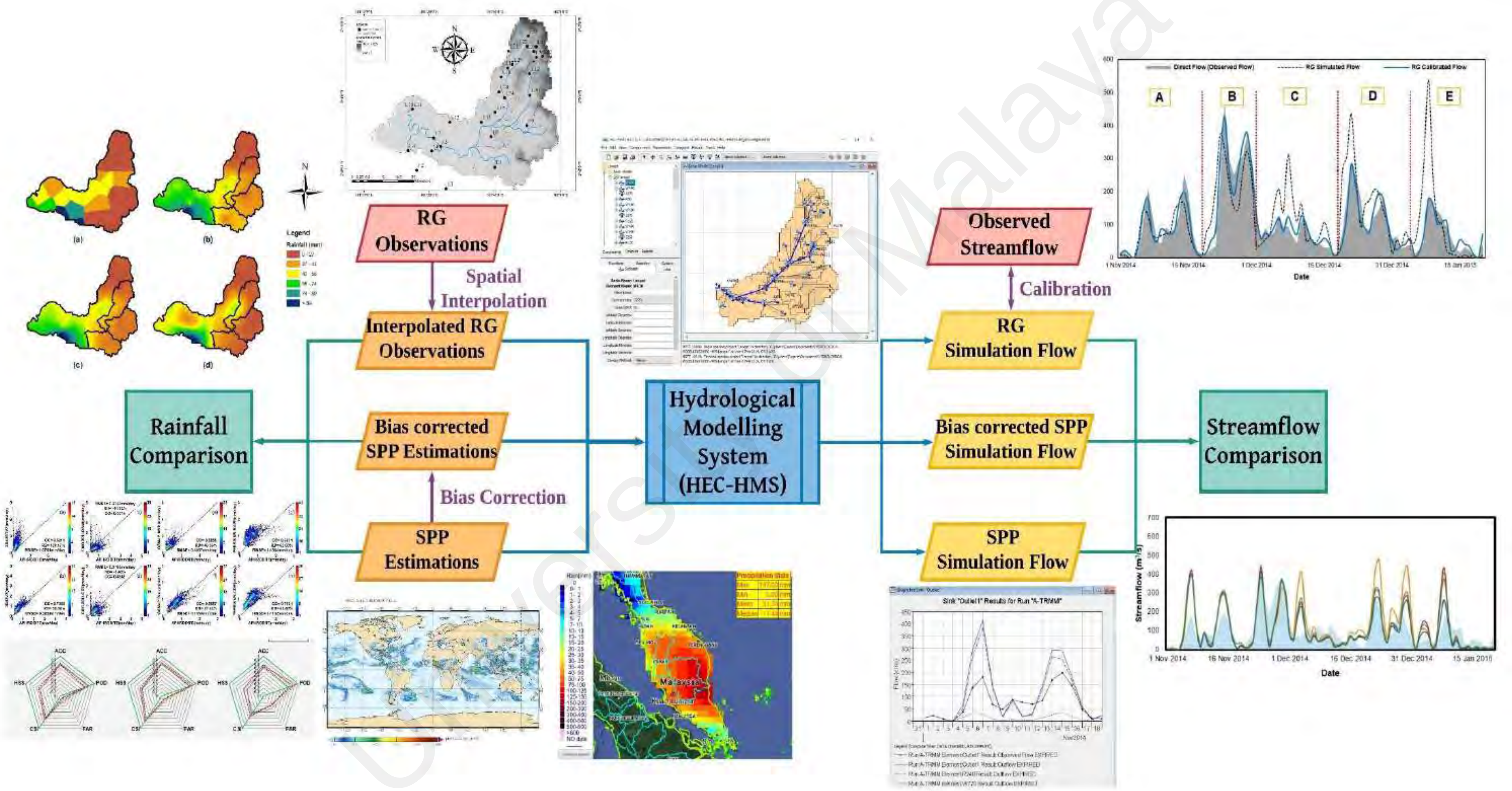

Figure 1.1: Conceptual framework of research

1.6 Significance of the Study

Precipitation or rainfall is a vital element in the hydrological cycle regardless of whether one is primarily concerned with climate-scale, regional, or local hydrology. Nevertheless, the extreme transience and spatial inhomogeneity of rainfall make it one of the most challenging variables as an input to the hydrological models particularly in the regions for which their rain gauges and radar observations are sparse. Hence, accurate and reliable precipitation information is therefore necessary to ensure better water resources management and decision-making. At present, there are several SPP are freely available publicly of which their huge potential benefits should be explored by the hydrological community as an alternative source to overcome the limitation of ground observation techniques. Recent development in SPP estimations is the multi-sensor technique that combines the advantages of both geostationary (high temporal resolution) and polar-orbiting satellites (direct relation) data. Malaysia, as a tropical country, is prone to annual flooding while experiencing a major flooding event at least once every five years where multiple states are affected. Towards the end of the year, northeast monsoons cause massive heavy downpours of rain, particularly in the eastern states. Despite several flood mitigation initiatives, forecasting and warning system efforts have been undertaken by the various agencies, particularly the DID, under the Ministry of Natural Resources and Environment, present countermeasures remain insufficient as experienced during the December 2014 – January 2015 flood crisis, where close to 250,000 residents were displaced. Since not many studies had been implemented in Malaysia, these advance satellite data are important and crucial to be investigated for this country. Also, evaluation of atmospheric parameters between ground observation and satellite image should be done by our researchers in Malaysia so that future researchers can make use of these alternative data other than rain gauge to predict future events in Malaysia. Moreover, this will be beneficial for the SPP's sensor and algorithm developers to assess the capability of SPP in high precipitation variability regions.

1.7 Organization of the Thesis

The thesis comprises of six chapters dealing with various aspects of dynamic response and probabilistic analysis. Chapter 1 gives general introduction of the research. Chapter 2 reviews various papers that have been done in order to have a better understanding and explanation of the relevance of the study. This part is much helpful as a good research study can only be achieved when there is a good basic knowledge of the study.

Chapter 3 provides a thorough evaluation of the selected SPP estimations for 2014-2015 extreme flood events that happened in the three different river basins in Peninsular Malaysia, i.e. Langat, Kelantan, and Johor river basins. This chapter covered the first and second objectives of this research. The first approach is the validation of the spatial interpolation methods applied to the rain gauge network. Next, the comparison between SPP and interpolated rain gauge observations at different geographic locations of the selected river basins were conducted. The third approach is the assessment of rain detection and capturing storms abilities by these selected SPP at those river basins.

Chapter 4 provides bias-adjustment for the SPP estimations. This chapter attempts to improve the SPP estimations by adopting bias correction (BC) schemes and produce more accurate predictions (Refer to the third objective) before the data are ready to be input in the hydrologic modeling. The selected bias correction schemes are described. Next, this section provides a comparative analysis between the raw and bias-adjusted SPP estimations. Moreover, in order to evaluate the uncertainty of the BC parameters applied on the SPP rainfall and whether these parameters can be applied in a similar event of different time period, this chapter has included an addition of four flood events of the same month as 2014-2015 floods (December and January) for the purpose of sensitivity analysis.

Chapter 5 covers the final objective of this research whereby both raw and bias-adjusted SPP estimations will be applied to the hydrological modeling (HEC-HMS). The purpose of this chapter is to demonstrate the applicability of SPP in flood prediction using rain gauge optimized parameters. Description of the model and simulation process are discussed in this chapter. Apart from that, this section provides a comparative analysis of flood prediction with and without bias-adjustment SPP estimations.

Finally, Chapter 6 draws the conclusions for every objective of this research and provides general recommendations for future studies.

CHAPTER 2: LITERATURE REVIEW

2.1 Introduction

This literature review aims to address various aspects of the use of satellite precipitation products (SPP) for hydrological applications. This chapter will first describe the monsoon weather systems in Southeast Asia followed by that for Malaysia specifically. Next, a review on different types of rainfall measurements including the ground-based measurements and remote sensing technologies is discussed. SPP is the main concern of this research, a review of SPP estimation techniques and different types of error depending on the quality of the measurements made by the sensors as well as climate, topography, season, and the local climatic regime was present. Finally, this chapter discusses SPP-forced hydrological modeling.

2.2 Monsoon weather systems in Southeast Asia

Southeast Asian countries include East India, South China, Myanmar, Laos, Vietnam, Thailand, Malaysia, Singapore, Kampuchea, Indonesia, Borneo, the Philippine islands, Portuguese Timor and western New Guinea as illustrated in Figure 2.1. These countries are influenced by the monsoon which is a large-scale seasonal reversal of the wind regime (Serreze & Barry, 2010).

Figure 2.1: Southeast Asia

Monsoonal areas receive summer rainfall maximums and most of the double rainfall maximums. This monsoon not only influences Asian countries but also breaches beyond the tropical latitudes. Monsoon rainfall can also affect regions that were not originally considered as monsoonal (Serreze & Barry, 2010). The two main monsoon regimes are specifically named the northeast monsoon (winter monsoon), which happens from November to March annually, and the southwest monsoon (summer monsoon) from late May to September. Furthermore, October is the transition month from the southwest to northeast monsoon seasons (Cruz *et al.*, 2013). The East Asian summer monsoon (EASM) happens when rainfall reaches a maximum during the boreal winter, whereas the East Asian winter monsoon (EAWM) happens during boreal summer where rainfall reaches maximum. The EAWM is an atmospheric flow over Asia and is varies greatly depending on the Siberian High (SH) and the Arctic Oscillation (AO) (Wang *et al.*, 2012).

The SH refers to the semi-permanent system that accumulates cold, dry air in northeastern Siberia. It reaches its maximum intensity in winter and accounts for the lowest temperatures and the highest pressures in weather systems. On the other hand, the AO, also known as the Northern Hemisphere annular mode of atmospheric circulation, is categorized into two phases by looking at the characteristics of the wind that circulates the Arctic in an anti-clockwise direction (NOAA, 2012). When the wind is strong, the circulation remains in the Arctic Circle. This is termed as the positive phase. During the negative phase, the high pressure at the North Pole and lower pressure at mid-latitudes (OSS, 2013) result in the wind moving towards the tropics. The weather and climate of the Arctic affect the monsoon seasonality indirectly. The Arctic ice sheets control the intensity of SH which influences the EAWM – a strong SH results in a strong EAWM. This is also recorded by the methods of measuring the grain size of loess done by many scientists as an indicator of the intensity of EAWM. A stronger wind is able to carry coarser dust (Wang *et al.*, 2012). Chinese loess records showed that there has been an increase in grain size suggesting that the strength of the EAWM has increased during the Holocene (Wang *et al.*, 2012). The increased dust deposition has been associated with drier and cooler EAWM conditions (Porter, 2001).

The EASM however, is dominated by the Western Pacific Subtropical High (WPSH) (SOEST, 2013; Wang *et al.*, 2013; Zhou *et al.*, 2009). Findings of the study done by Wang *et al.* (2013) showed that positive WPSH–ocean interaction can provide a source of climate predictability and highlight the importance of subtropical dynamics in understanding monsoon and tropical storm predictability. Zhou *et al.* (2009) stated that the change in atmosphere temperature partly affected the WPSH which directly influences the EASM. Since the late 1970s, the WPSH had shifted westward for reasons unknown to date. Referring to the study of Zhou *et al.* (2009), the westward shift of the WPSH from the mean position of the western edge (133.5°E) is 14° during the 1980–1999 (119.5°E).

It was suggested that the westward shift of EASM is due to the atmosphere's response to the observed Indian Ocean–western Pacific (IOP) warming (Huang & Yan, 1999; Zhou *et al.,* 2009). The Himalayan uplift or the Tibetan Plateau is also another factor that influences the monsoon rainfall onset dates (Kilaru *et al.*, 2013). The rate of growth of the Tibetan Plateau was faster than its erosion process possibly (Mishra & Kumar, 2014). The decrease in rainfall over major parts of the region may account for the slow erosion process. This has been argued as a factor that promoted the monsoon strengthening in Asia (Reuter *et al.*, 2013). The increased convection at high temperatures results in more rainfall in the leeward region. This may also be a contributor to the flooding in Indian regions.

2.3 Weather of Malaysia

Malaysia is located at Southeast Asia and lies near the Equator, between 1°–8°N latitude and 99°–120°E longitude. Malaysia has a total land area of 329,758 km^2 of which is divided into two main parts: (1) Peninsular Malaysia (PM) (131,598 km^2), located in the south of continental Eurasia; and (2) East Malaysia (EM) (198,160 km^2) in the northwestern coastal area of the island of Borneo. The two areas are 531 km apart, separated by the South China Sea.

Malaysia has a tropical rainfall climate. High temperatures and high humidity prevail with an average temperature of 27˚C. During the day, the temperature rises above 30°C year-round and during the night temperature rarely drop below 20°C. Inland regions are slightly cooler, with an average daytime temperature of 26˚C, while the upper altitudes have an average daytime temperature of 23˚C.

The climate of Malaysia is subjected to the Southeast Asia Maritime Continent monsoon, which is part of the larger Asian–Australian monsoon system (Tangang *et al.*, 2012). According to Dale (1974), the rainfall pattern in Peninsular Malaysia was divided into four periods based on the Southeast Asia monsoon, i.e. the southwest monsoon (SWM), northwest monsoon (NEM) and two inter-monsoon (IM) seasons.

Precipitation from the NEM starts in November and ends in February, while the SWM brings rain from May to August. The NEM brings heavy precipitation on the east coast of Peninsular Malaysia and in the northeast of the East Malaysia region as a result of orography, while the SWM brings relatively less precipitation, particularly on the west coast of the PM because of the shield provided by Indonesia. By contrast, the two IM seasons, i.e., from March to April and from September to October, bring heavy precipitation that normally occurs as convective rain.

2.4 Ground-based rainfall measurement

2.4.1 Rain gauge measurement

Rain gauge, also known as an udometer, pluviometer, or an ombrometer (as shown in Figure 2.2) was the most common instrument used to measure how much rain has fallen. There are several types of rain gauge that are usually used to collect rainfall depth such as tipping-bucket rain gauge, weighing precipitation gauge, and telemetering rain gauge. This instrument measures directly the precipitation and had been the only available information from which to derive long records of reference precipitation over many years (Tapiador *et al.*, 2012; Yilmaz *et al.*, 2005). However, rain gauges are considered as point measurement which cannot represent for the environment (de Coning, 2013; Habib *et al.*, 2012). Also, many regions of the world including developing countries, oceans and mountains are ungauged (Behrangi *et al.*, 2011; Collischonn *et al.*, 2008). Apart from that, the instruments do malfunction and back-up systems may not always provide accurate data (Strangeways, 2004).

Rain gauges also may underestimate on true precipitation due to significant bias arising from coarse spatial resolution, location, wind, and mechanical errors (de Coning, 2013; Groisman & Legates, 1994; Yilmaz *et al.*, 2005). Precipitation can also be estimated using weather radar due to its continuous spatial coverage (Habib *et al.*, 2012) but it has difficulties in hardware calibration (Yilmaz *et al.*, 2005). The area covered by weather radar is still limited, the precipitation can be undetected or rate can be underestimated as distance from the radar increases. (Diederich *et al.*, 2015; Gu *et al.*, 2010; Scofield & Kuligowski, 2003). Moreover, the accuracy of the reflectivity values can be influenced by fixed targets such as ground clutter, beam block or anomalous propagation (de Coning, 2013; Diederich *et al.*, 2015).

Figure 2.2: Rain Gauge

Rain gauge is cheap and easy to install and calibrate and has been used for decades, and thus the only source available from which it is used to derive a long term records of reference precipitation (Tapiador *et al.*, 2012). However, it has several problems. Firstly, these precipitation measuring stations sometimes fail in providing a continuous record of precipitation. According to Suhaila *et al.* (2010), it was found that a percentage of missing values was less than 10% for the period 1975 to 2004. Besides, the instruments do malfunction and back-up systems may not always provide accurate data (Strangeways, 2004). The rain gauges may underestimate the true precipitation due to significant bias arising from coarse spatial resolution, location, wind, and mechanical errors (Groisman & Legates, 1994; Yilmaz *et al.*, 2005).

In order to determine the rainfall-runoff in the river basins, the spatial distribution of rainfall over a basin is required. Rain gauges can provide only fractional coverage of the overall spatial domain. Thus, this often resulted in inability to provide an accurate representation of the variability in a rainfall field. Considering this, a network of gauges (consisting of a series of gauges distributed throughout the basin) is used to produce a spatial distribution and approximate rainfall accumulations at ungauged locations. Spatial distribution of rainfall from point rain gauge values can be determined using various spatial interpolation techniques such as Thiessen Polygon, Inverse distance weighting (IDW), Kriging and Spline. Rainfall fields, however, often exhibit a high degree of spatial variability (Tao, 2009) which is often uncaptured through the interpolation of point rain gauge values that generally produce a uniform rainfall field (Sinclair & Pegram, 2005). Previous researchers had investigated the effect of gauge network design on interpolation accuracy. It was found that the interpolation accuracy of rainfall data sets was dependent on the optimal network density and spacing (Rodríguez-Iturbe & Mejía, 1974; Xu *et al.*, 2013). Nevertheless, optimal gauge density and spacing, for the most part, are never been achieved in a river basin (Smith *et al.*, 2007). Huff (1970) demonstrated that a rain gauge network density of one gauge per 65 km^2 is required in order to achieve an average sampling error in recorded rainfall accumulations of less than 5% for six-hour rainfall accumulations. The density required, however, will change depending on operational considerations. According to the United State Army Corps of Engineers (USACE) (1996), the optimal network design should consist of evenly distributed gauges at a spatial density determined by:

$$N = A^{0.33} \tag{2.1}$$

where N = the number of gauges, and A = the area of the basin in squared miles. The World Meteorological Organization (WMO) (2008) recommends rain gauge network densities dependent on catchment type (refer to Table 2.1).

Table 2.1: Recommended minimum densities of rain gauge stations (WMO, 2008)

Physiographic Unit	Area per station (km^2)
Coastal	900
Mountains	250
Interior plains	575
Hilly/ undulating	575
Small islands	25
Polar/ arid	10,000

Highly variable rainfall fields have a demonstrated effect on runoff modeling (Schilling & Fuchs, 1986). The effect of rainfall field variability was investigated by Faurès *et al.* (1995) who studied the effect of varying gauge density and placement on hydrological modeling results for a watershed in southeastern Arizona, United State. By varying the gauges used to generate the rainfall input for the model, they found that the peak runoff and the runoff volume varied substantially with a coefficient of variation which ranged from 9% to 76% and 2% to 65%, respectively. This study indicated that in an environment dominated by high-intensity rainfall events with considerable spatial variability, rain gauge density and placement can strongly influence predicted stream flows from hydrological modeling, leading to an increase in model uncertainty results.

The errors within gauge measurements due to systematic and calibration issues also often lead to considerable error in subsequent modeling efforts.

2.4.2 Automatic Weather Stations (AWS)

In recent years, weather monitoring has become increasingly automated. This automated weather system (as shown in Figure 2.3) consisting of the following major components:

- A suite of meteorological sensors housed in instrument shields and connected to a field processing unit (data-logger) by means of shielded cables
- A field-processing unit (data-logger) of data acquisition, processing, storage, and data transmission; and
- Peripheral equipment such as stabilized power supply, modem, built-in-diagnostics and local terminals for manual entry, data editing, and display.

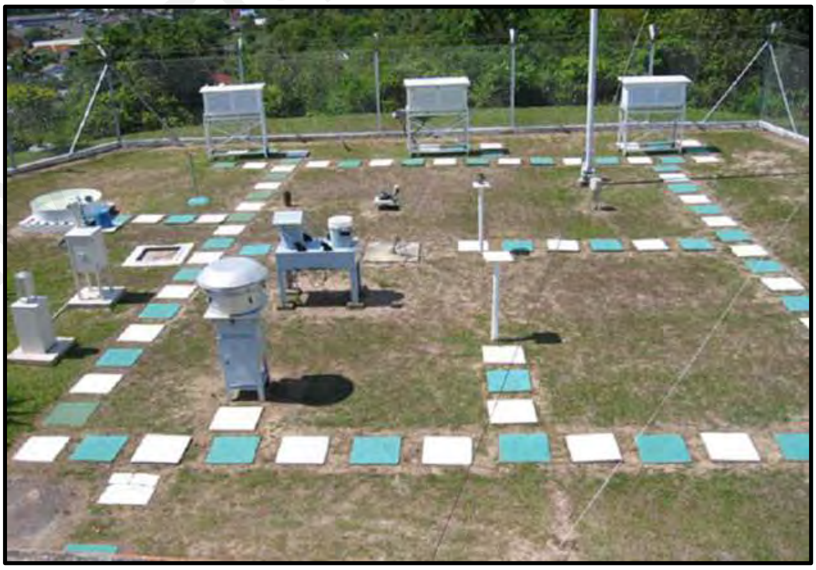

Figure 2.3: Meteorological Station in Mersing

(Source: Malaysian Meteorological Department)

The AWS measures precipitation (amount of rainfall), atmospheric pressure, temperature, humidity, wind speed and direction, and global solar radiation, updating the data every minute, 24 hours a day without human intervention.

2.4.3 Weather radar

Radar is an acronym for ‘Radio Detection and Ranging’, and it is a ground-based and active remote sensing equipment. The details on the use of weather radar in weather forecasting will be explained in Section 2.5.1.

2.5 Remote Sensing Applications in Weather and Climate

Remote sensing refers to the activities of obtaining information about an object by a sensor without being in direct contact with the object. Applications of remote sensing span a wide range of fields, including meteorology, hydrology, oceanography, geologic studies, etc. In the realm of meteorology, weather radar and satellites are the common remote sensors in the weather and climate measurement due to the ways in which the atmosphere and other earth systems interact with the electromagnetic spectrum (EMS) (Figure 2.4). The detail on the principle of operation of weather radar and satellites will be discussed in the next section.

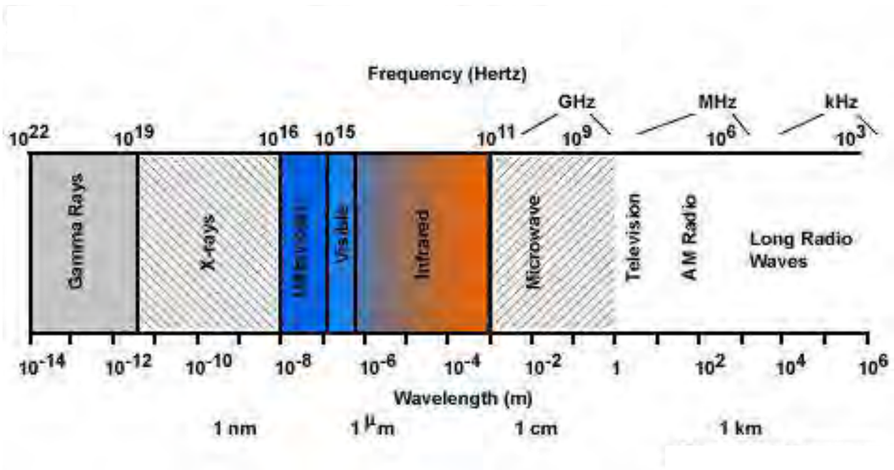

Figure 2.4: The Electromagnetic Spectrum
(Source: Laing & Evans, 2011)

Generally, remote sensing systems can be classified into active and passive types in accordance with the source of electromagnetic radiation. Passive sensors (Figure 2.5a) can only be used to detect radiation when the radiation is available. Remote sensing of objects that reflect solar radiation is possible only when the sun is illuminating the earth. Since there is no reflected radiation available from the sun at night, cloud images in the visible channel are only available in the day. On the other hand, remote sensing of objects in the thermal infrared channel can be performed day or night as long as the objects radiate enough amount of thermal infrared radiation.

On the other hand, active sensors (Figure 2.5b) generate and transmit their own energy and have the advantage of being independent of solar radiation and the time of the day. It can be used for examining objects in wavelengths that are not sufficiently provided by the sun, such as microwaves. However, active sensors require the generation of a fairly large amount of radiation to adequately illuminate an object.

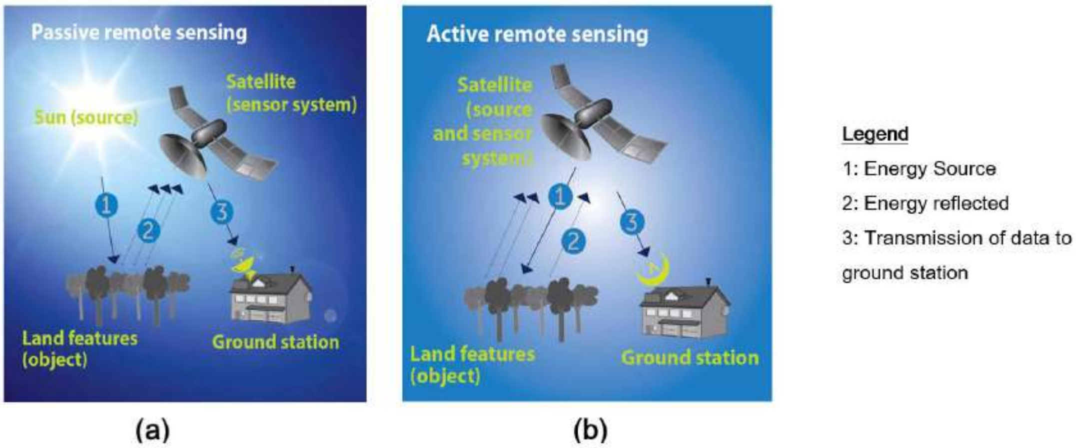

Figure 2.5: Passive and active remote sensing

(Source: http://atlas.sansa.org.za/atlas-intro_to_rs.html)

2.5.1 Weather Radar

"Weather radar measurement is a complex process to make quantitative estimation of rainfall due to involving complicated and sophisticated hardware with both electronic and mechanical subsystems, signal processing, propagation and interaction of electromagnetic waves through the atmosphere and with the ground, image analysis, and quality control, physics of precipitation processes, optimal estimation and uncertainty analysis, database organization and data visualization and hydrologic applications using electromagnetic wave" (Krajewski & Smith, 2002). However, it was useful for the input of runoff and flood prediction models, validation of satellite remote sensing algorithms as well as for statistical characterization of extreme rainfall frequency. In the case of rainfall, the raindrop size and distribution are related to the reflectivity using the Marshall-Palmer reflectivity droplet size ratio, Z-R (Marshall and Palmer, 1948), following:

$$Z = aR^b \tag{2.2}$$

where Z is the reflectivity factor measured by the radar station (dbz), R is the rainfall intensity (mm/hr), and a and b are empirical coefficients determined during calibration. Figure 2.6 shows one of the weather radar stations in Miri, Sarawak, Malaysia and Figure

2.7 shows a sample of radar observation provided by the Malaysian Meteorological Department (MMD).

Figure 2.6: Weather radar in Miri, Sarawak, Malaysia

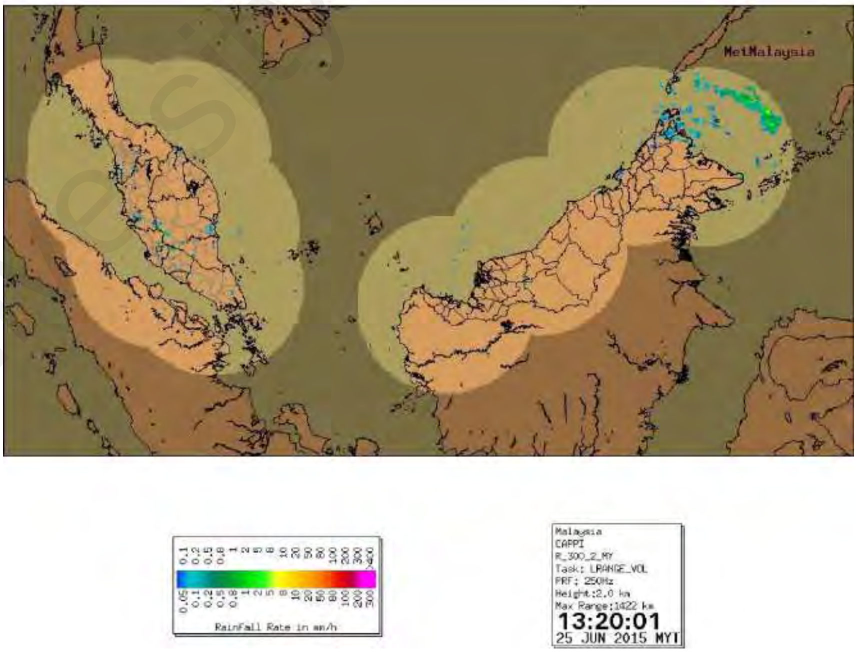

Figure 2.7: Sample of radar observation in Malaysia

(Source: MMD)

Creutin *et al.* (2000) characterized three major sources of radar error for quantitative precipitation estimation:

(1) Electronic instability and miscalibration of the radar system and *Z-R* relationship;

(2) Beam geometry; and

(3) Fluctuation in atmospheric conditions.

All three categories of errors can have a considerable effect on the ability to use radar in hydrological modeling applications. According to Golding (2009), it is the above sources of error that limit the widespread use of radar in hydrological modeling. The first error outlined by Creutin *et al.* (2000) relates to the use of the Marshall-Palmer relationship introduced in Equation (2.2) above. This relationship can be calibrated at each radar location. Once calibrated, the coefficients are generally held constant (Steiner & Smith, 2000). Each droplet, however, does not hold true to the same ratio. Furthermore, the ratio does not hold true for each storm event and consequently will tend to either underestimate or overestimate the rainfall rate. Vieux and Bedient (1998) and Morin *et al.* (2006) investigated the effect of manipulating the Marshall-Palmer relationship on simulated hydrographs and found that small manipulations in this relationship can cause substantial changes in the simulated hydrograph. The second and third categories identified by Creutin *et al.* (2000) are dependent on the radar environment. These errors include beam broadening, clutter, anomalous propagation, visibility effects, variability in time and space of the vertical profile of reflectivity (VPR), beam power attenuation and issues related to the microphysics of precipitation. These errors affect the measurement of reflectivity from the atmosphere and can result in substantial measurement uncertainty. For example, Michelson and Koistinen (2000) demonstrated how beam broadening in a study conducted in the Baltic Sea caused radar accuracy to deteriorate the further the beam traveled. Furthermore, spatio-temporal sampling errors can result from the fact that radar measures rainfall at substantial heights above the ground. Between the measurement location and the ground, the rainfall can move substantial lateral distances or even evaporate before reaching the ground. Errors in reflectivity result in errors in the subsequent rainfall estimation.

2.5.2 Weather Satellites

Satellite sensors are the only instrument to measure precipitation on a global scale with short revisit time. In this era of globalization, there are various types of satellite products used in the study of weather and climates. Figure 2.8 shows the global satellite observation system.

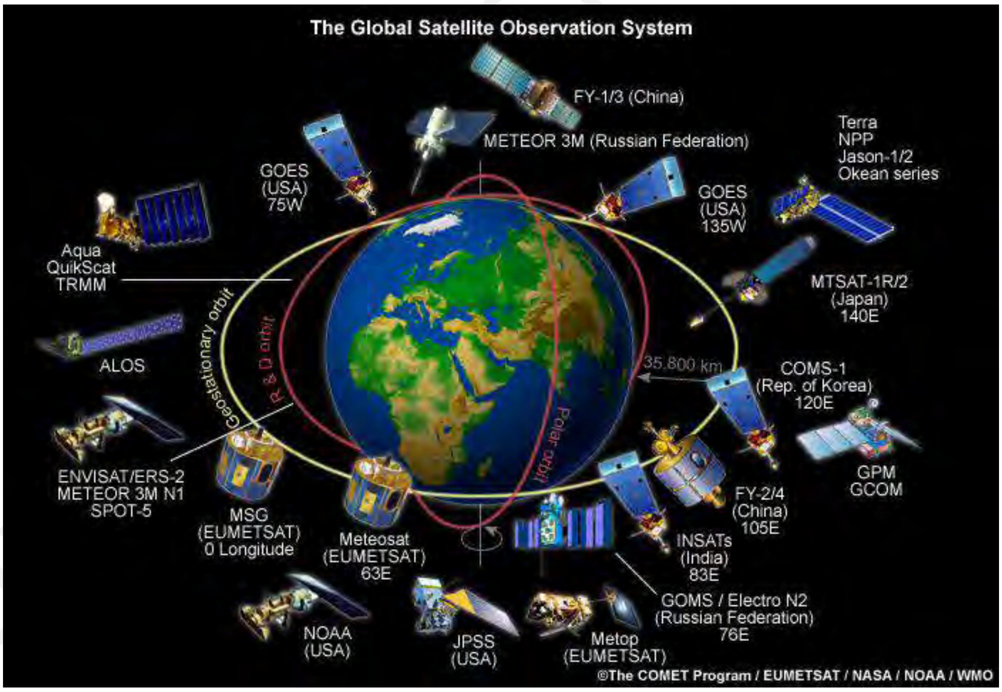

Figure 2.8: The global satellite observation system

A distinction is made between sensors deployed on polar-orbiting and geostationary satellites. Polar-orbiting satellites can sense the whole globe but have a relatively low revisit time which limits its temporal resolution, whereas geostationary satellites hold a high temporal resolution but cover a limited but constant area. In addition, they operate about two orders of magnitude higher in space compared to the polar-orbiting satellites. Passive microwave (PMW) instruments have large antenna sizes and, consequently, cannot operate on geostationary satellites. However, plans exist to deploy microwave sounders on geostationary satellites (Lambrigtsen *et al.*, 2006). The so-far deployed visible (VIS) and infrared (IR) sensors retrieve information mainly from the cloud top. Cloud top information is used to indirectly derive the precipitation rate, which can lead to erroneous detection of precipitation from non-convective high clouds with cold cloud tops (Kidd & Levizzani, 2011).

PMW sensors represent the second commonly used type of satellite instruments to estimate precipitation from space. They provide a more physically complete image of the atmospheric water content compared to VIS/IR satellite sensors (Levizzani *et al.*, 2007). Whereas low-frequency channels serve to directly detect medium-to-large water droplets below the freezing level, high-frequency channels can infer smaller particles and specifically ice particles indirectly from scattering above the freezing level. As a downside, particularly the low-frequency channels have a coarse spatial resolution of several tens of kilometers in diameter. In contrast, active microwave sensors reach much higher spatial resolutions but with a very narrow swath width. Due to the low swath width, these spaceborne radars commonly serve as a calibrator for PMW sensors or for case studies

2.6 Satellite Precipitation Products (SPP)

Satellite precipitation estimates can be derived from a range of observations from many different sensors, including Geostationary (GEO) satellites and Low Earth Orbiting (LEO) satellites (Kidd & Huffman, 2011; Serrat‐Capdevila *et al.*, 2014). Five operational GEO satellites are required to ensure full West-East (and ~70 °N to 70 °S) coverage and provide imagery on a frequent and regular basis (i.e., every 30 min). LEO satellites generally cross the Equator at the same local time on each orbit, providing about two overpasses per day. Rainfall can be inferred from visible images since thick clouds, that are more likely to be associated with rainfall, tend to be brighter than the Earth's surface. Infrared (IR) imagery, which is available night and day, is potentially more useful since heavier rainfall tends to be associated with larger, taller clouds with colder cloud tops. Passive Microwaves (PMW) represent a useful alternative, as emissions from rain droplets lead to an increase in PMW radiation and scattering caused by precipitating ice particles leads to a decrease in PMW radiation.

A growing number of techniques have been developed that exploit the synergy between polar-orbiting retrievals (infrequent, more direct) and geostationary observations (frequent, less direct) and that blend IR radiances with PMW observations (Turk *et al.*, 2000). TMPA (Huffman *et al.*, 2007), is one of the examples that ingests data from PMW imaging with sounding sensors and geostationary IR data. Other techniques have used Artificial Neural Networks (ANNs) to derive precipitation estimates by combining information from multi-channel and multi-sensor observations like the PERSIANN (Hsu *et al.*, 1997). Other techniques use IR data as a measure of cloud movement to morph the PMW observations between successive satellite overpasses. Examples of current state-of-the-art methodologies are the CMORPH (Joyce *et al.*, 2004) and the GSMaP (Kubota *et al.*, 2007). Recently, the National Aeronautics and Space Administration (NASA) and Japan Aerospace Exploration Agency (JAXA) GPM in coordination with the Goddard Earth Sciences Data and Information Services Center (GES-DISC) released the Integrated Multi-satellitE Retrievals for GPM (IMERG) (Huffman *et al.*, 2015), which merges precipitation estimates from PMW and IR sensors and monthly surface precipitation gauge analysis data to provide half-hourly precipitation estimates on a 0.1° grid over the 60° N-S domain.

2.7 Errors of Satellite Precipitation Estimations

Several studies had validated SPP through comparison with gauge and radar rainfall estimates in different parts of the world and under different climatic conditions (Ebert *et al.*, 2007; Gottschalck *et al.*, 2005; Maggioni *et al.*, 2016; Stampoulis & Anagnostou, 2012; Tian & Peters-Lidard, 2010) and found that the SPP are subjected to different types of error depending on the quality of the measurements made by the sensors as well as climate, topography, season, and local climatic regime. In this section, we summarize the main sources of errors of these products that may limit their use in hydrologic modeling to monitor and predict floods.

2.7.1 The density of ground-based rainfall measurement

The errors in SPP are commonly assessed with respect to ground-based rainfall measurements such as rain gauge or weather radar. Lacking a sufficiently dense rain gauge coverage is the main obstacle for a proper evaluation of the satellite retrievals (Kidd *et al.*, 2017; Maggioni & Massari, 2018; Massari *et al.*, 2017). Thus, this poses a challenge not only for the mere validation of SPP but also for the understanding of how SPP uncertainties propagate into hydrologic simulations and using rain gauge information for correcting the bias in SPP prior to their use in hydrologic models.

For example, Anagnostou *et al.* (2010) presented cross-validation of the rainfall gauges based on an independent small-scale in Oklahoma. As the rain gauge network was relatively dense (100-m inter-gauge distances), they had demonstrated the need to benchmark reference data sources prior to their quantitative use in validating remote sensing retrievals. This reference can be easily obtained from the United States, Europe, Australia, and China that having relatively high rain gauge density (Refer Figure 2.9).

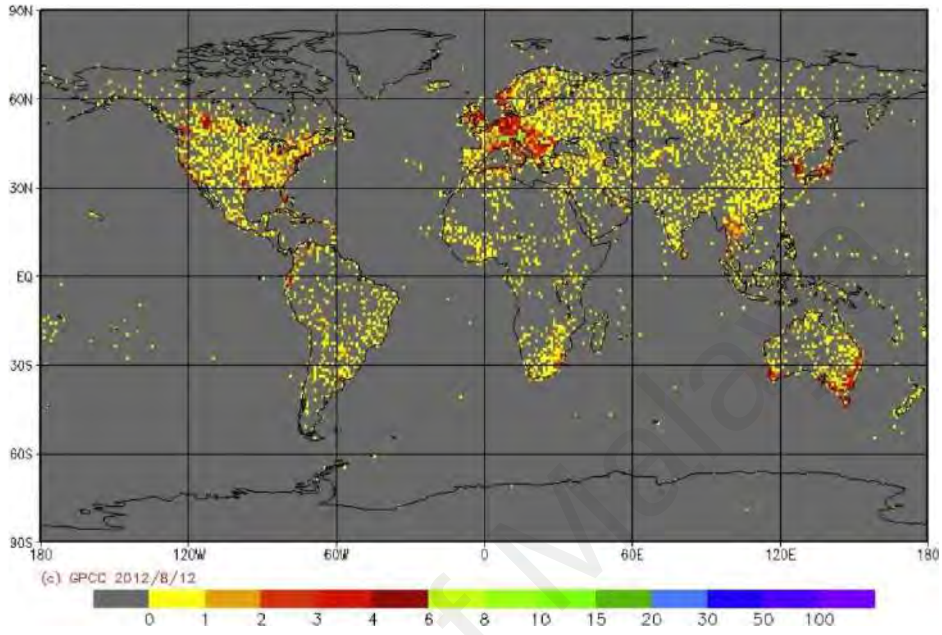

Figure 2.9: Number of stations used by the GPCC

(Source: The Climate Data Guide: GPCC: Global Precipitation Climatology Centre)

In order to adopt the rain gauge measurements as the benchmark or reference points for the evaluation and validation of SPP, the temporal sampling uncertainties (related to observation frequency) and the spatial sampling error (related to rain gauge density) are considered. In particular, temporal sampling uncertainties increase with the sampling interval according to a scaling law and decrease with an increasing averaging area with no strong dependence on local orography (Villarini *et al.*, 2008). On the other hand, spatial sampling uncertainties tend to decrease for increasing accumulation time, with no strong dependence on the gauge location within the pixel or on the gauge elevation.

2.7.2 Rain detection, systematic, and random errors of SPP

SPP estimations can be affected by detection, systematic, and random errors. Detection errors include false alarms (when the satellite estimate is larger than zero, but in fact, it does not rain) and missed rain (when the satellite estimate is zero, but there is rain at the ground). When the satellite correctly detects rainfall, the estimated rain rate may be characterized by systematic (or bias) and/or random errors. Biases arise from systematic problems, whereas the random error depends on the remote sensing measurement (retrieval error) and the lack of continuity in the coverage by LEO satellites (sampling error) (Bennartz & Petty, 2001). Typical sources of retrieval error are due to beam-filling issues and sub-pixel inhomogeneity in the rainfall field (Kummerow, 1998) and to the difficulties in estimating the impact of solid hydrometeors (Bennartz & Petty, 2001). Nevertheless, sampling errors are determined by the satellite orbit, swath width and space-time characteristics of the rainfall fields themselves (Chang & Chiu, 1999). Errors in rain detection and in precipitation rate estimation can both play an important role in water cycle applications such as flood forecasting, land surface modeling, etc.

2.7.3 Seasonality, storm type, and topography

The performance of SPP can also be influenced by seasonal precipitation patterns, type of storm, and topography (Dinku *et al.*, 2010; Ebert *et al.*, 2007; Gottschalck *et al.*, 2005; Moazami *et al.*, 2013; Tian & Peters-Lidard, 2007). For instance, Ebert et al. (2007) compared to near real-time SPP with numerical weather models in Australia, the US, and Northwestern Europe. They found that SPP performed better than models for convective storms (summer) and from the tropics to mid-latitudes. In these cases, retrieval uncertainty is the primary error source, mainly caused by the IR inaccuracy with stratiform precipitation and snow cover. In semi-arid climates (northern Mexico), large false alarm rates are observed due to raindrop evaporation before reaching the surface.

Moazami *et al.* (2013) and Dinku *et al.* (2010) detected a similar behavior in Iran and Eastern Africa, respectively.

Tian and Peters-Lidard (2010) reported that the spread of global estimates systematically depends on seasonality, location and rain rate with the largest standard deviations among products at high latitudes (>40°) and during the cold seasons. Low deviations were noted in tropical regions with intense convective precipitation and higher in cold regions with a complex topography and light rainfall events, along with coastlines and over water bodies (Kubota *et al.*, 2009). In summary, the more the precipitation regime tends toward deep convection, the more accurate the satellite estimates are. Despite the SPP have higher accuracy during summers, in this season they are characterized by a considerable positive bias which may largely impact hydrologic model predictions when SPP are used as forcing data.

High-mountain regions are among the most challenging environments for SPP measurements due to extreme topography and large weather and climate variability. Apart from that, these regions are typically characterized by a lack of in situ ground observations. Hong *et al.* (2007) evaluated the impact of topography on PERSIANN-Cloud Classification System (PERSIANN-CCS) performances in western Mexico and found the satellite managed to capture the spatial distribution and timing of diurnal convective rainfall, but showed elevation-dependent biases, underestimating light rain at both high elevations and early in the day and overestimating precipitation rates at low elevation. Elevation-dependent trends with underestimation at higher elevation for CMORPH and TRMM 3B42RT were also observed in Ethiopia and Colombia (Dinku *et al.*, 2007; Hirpa *et al.*, 2010). A similar case was found by Guo *et al.* (2017) in central Asia where significant elevation-dependent errors were observed in eight SPP especially at altitudes higher than 3000 m with large miss precipitation errors and poor detection capabilities. Nevertheless, in some regions of the world, such as the Kabul basin in

Afghanistan (Ghulami *et al.*, 2017), a relatively good detection of both amount and distribution of precipitation was observed.

2.8 Hydrological modeling studies in Malaysia

Hydrological models are vital components and essential tools for water resources and environmental planning and management (Devia *et al.*, 2015). Recently, several studies have been conducted in examining the compatibility of model results with in-situ streamflow measurements (Easton *et al.*, 2010; Gao *et al.*, 2010; Grillakis *et al.*, 2010; Halwatura & Najim, 2013; Park & Markus, 2014). Some modelers are of the view that even the use of complex modeling techniques, it does not give better assessment due to soil heterogeneity and climatic changes that play vital roles in the behavior of streamflow.

In Malaysia, several public domain hydrologic models that range from physically-based models, empirical models and conceptual models are in use, including the Hydrologic Modeling System (HEC-HMS), Soil Water Assessment Tool (SWAT), MIKE-SHE, Artificial Neural Network (ANN). Abdulkareem *et al.* (2018) had conducted a study on evaluating the hydrological models used in Malaysia, determine the coverage of the hydrological models in major river basins. The results of the review showed that 65% of the studies conducted used physical-based models, 37% used empirical models while 6% used conceptual models. Of the 65% of physical-based modeling studies, 60% utilized HEC-HMS an open-source model, 20% used SWAT (public domain model), 9% used MIKE-SHE, MIKE 11 and MIKE 22, Info works occupied 7%, and the others occupied 4%. Thus, indicating a preference for open access models in Malaysia. In the case of empirical models, 46% from the total of empirical researches in Malaysia used ANN, 13% used Logistic Regression (LR), while Fuzzy logic, Unit Hydrograph, Auto-regressive integrated moving average (ARIMA) model and support vector machine

(SVM) contributed 8% each, whereas the remaining proportion is occupied by Numerical Weather Prediction (NWP), Land Surface Model (LSM), Frequency Ratio (FR), Decision Tree (DT) and Weight of Evidence (WoE).

2.9 SPP forced hydrological models

SPP estimations are increasingly becoming more applicable in hydrological studies (Alazzy *et al.*, 2017; Bajracharya *et al.*, 2015; Ciabatta *et al.*, 2016; Li *et al.*, 2018; Pakoksung & Takagi, 2016; Tramblay *et al.*, 2016; Wang *et al.*, 2016; Wang *et al.*, 2018; Zulkafli *et al.*, 2014). Maggioni and Massari (2018) reviewed that the intrinsic quality of SPP, the basin size, the SPP resolution, and the choice of the hydrologic model has been shown to impact the error propagation from the precipitation forcing to the output. However, the quantification of these effects had not consented. In some cases, the error is shown to increase with the catchment area (Falck *et al.*, 2015). However, in others, there is no change in the error magnitude was observed as a function of the basin size (Pan *et al.*, 2010). SPP resolution has been shown to play a more important role than the error associated with SPP and its impact on the streamflow simulations strongly depends on the catchment area (Nikolopoulos *et al.*, 2010). Nevertheless, different models show different performances for different SPP suggesting the existence of interconnections between models and their precipitation forcing (Qi *et al.*, 2016).

2.10 Summary

Accurate and reliable precipitation data are the basis for hydro-climatological studies. SPP estimations have provided alternative precipitation data for regions with sparse rain gauge measurements. Despite the continuing great efforts to develop fine resolution SPP, the errors of SPP estimates cannot be removed completely due to the characteristics of the retrieval errors that vary in different climatic regions, seasons, and surface conditions. At the same time, we'd expect to see an increase in extreme flood events, it is crucial for the hydrologists and climatologists to investigate and enhance the available SPP datasets for extreme floods around the world.

CHAPTER 3: EVALUATION OF RAW SATELLITE PRECIPITATION PRODUCTS FOR EXTREME FLOOD EVENTS IN MALAYSIA

3.1 Introduction

This chapter evaluates the three advanced satellite precipitation products (SPP), i.e. CMORPH, TRMM 3B42V7, and PERSIANN against the ground observation to evaluate their performances during the 2014-2015 extreme flood events at three river basins, i.e. Kelantan, Langat and Johor river basin located at the northern, west and south part of Peninsular Malaysia, respectively. As SPP rainfall estimates are continuous and represent areal rainfall whereas gauge observed rainfall is at a particular point in location, therefore comparisons between both datasets are done by converting the point rainfall values into areal using several interpolation techniques. Then, a comparative evaluation of various rainfall interpolation methods used to transform the point-based rain gauge data to areal precipitation was performed. The purpose of this evaluation is to find out the most suitable method for the rain gauge observations to compare with the grid-based satellite estimations. Moreover, this study presents the rain detection and capturing storm ability of every SPP over three river basins.

3.2 Review on Previous SPP Studies

Numerous studies on evaluating the performance of weather satellites which have been done varies with location, season, topography, climatology, and so on (Dinku *et al.*, 2008; Jiang *et al.*, 2016; Luo *et al.*, 2017; Moazami *et al.*, 2013; Tan *et al.*, 2015). In Malaysia, Varikoden *et al.* (2010) and Semire *et al.* (2012) evaluated the TRMM 3B42V6 daily and monthly data, respectively, and found that 3B42V6 performed well over Malaysia with about 15% error bias at monthly scale. Later then, Tan *et al.* (2015) found that CMORPH, TRMM, and PERSIANN satellite products performed better in the northeast monsoon compared to the southwest monsoon. These products also showed better performances occurred in eastern and southern Peninsular Malaysia (Kelantan, Terengganu, Pahang and Johor) and in the north of East Malaysia (Sabah), which receives higher rainfall during the northeast monsoon, whereas poor performances occurred in the western and dryer Peninsular Malaysia.

In China, Xue *et al.* (2013) evaluated two versions of TRMM 3B42 (V6 and V7) products in the mountainous Wangchu Basin of Bhutan using rain gauge data. The results showed that TRMM 3B42V7 product had a significant upgrade from the 3B42V6 product in precipitation accuracy and can serve as input to distributed hydrological modeling in that study area. Jiang *et al.* (2012) evaluated the performance of near real-time satellite products, i.e. CMORPH and two models of TMPA satellite – 3B42V6 and 3B42RT from the year 2003 to 2008 (6 years) in the Mishui Basin in South China. They found that the 3B42V6 satellite underestimated the rainfall precipitation of about 4 %, while the other two underestimated largely of about 40%. Later, Jiang *et al.* (2016) evaluated the latest version of TRMM 3B42V7 with CMORPH over 12 years starting from the year 2000 – 2011 in two different latitude basins of China and found that both satellite products overestimated precipitation over the high-latitude Laoha river basin and underestimated for the low latitude Mishui Basin. Chen *et al.* (2014) evaluated the performance of CMORPH and PERSIANN products during flood events in Beijing, China in July 2012. The results showed that both CMORPH and PERSIANN were not comparable to the dense rain gauge observations. CMORPH overestimated the daily accumulated rainfall whereas PERSIANN underestimated the daily accumulated rainfall.

Gottschalck *et al.* (2005) evaluated the performance of PERSIANN and TRMM 3B42RT over the Continental United States (CONUS) and found that both PERSIANN and 3B42RT overestimated precipitation over the central CONUS and western mountains during the spring and summer. However, during the fall and winter months, PERSIANN underestimated precipitation in the western mountains and 3B42RT overestimated it. Later on, Tian and Peters-Lidard (2007) furthered the work by evaluating CMORPH over the CONUS and found that there was an underestimation over the northeast during the summer months, but a severe overestimation over the central CONUS and mountain west during the summer and spring months.

Some researchers evaluated the performance of SPP by point to pixel comparison (Bajracharya *et al.*, 2015; Ghaju & Alfredsen, 2012; Hughes, 2006) and some of that compared in terms of mean areal precipitation by implementing rainfall interpolation method. None of the researchers thus far did an evaluation on which interpolation method is the best to be compared with the grid-based satellite estimations. Most of the researchers used the inverse distance weighting (IDW) technique to interpolate the rain gauge data and evaluated the performance of TRMM 3B42 by direct comparison of the mean rainfall (Collischonn *et al.*, 2008; Tan *et al.*, 2015; Tuo *et al.*, 2016). Liu *et al.* (2012, 2015) used the Thiessen Polygon method to convert the point-based rain gauge observations into areal precipitation. Akbari *et al.* (2011) used the Kriging method on the existing gauge network to explain the storm pattern over Klang watershed and to compare with TRMM rainfall estimation.

3.3 Description of the study area

This study focuses on a huge tragedy of flood that happened at the end of 2014. This extreme flood event hit certain countries such as Indonesia, Malaysia, Thailand and the Philippines where heavy rains fall due to the southeast monsoon blowing across the South China Sea, making the sea warmer than usual. In Malaysia, extreme floods that occurred on 15 December 2014 – 3 January 2015 have been considered as the worst flood events in decade. During this event, most of the rivers in Kelantan, Pahang, Perak, and

Terengganu had reached dangerous levels. More than 200,000 people were affected and 21 people were killed due to this natural disaster (Akasah & Doraisamy, 2015). In this study, three river basins are chosen mainly based on their history of great flood, varies in basin size and different geographic location. As shown by Figure 3.1, Kelantan, Langat, and Johor river basins are located at the northern, western and southern parts of Peninsular Malaysia, respectively. Further explanation of these study areas is discussed in the following section.

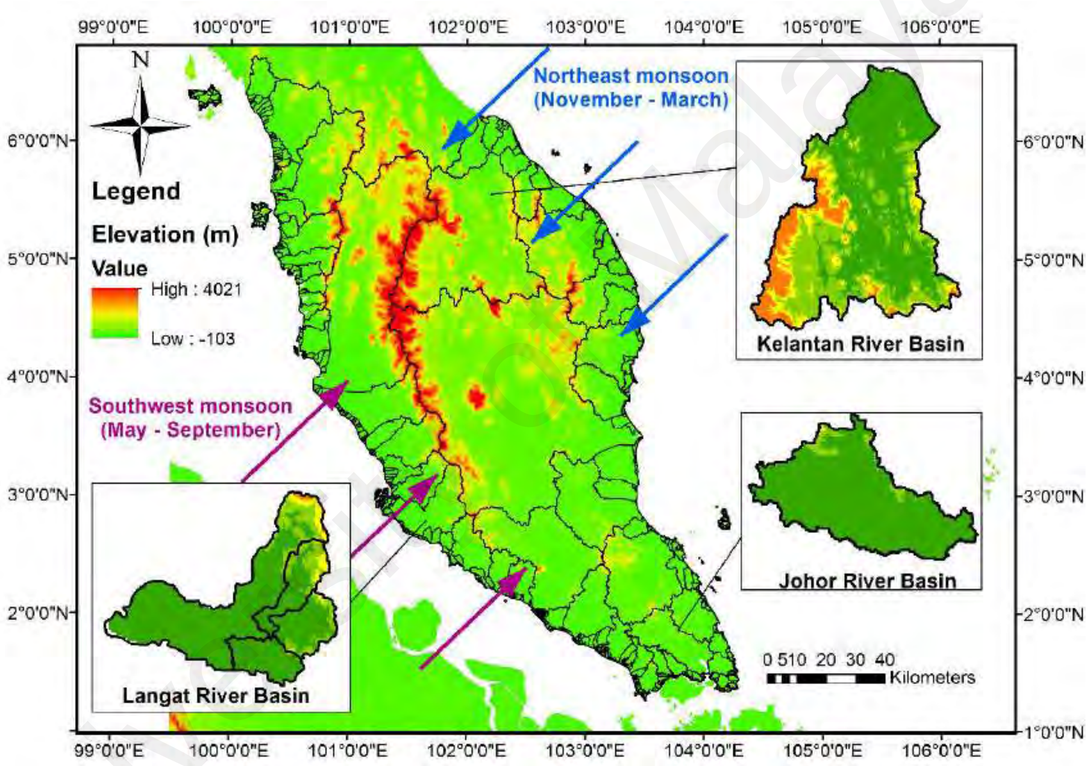

Figure 3.1: Location of the study areas.

3.3.1 Langat river basin

Langat river basin covers the state of Selangor and Negeri Sembilan and also a portion of the Federal Territory of Putrajaya, Kuala Lumpur, and Klang, and Petaling Jaya district. The basin has a total catchment area of about 2,350 km^2. The larger part of the basin totaling 1,900 km^2 occupies the south and south-eastern parts of the state of

Selangor. The basin is located between latitudes 1°30′–2°10′N and longitudes 103°20′–104°10′E. There are three major tributaries, i.e. Langat River (is the main river), Semenyih River and Labu River. The Langat River, has a total length of about 180 km, draining from the main range (Banjaran Titiwangsa) at the Northeast of Hulu Langat District in south-southwest direction into the Straits of Malacca. Both Langat River and Semenyih River originate from the hilly and forested areas in the western slope of Banjaran Titiwangsa, northeast of Hulu Langat. This water catchment is important as it provides raw water supply and other amenities to approximately 1.2 million people within the basin. Important conurbations served include towns such as Cheras, Kajang, Bangi, Government Centre of Putrajaya and others. There are two reservoirs (Semenyih and Hulu Langat) and 8 water treatment plants (4 of which operate 24 hours), which provide clean water to the users after undergoing treatment. In terms of climate, high rainfall and high humidity occur at various periods throughout the year. The mean areal annual rainfall of this basin is 1994.1 mm. The highest recorded monthly rainfall was about 327.1 mm occurred in November (i.e. during the northeast monsoon) while the lowest was 97.6 mm in June (i.e. during the southwest monsoon).

3.3.2 Kelantan river basin

Kelantan river basin is one of the major basins in Malaysia which is located at the North-Eastern part of Peninsular Malaysia at latitudes 4° 40' N to 6° 12' N and longitude 101° 20' E to 102° 20' E. The maximum length and breadth of the catchment are 150 km and 140 km, respectively. The river is about 248 km long and drains an area of 13,100 km^2, occupying more than 85% of the State of Kelantan. The basin has an annual rainfall of about 2,500 mm much of which occurs during the North-East Monsoon between mid-October and mid-January. The mean annual temperature at Kota Bharu is 27.5 °C with a mean relative humidity of 81%. The mean flow of the Kelantan River measured at

Guillemard Bridge (5.76° N, 102.15° E) is 557.5 m^3/s. The entire basin contains large areas of tropical forested mountains, lowland forest, and limestone hills. Currently, there are many activities involving land-use changes from lowland forest to vegetation and urban area. In terms of climate, southwest and northeast monsoons hit Peninsular Malaysia annually (Sow *et al.*, 2011; Tangang *et al.*, 2007). The northeastern monsoon produced heavy rains and thunderstorms between November and March. From May to September, another inter-monsoon comes from the southwest and hits places like Kelantan, bringing the most rainfall to the study area. During the 2014-2015 flood events, Kelantan was the most seriously affected state that had the most evacuees with more than 20,000 people (Akasah & Doraisamy, 2015).

3.3.3 Johor river basin

Johor river basin is located at the southern part of Peninsular Malaysia with the latitudes ranging from 1°30′–2°10′N and longitudes 103°20′–104°10′E. The catchment covers four districts of Johor State: Kota Tinggi, Kluang, Kulai Jaya, and Johor Bahru. It has a surface area of about 1,652 km^2. The main river, Johor River is 122.7 km long and originates from Gunung Belumut (the second-highest mountain in Johor) in the north of the basin. The river flows in a north-south direction and then southwest into the Strait of Johor. This basin is covered mostly by rubber and oil plant plantation. This catchment has an average annual rainfall of 2500 mm. Like the Kelantan river basin, the climate in the Johor river basin is a tropical monsoon climate, divided into the northeast monsoon (November–February), and the southwest monsoon (May-August) (Sow *et al.*, 2011; Tangang *et al.*, 2007). Flooding events frequently occur in December where the highest rainfall and peak streamflow are recorded.

3.4 Data Acquisition

3.4.1 Rain gauge network

The daily rainfall data starting from 1st December 2014 until 31st January 2015 (62 days) were acquired from the 50 operating rain gauge stations in the Kelantan river basin, 28 stations in Langat river basin and 18 stations in Johor river basin. All data were collected from the DID. The list of stations with detailed information including station name, district, river, latitude, and longitude for those three river basins is attached in Appendix A. Figure 3.2 shows the distribution of rain gauge network for all three river basins. For Langat river basin, as shown in Figure 3.2(a), more stations are concentrated at latitudes 3°00′–3°15′N and longitudes 101°45′–102°00′E, but fewer active stations were found at the south-eastern portion of the basin. For the Kelantan river basin, as shown in Figure 3.2(b), most of the rain gauge stations are installed at lower elevations in the northern portion of the basin, only a few stations are found at the southeastern portion of the basin. Not many rain gauge stations are active during the selected event in Johor River Basin, in fact, some grids are found with only one station, as shown in Figure 3.2(c).

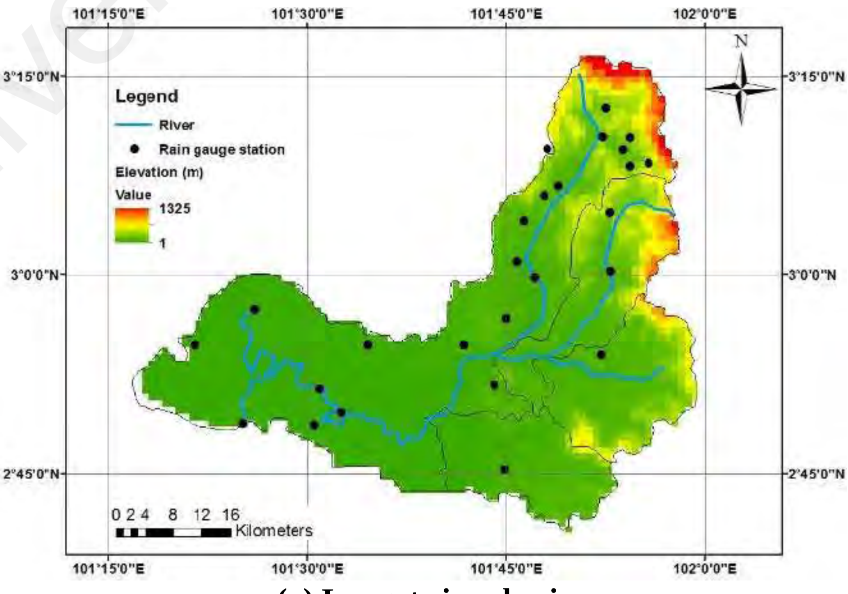

(a) Langat river basin

Figure 3.2: Distribution of rain gauge stations in (a) Langat, (b)Kelantan and (c) Johor river basin.

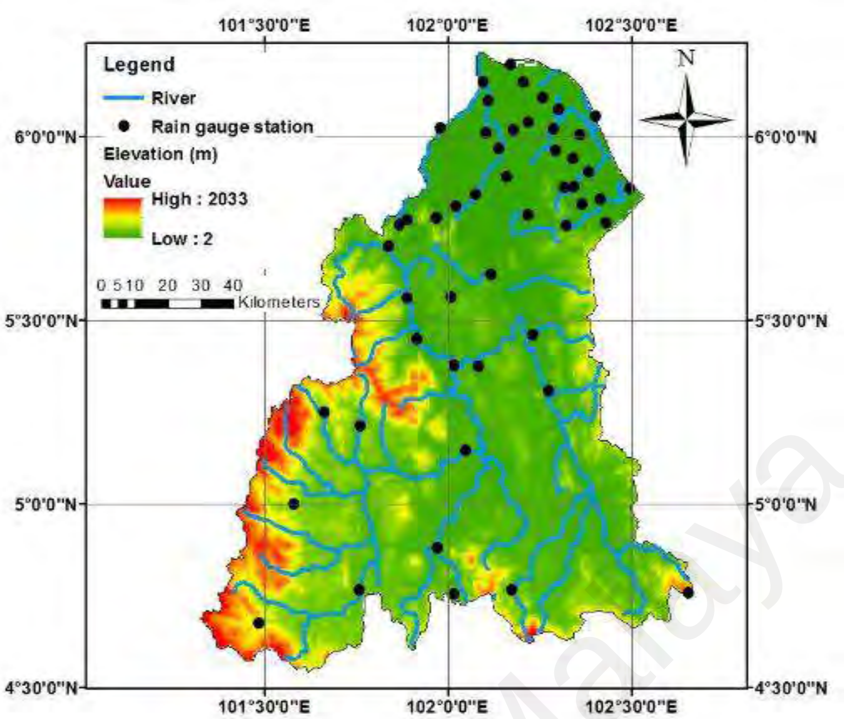

(b) Kelantan river basin

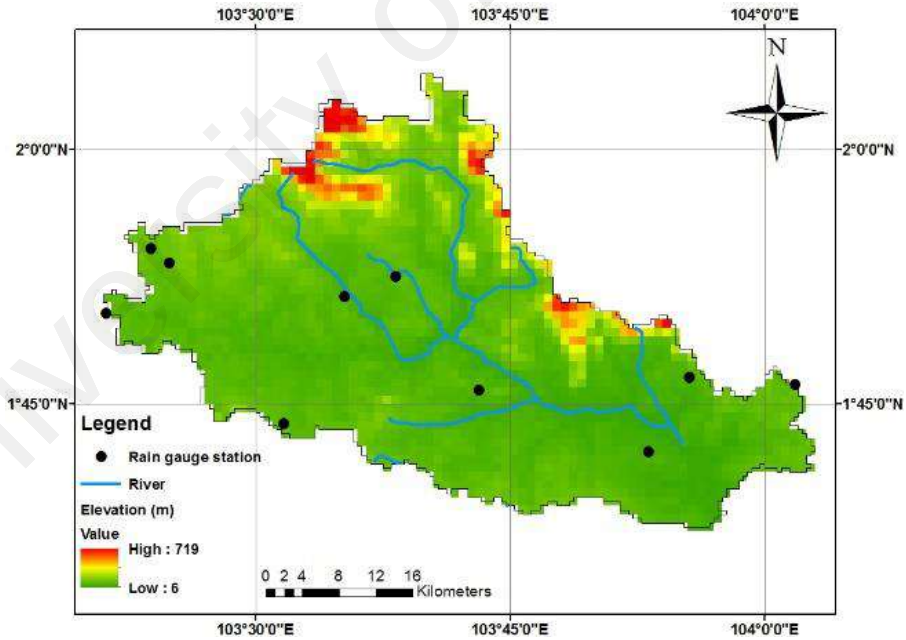

(c) Johor river basin

Figure 3.2, continued

3.4.2 Satellite rainfall estimations

Three satellite-derived rainfall products chosen for this study, i.e. TRMM 3B42 V7, CMORPH, and PERSIANN. The selected resolution for each satellite product is summarized in Table 3.1.

Table 3.1: Information about satellite precipitation products (SPP)

Satellite Products	Spatial Resolution	Temporal Resolution	Spatial Coverage	Data Source
TRMM	0.25°	Daily	50°N – 50°S	http://mirador.gsfc.nasa.gov
CMORPH	0.25°	Daily	60°N – 60°S	ftp://ftp.cpc.ncep.noaa.gov/precip/global_CMORPH
PERSIANN	0.25°	Daily	60°N – 60°S	http://www.ngdc.noaa.gov/

The Tropical Rainfall Measuring Mission (TRMM) is NASA's first mission dedicated to observing and understanding the tropical rainfall and how this rainfall affects the global climate. It is a joint mission with the Japan Aerospace Exploration Agency (JAXA). This product is a combined microwave-infrared precipitation product (Huffman *et al.*, 2007), providing precipitation for the spatial coverage of 50°N – 50°S at the latitude-longitude resolution. The primary instruments for measuring precipitation are the Precipitation Radar (PR), the TRMM Microwave Imager (TMI), and the Visible and Infrared Scanner (VIRS). Additionally, TRMM will carry the Lightning Imaging Sensor (LIS) and the Clouds and the Earth's Radiant Energy System (CERES) instrument. These instruments can function individually or in combination with one another. The latest version of this product, 3B42V7, can be freely downloaded from Goddard Earth Sciences Data and Information Services Centre (http://mirador.gsfc.nasa.gov). In this study, the daily aggregated TRMM 3B42V7 observations at the spatial resolution of 0.25° were analyzed.

The National Oceanic and Atmospheric Administration's (NOAA) Climate Prediction Center (CPC) morphing technique (CMORPH) (Joyce *et al.*, 2004) was available since December 2002 at various spatial and temporal resolutions (e.g. 8 x 8 km^2, 0.25° x 0.25° ; 30 min, 3 hourly, and daily) for regions that are situated between 60° N and 60° S. Due to its near-real-time availability and high temporal and spatial resolution, this satellite product was useful in any hydrologic and water resources application (Habib *et al.*, 2012). This satellite product combines various passive microwave (PMW) rain estimates such as TRMM Microwave Imager (TMI), Special Sensor Microwave Imager (SSM/I), Advanced Microwave Sounding Unit (AMSU), and Advanced Microwave Scanning Radiometer for Earth Observing System (AMSR-E), but calibrates against TMI values (Sohn *et al.*, 2010). However, due to insufficient global coverage by microwave measurements at a 30 minutes time scale only, vast areas may have gaps where PMW estimates are not available. To fill these gaps, microwave-based rainfall values are interpolated with time according to the propagation of cloud systems obtained from geostationary infrared (IR) based motion vectors (Joyce *et al.*, 2004). In the latest CMORPH Version 1.0, bias correction was conducted by adjusting the satellite estimates against a daily rain gauge analysis and can be accessed from the ftp: (ftp.cpc.ncep.noaa.gov/precip/global_CMORPH). Three spatial and temporal resolutions can be selected: 8 km-30 min, 0.25°-3 hourly, and 0.25°-daily. In this study, the 0.25°-daily bias-corrected Version 1.0 CMORPH data were used.

Precipitation Estimation from Remotely Sensed Information using Artificial Neural Networks (PERSIANN) (Hsu *et al.*, 1997; Sorooshian *et al.*, 2000) was an automated system developed for the estimation of rainfall from geosynchronous satellite longwave infrared imagery (GOES-IR). This product can provide precipitation data for the spatial coverage of 60°N – 60°S. In this study, the bias-corrected PERSIANN data, which maintains the total monthly precipitation estimation with GPCP at the spatial resolution of 0.25° and daily temporal resolution were downloaded from the following website (http://www.ngdc.noaa.gov/).

3.5 Methods

3.5.1 Interpolation of rain gauge precipitation

Rain gauge measurement is considered as a point precipitation measurement and it cannot represent the volume of precipitation falling over a given catchment area. Therefore, dense rain gauges with spatially distributed are crucial as true representative precipitation of the area. However, often a very dense rain gauge with spatially distributed is practically difficult to find in most countries. When a limited number of rain gauge is compared to the satellite products, point-to-grid precipitation is insufficient for the large variability of rain gauge associated with the spatial and temporal resolution of satellite products. Therefore, conversion to a gridded surface from rain gauge data at the same resolution of the satellite data by the interpolation method is applied to overcome the large variability issue (Lo Conti *et al.*, 2014). As a result, a comparative evaluation of a set of interpolation methods was performed in this study for all river basins using the Geographical Information System (GIS) platform. Given a limited number of rain gauges stations by DID, several interpolation methods chosen were Arithmetic Mean (AM) (Anctil *et al.*, 2006; Creutin & Obled, 1982; Shaw & Lynn, 1972), Thiessen Polygon (TP) (Thiessen, 1911), Inverse Distance Weighting (IDW) (Di Piazza *et al.*, 2011; Ly *et al.*, 2011; Ly *et al.*, 2013; Wagner *et al.*, 2012), Ordinary Kriging (OK) (Buytaert *et al.*, 2006; Zhang & Srinivasan, 2009) and Spline (SP) (Franke, 1982; Hutchinson, 1995; Mitáš & Mitášová, 1988; Tait *et al.*, 2006). Details of each interpolation are described below.

3.5.1.1 Arithmetic Mean (AM)

This method consists of computing the arithmetic average of the values of the precipitation for all stations within the area. Since this method assigns equal weight to all stations irrespective of their relative location and other factors, it should be adopted in area where rainfall is uniformly distributed. The average precipitation of the basin is computed using Equation (3.1)

$$\bar{P} = \frac{\sum_{i=1}^{n} P}{n} \tag{3.1}$$

where average precipitation is over an area, P is the precipitations at individual station i, and n is the number of stations.

3.5.1.2 Thiessen Polygon (TP)

Thiessen polygon is also a simple and straight forward technique that was introduced to estimate equivalent uniform depth (Thiessen, 1911). This technique assumes that an average value over the same area of a Thiessen polygon is taken to be equivalent to the point value located at the centroid of this polygon. For every basin, encompassing n Thiessen polygons, the areal rainfall over the basin (P_T) is computed from

$$P_T = \sum_{i=1}^{n} T_i P_i \tag{3.2}$$

where P_i is the observed rainfall at the centroid of the ith polygon, and the weighting factor T_i is given by

$$T_i = \frac{A_i}{A_T} \tag{3.3}$$

where A_T is the total area of the basin, and A_i is the area defined by the intersection of the Thiessen polygon and the basin boundary. The Thiessen polygon technique is suitable for application over relatively flat and expansive areas. However, this technique assumes that precipitation varies linearly between stations and is therefore unsuitable for use in mountainous regions which have an effect on the precipitation amount.

3.5.1.3 Inverse Distance Weighting (IDW)

IDW assigns weights to neighboring observed values based on the distance to the interpolation location and the interpolated value is the weighted average of the observations. In standard IDW, the interpolated value is estimated by a weighted mean of the observations and the weights are proportional to a negative power of geographical distances d_i between the point of interpolation and the considered observation points. Typically, not all observations P_i are considered in the estimation of the interpolating value P_0 but only n neighboring with

$$P_0 = \frac{\sum_{i=1}^{n} P_i \omega_i}{\sum_{i=1}^{n} \omega_i} \tag{3.4}$$

and the weights

$$\omega_i = \frac{1}{d_i^{\lambda}} \tag{3.5}$$

The power λ of distance has to be chosen appropriately depending on the interpolated variable. Spatially smoother variables show larger spatial dependence and thus like smaller values of λ than spatially rougher fields. Generally, it is assumed that the separation of close-by observations increases faster than linear with station distance and often a power λ of two (2) is assumed.

3.5.1.4 Kriging

Kriging assumes that the distance or direction between sample points reflects a spatial correlation that can be used to explain variation in the surface. The Kriging tool fits a mathematical function to a specified number of points, or all points within a specified radius, to determine the output value for each location. Like IDW, it weights the surrounding measured values to derive a prediction for an unmeasured location. The general formula for both interpolators is formed as a weighted sum of the data:

$$\hat{Z}(s_0) = \sum_{i=1}^{n} \lambda_i Z(s_i) \tag{3.6}$$

where $Z(s_i)$ is the measured value at the *i*th location, λ_i is an unknown weight for the measured value at the *i*th location, s_0 is the prediction location and *n* = the number of measured values.

However, the weights λ_i in the kriging method are based not only on the distance between the measured points and the prediction location but also on the overall spatial arrangement of the measured points. To use the spatial arrangement in the weights, the spatial autocorrelation must be quantified. Thus, in ordinary kriging, the weight, λ_i, depends on a fitted model to the measured points, the distance to the prediction location, and the spatial relationships among the measured values around the prediction location.

3.5.1.5 Spline

The Spline tool uses an interpolation method that estimates values using a mathematical function that minimizes overall surface curvature, resulting in a smooth surface that passes exactly through the input points.

The algorithm used for the Spline tool uses the following formula for the surface interpolation:

$$S(x,y) = T(x,y) + \sum_{i=1}^{n} \lambda_i R(r_i) \quad (3.7)$$

where i is the index of point, n is the total number of points, λ_i are coefficients found by the solution of a system of linear equations, r_i is the distance from the point (x,y) to the ith point. $T(x,y)$ and $R(r)$ are defined differently, depending on the type of spline.

There are two Spline types: Regularized and Tension. The Regularized type creates a smooth, gradually changing surface with values that may lie outside the sample data range. The Tension-type controls the stiffness of the surface according to the character of the modeled phenomenon. It creates a less smooth surface with values more closely constrained by the sample data range. In this study, the Regularized option was used in this analysis. Therefore, $T(x,y)$ and $R(r)$ are computed using Equation (3.8) and (3.9) respectively.

$$T(x,y) = \ a_1 + a_2 x + a_3 y \quad (3.8)$$

where a_i are coefficients found by the solution of a system of the linear equation.

$$R(r) = \frac{1}{2\pi} \left\{ \frac{r^2}{4} \left[\ln\left(\frac{r}{2\tau}\right) + c - 1 \right] + \tau^2 \left[K_0\left(\frac{r}{\tau}\right) + c + \ln\left(\frac{r}{2\pi}\right) \right] \right\} \quad (3.9)$$

where r is the distance between the point and the sample, τ^2 is the weight parameter, K_0 is the modified Bessel function and c is a constant equal to 0.577215.

3.5.2 Evaluation indexes

The performance of satellite precipitation products with respect to rain gauge datasets was assessed based on a specific set of widely applied criteria in this field. Evaluation criteria used in this study comprises of quantitative and categorical indexes of which representing precipitation values and precipitation occurrences, respectively.

3.5.2.1 Quantitative evaluation indexes

There are six quantitative evaluations used in this study to measure the differences between the satellite products and rain gauge datasets. These quantitative evaluations are the coefficient of determination (R^2), coefficient of Pearson Correlation (CC), bias, mean absolute error (MAE), root mean square error ($RMSE$) and normalized root mean square error ($NRMSE$). CC explains the relationship between the actual values of two variables (independent and dependent) while R^2 measures how well the independent variable explains the dependent variable in a regression. Both values range between 0 (no correlation) to 1 (perfect correlation). The percentage bias ($PBias$) describes the degree to which the observed value is overestimated or underestimated. The mean absolute error (MAE) represents the average magnitude of the error. $RMSE$ indicates how closely the satellite observation predicts the measured values and $NRMSE$ evaluates the reliability of SPP. Equations (3.10) to (3.15) show the aforementioned quantitative evaluations.

$$R^2 = 1 - \frac{\sum_{i=1}^{n}(S_i - G_i)^2}{\sum_{i=1}^{n}(G_i - \bar{G})^2} \tag{3.10}$$

$$CC = \frac{\sum_{i=1}^{n}(G_i - \bar{G})(S_i - \bar{S})}{\sqrt{\sum_{i=1}^{n}(G_i - \bar{G})^2}\sqrt{\sum_{i=1}^{n}(S_i - \bar{S})^2}} \tag{3.11}$$

$$PBias = \left(\frac{\sum_{i=1}^{n} S_i}{\sum_{i=1}^{n} G_i} - 1\right) \times 100\% \tag{3.12}$$

$$MAE = \frac{\sum_{i=1}^{n}|S_i - G_i|}{n} \tag{3.13}$$

$$RMSE = \sqrt{\frac{\sum_{i=1}^{n}(S_i - G_i)^2}{n}} \tag{3.14}$$

$$NRMSE = \frac{RMSE}{\bar{G}} \tag{3.15}$$

where *S* and *G* represents satellite/gridded and gauge precipitation, respectively, and *n* is the total number of measurements, *i* is the index of data, $\bar{S}$ is the average value of S_i and $\bar{G}$ is the average value of G_i.

3.5.2.2 Categorical evaluation indexes

In order to assess the rainfall detection and capturing storm capabilities, five categorical evaluation indexes including the accuracy (*ACC*), probability of detection (*POD*), false alarm ratio (*FAR*), critical success index (*CSI*) and Heidke Skill Score (*HSS*) were accessed to discriminate between rain/no-rain events (days).

ACC represents the level of agreement between the satellite estimate and the rain gauge precipitation data. *POD* measures how well SPP correctly detected rainfall for all the actual occurrences of rainfall detected by the rain gauges. *FAR* measures how often SPP detected rainfall when actually there was no rainfall. *CSI* measures the fraction of a gauge's precipitation that was correctly detected by the SPP. *HSS* measures the fraction of correct SPP estimates without considering random matches. The equations used to calculate these quantities have all been given by Mashingia *et al.* (2014). Equations (3.16) to (3.20) below show the formulas of the aforementioned categorical statistics. The quantities *A*, *B*, *C*, and *D* are computed based on the contingency table (Table 3.2) where *A* represents hits (event forecast to occur, and did occur); *B* represents false alarm (event forecast to occur, but did not occur); *C* means misses (event forecast not to occur, but did occur); *D* is known as correct negative (event forecast not to occur, and did not occur) and n is the sum of *A*, *B*, *C*, and *D*.

Accuracy, $ACC = \frac{A+D}{n}$ (3.16)

Hit Rate/ Probability of detection, $POD = \frac{A}{A+C}$ (3.17)

False Alarm Ratio, $FAR = \frac{B}{A+B}$ (3.18)

Critical Success Index, $CSI = \frac{A}{A+B+C}$ (3.19)

Heidke Skill Score, $HSS = \frac{2(A \cdot D - B \cdot C)}{(A+C) \cdot (C+D) + (A+B) \cdot (B+D)}$ (3.20)

Table 3.2: Contingency table for comparing gauge and satellite precipitation estimate

	Gauge ≥ Threshold	Gauge < Threshold
Satellite ≥ threshold	*A*	*B*
Satellite < threshold	*C*	*D*

ACC, *POD*, *FAR*, and *CSI* range from 0 to 1, with 1 being the perfect score for *ACC*, *POD*, and *CSI* and 0 being the perfect score for *FAR*. The *HSS* ranges from −∞ to 1, with 1 being a perfect score, 0 means no skill, negative HSS indicates that the forecast is worse than the gauge observation.

3.6 Results and Discussions

3.6.1 Evaluation of various interpolation methods for rain gauge observations

During the extreme floods, the highest amount of rain over the Kelantan river basin is observed on 17th December 2014 as 205.72 mm/day. On the other hand, for the Langat river basin and Johor river basin, the highest total amount of rainfall over the basin are 37.45 mm/day on 22nd December 2014 and 49.31 mm/day on 25th December 2014, respectively. From this rainfall data, we can observe the highest rainfall pattern that hit these three basins in response to time. As the northeast monsoon season brings in rainfall from the north towards the western and southern, thus the first hit is on the 17th (Kelantan) followed by 22nd (Langat) and 25th (Johor). This rainfall pattern seems to follow the northeast season circulation.

The analysis begins with the result from several interpolation methods such as Arithmetic mean (AM), Thiessen polygon (TP), inverse distance weighting (IDW), ordinary kriging (OK) and spline performed on rain gauge daily precipitation to produce mean areal precipitation. The purpose of this interpolation is to examine the accuracy of spatial interpolation output when various interpolation methods are performed. Generally, this study found that the trend between five interpolation methods in computing the mean areal precipitation is almost similar for every basin. All interpolation methods performed based on rain gauge data exhibit somewhat a similar pattern with values are quite close across all the methods even though the result shown by the Kelantan river basin for the highest rainfall performed by an average method is a bit different from other methods, as shown in Table 3.3.

Table 3.3: Highest areal rainfall of each interpolation method during 2014-2015 flood events.

River Basin	Highest Areal Rainfall of the Flood Events (mm/day)				
	AM	**TP**	**IDW**	**OK**	**SP**
Kelantan	202.46	105.63	109.05	105.32	109.12
Langat	37.45	36.22	38.98	37.46	36.21
Johor	49.31	43.29	47.65	43.92	33.34

For each basin, four representative examples (TP, IDW, OK, and SP) of 248 precipitation maps created are shown in Figure 3.3 (Kelantan river basin), Figure 3.4 (Langat river basin) and Figure 3.5 (Johor river basin). These precipitation maps are from the peak (highest rainfall) of the flood events. AM is not shown as the mean precipitation computed represents the whole basin. The precipitation map for the Kelantan river basin shown in Figure 3.3 appears to be related to the geographic location of the area whereby the higher precipitation values (280 – 350 mm/day) in the northern zone is due to direct exposure to the South China Sea. For the Langat river basin (Figure 3.4), higher precipitation values (75 – 90 mm/day) are found at the south-western part of the basin which is in the low elevation area and very near to the sea. Higher precipitation values (50 – 110 mm/day) are found in the north-western part of the Johor river basin (Figure 3.5).

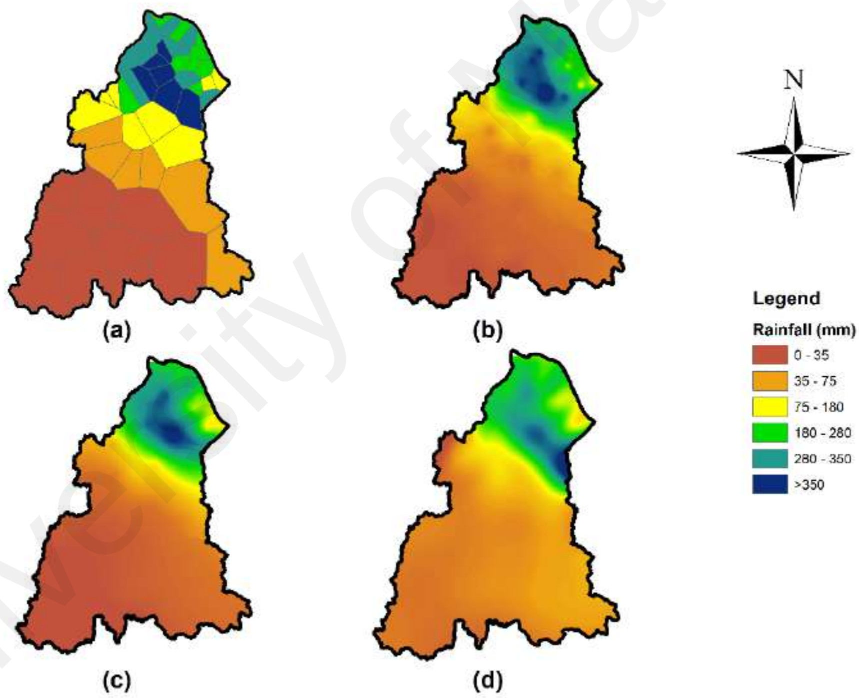

Figure 3.3: Results of interpolation methods for daily mean precipitation of the Kelantan river basin on 17th December 2014. (a) TP; (b) IDW (c) OK; (d) SP

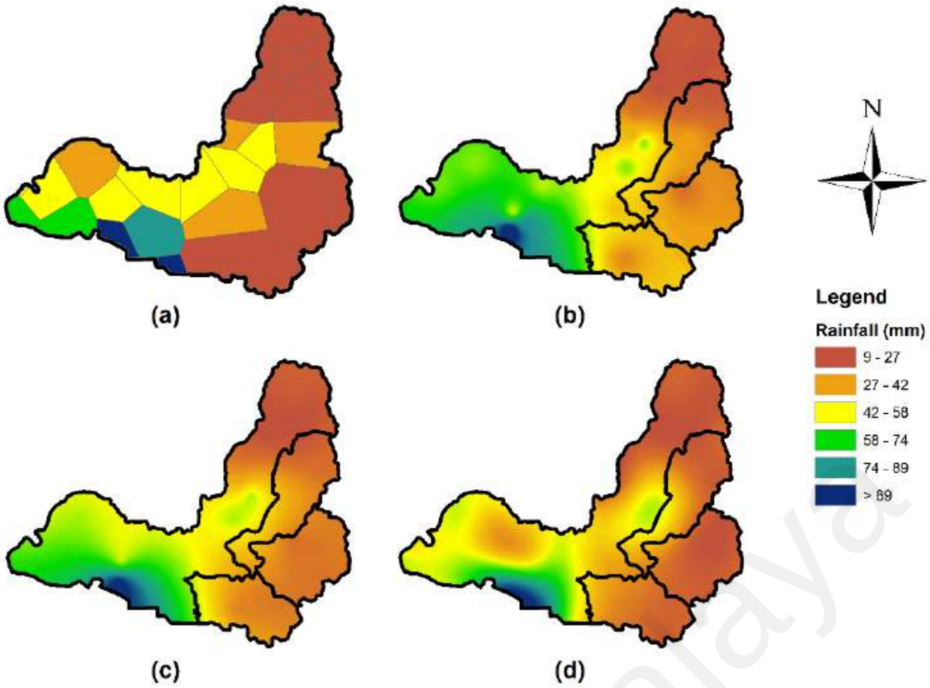

Figure 3.4: Results of interpolation methods for daily mean precipitation of the Langat river basin on 22nd December 2014. (a) TP; (b) IDW (c) OK; (d) SP

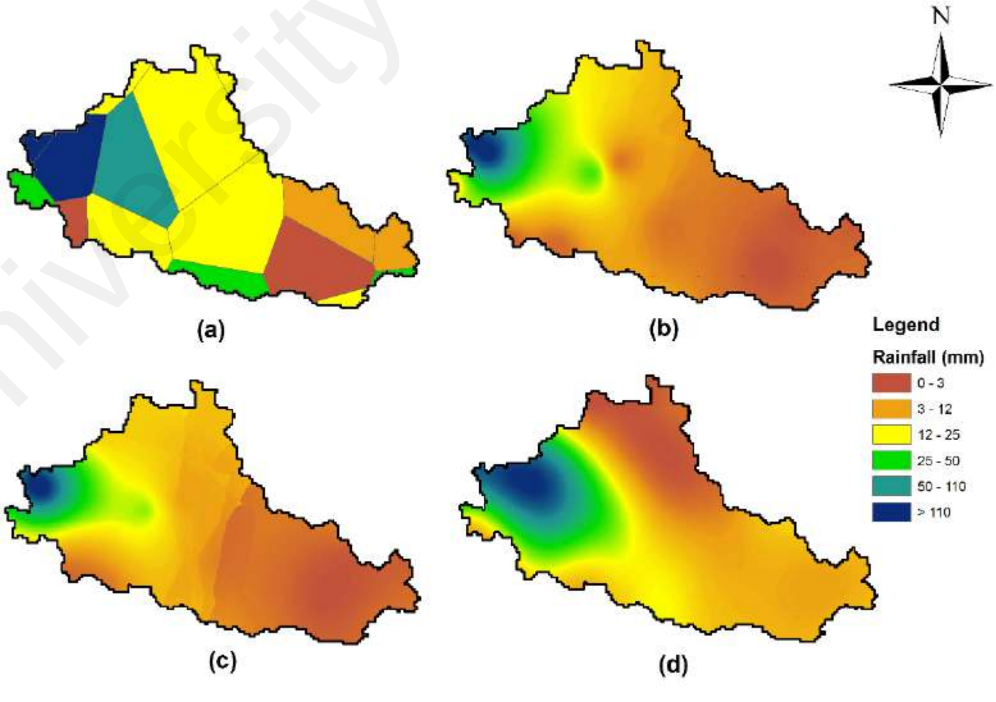

Figure 3.5: Results of interpolation methods for daily mean precipitation of the Johor river basin on 25th December 2014. (a) TP; (b) IDW (c) OK; (d) SP

3.6.2 Evaluation of SPP against interpolated rain gauge observations

In addition to the spatial representation of different interpolation methods, a comparison between all interpolation methods against satellite products is performed by observing their daily temporal data. Figure 3.6 – Figure 3.8 show daily temporal precipitation between the interpolated ground observations (i.e. AM, TP, IDW, OK and SP) and (a) CMORPH, (b) TRMM and (c) PERSIANN satellite observations for the 2014-2015 flood events at Langat, Kelantan and Johor river basin, respectively.

For the Kelantan river basin, the first and second highest rainfall occurs on the 16th and 22nd December 2014 given by all interpolation methods except the average method that reaches nearly between 150 – 200 mm/day. By comparing all five interpolation methods to the SPP (Figure 3.6), it is found that TRMM and CMORPH demonstrate the best performance as both of them capture the 16th December event quite comparable to the interpolation methods with the exception of the average method. Conversely, the amount of rainfall given by PERSIANN is slightly lower, i.e. less than 50 mm/day which implies the PERSIANN satellite is performed poorly for the Kelantan region. For the Langat river basin (Figure 3.7), all interpolation methods show somewhat good agreement, especially for the average method. A high rainfall value for Langat is found to occur three times, i.e. 20th December 2014, 22nd December 2014 and 8th January 2015 with the value between 30 – 40 mm/day. As in Kelantan, the SPP result for Langat exhibits the CMORPH and TRMM outperform the PERSIANN. This graphical result also shows that the TRMM is overestimated. The interpolation methods perform on the Johor river basin show that all methods produce a comparable result and the highest rainfall (30-50 mm/day) occurred on the 26th December 2014 (Figure 3.8). The 30 mm/day rainfall is observed from the average method. The SPP result seems not to be able to capture this event for the Johor river basin as none of them can correctly measure the highest rainfall.

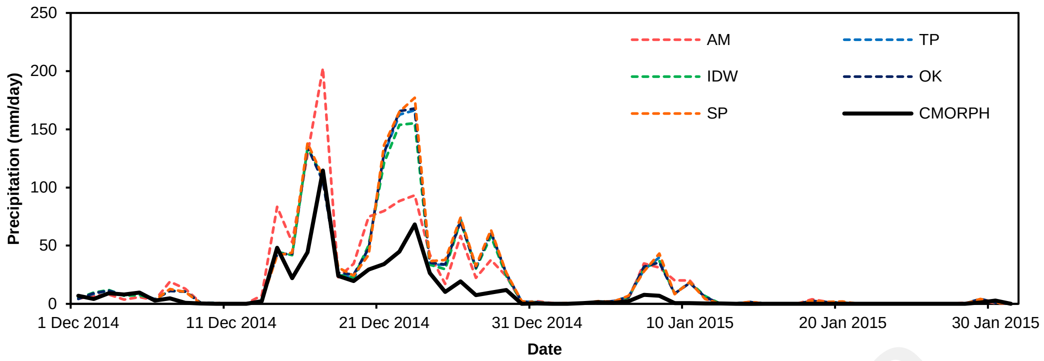

(a)

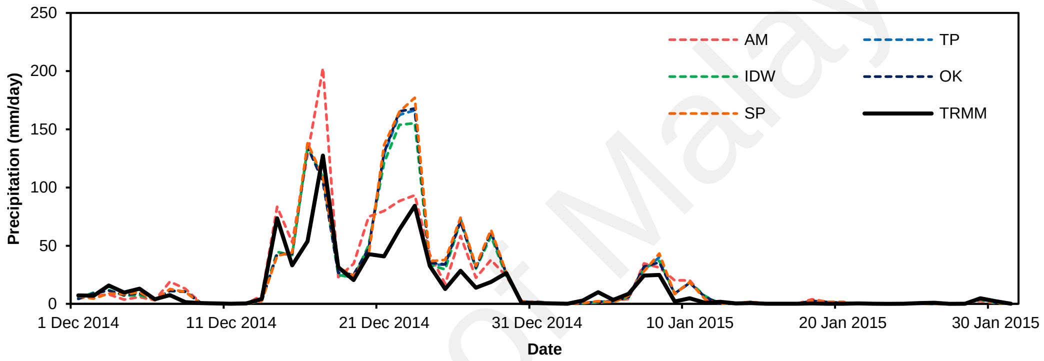

(b)

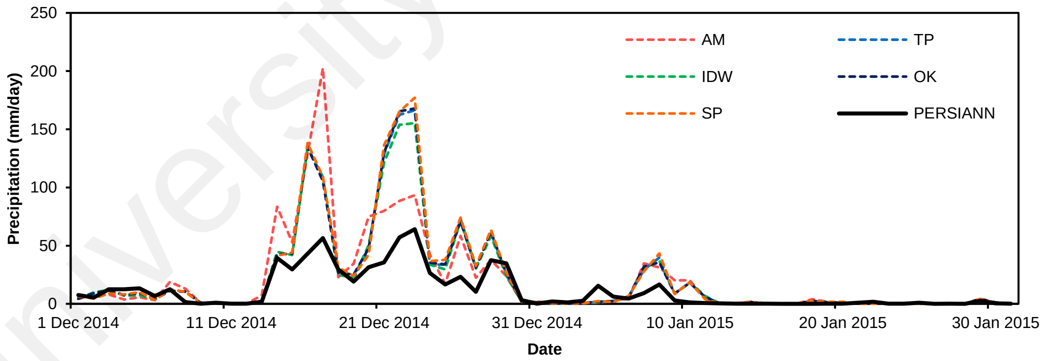

(c)

Figure 3.6: Comparison of daily mean precipitation series between interpolated ground observations and (a) CMORPH, (b) TRMM and (c) PERSIANN satellite observations for the 2014-2015 flood events at Kelantan river basin.

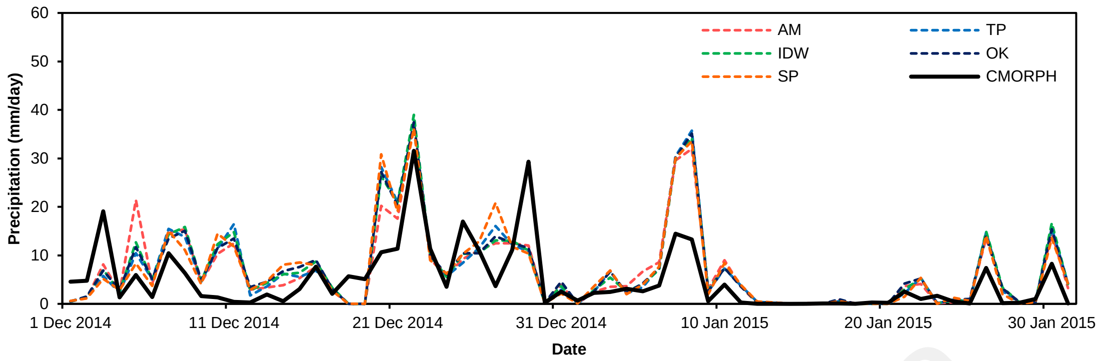

(a)

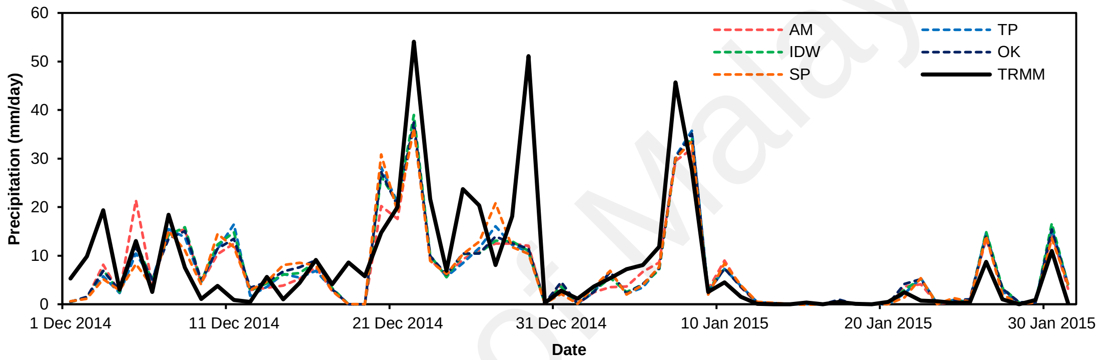

(b)

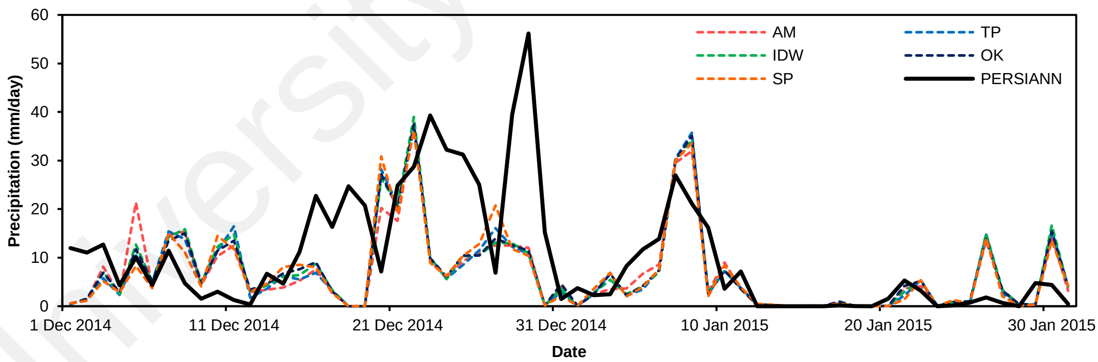

(c)

Figure 3.7: Comparison of daily mean precipitation series between interpolated ground observations and (a) CMORPH, (b) TRMM and (c) PERSIANN satellite observations for the 2014-2015 flood events at Langat river basin.

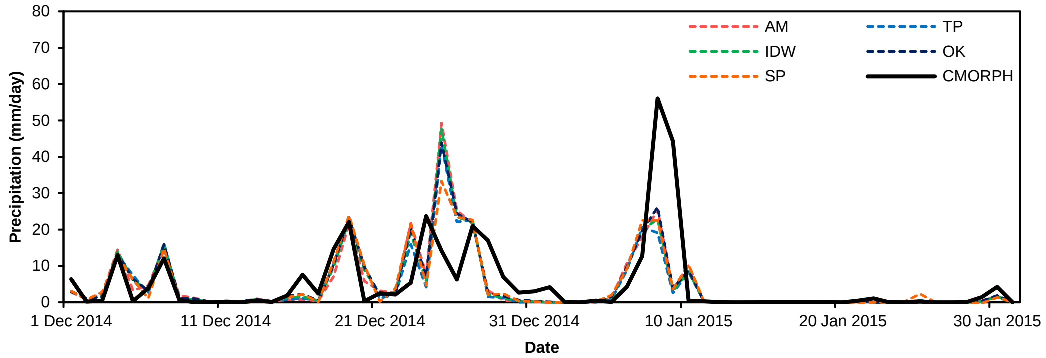

(a)

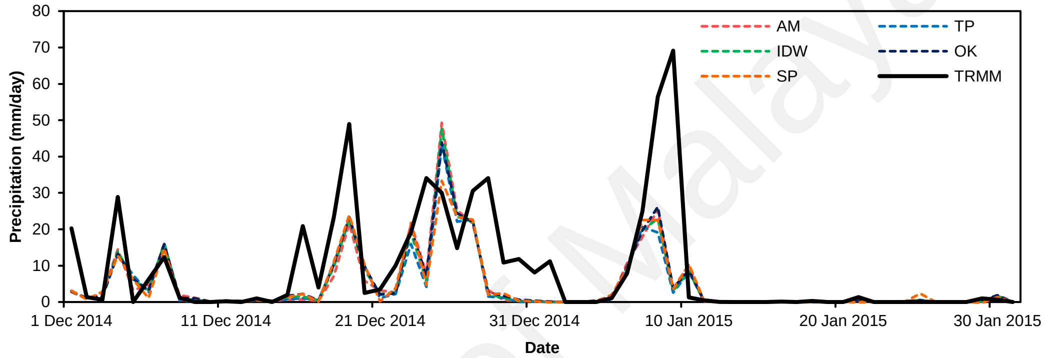

(b)

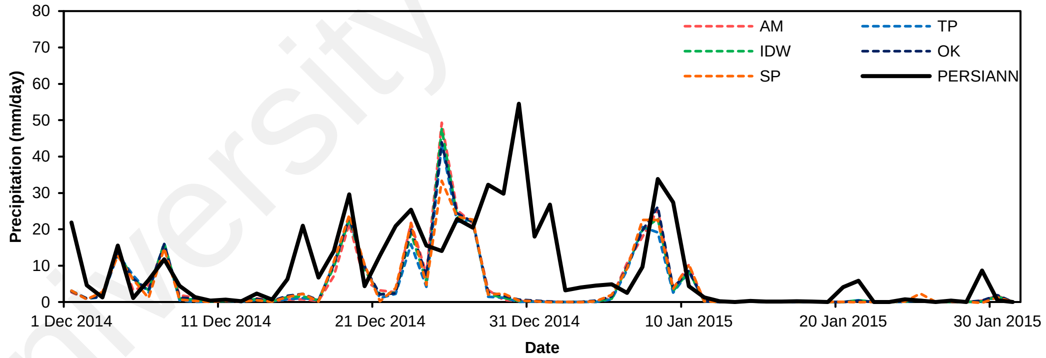

(c)

Figure 3.8: Comparison of daily mean precipitation series between interpolated ground observations and (a) CMORPH, (b) TRMM and (c) PERSIANN satellite observations for the 2014-2015 flood events at Johor river basin.

Figure 3.9 shows the scatterplots of averaged daily rainfall overall river basins for the three SPP versus the rain gauge observations. The scatter plot further demonstrates the SPP performance by comparing with each of the interpolation methods. For the Kelantan river basin, the average method displays slightly different in pattern as compared to the other methods. In addition, most of the data points are underestimated with less scattered. For the Langat river basin, the relatively scattered data points imply high variability in the SPP compared to all interpolation methods. Nevertheless, the TRMM shows a good agreement as indicated by the square plots. A similar trend can also be observed for the Johor river basin whereby a large variability given by the SPP.

Details statistical performance of the SPP for all river basins and using all interpolation methods are tabulated in Table 3.4 and accompanied by graphs in Figure 3.10. This result shows that the Kelantan river basin outperforms other river basins followed by Langat and lastly Johor river basin as indicated by the three SPP and based on all interpolation methods. Kelantan river basin is the largest basin followed by Langat and Johor river basin and this Kelantan river basin is geographically located near to the South China Sea that directly and highly influenced by heavy rainfall. The SPP results shown by this study are in accordance with the movement of the rainfall circulation of the northeast monsoon of which this monsoon circulation starts from the South China Sea towards the west and south of Peninsular Malaysia. It is interesting to suggest a new study in investigating the SPP performance during the southwest monsoon season of which the general monsoon circulation is opposite to the northeast monsoon by applying to the river basins that are situated in a different part of Peninsular Malaysia.

The R^2 given by all SPP in Kelantan is relatively high which is above 0.6 which implies all SPP perform better regardless of any interpolation methods. As we move further towards western, i.e. Langat river basin, the SPP gives slightly lower compared to the previous basin and it is found that the TRMM and CMORPH be able to perform about

50 to 60%. PERSIANN, however, not be able to measure accurately that resulted in a quite low R^2 value. The SPP performance becomes worse as we move down towards the south of Peninsular Malaysia, which was consistent with the findings by Tan *et al.* (2015). As evident by the Johor river basin, all SPP are performed poorly. In general, by comparing those three SPP for the three basins, it can be concluded that the CMORPH and TRMM be able to capture the extreme event with acceptable accuracy compared to the PERSIANN.

In terms of bias error, underestimate of actual rainfall for about 30% to nearly 60% are shown by all SPP for the Kelantan river basin given by all the interpolation methods. According to Thiemig *et al.* (2012), the significant underestimation of the SPP might be due to poor ability in estimating heavy rain (>10 mm/day). However, the under or overestimation is found to be smaller for the Langat river basin of which bias ranging up to 50% maximum for PERSIANN and 30% maximum for CMORPH. TRMM shows the lowest variability with less than 20%. As for the Johor river basin, the variability is somewhat higher as compared to the other basins. It is evident that TRMM and PERSIANN produce a relatively high bias value of more than 80%. Conversely, CMORPH performs better with about up to 10% overestimation.

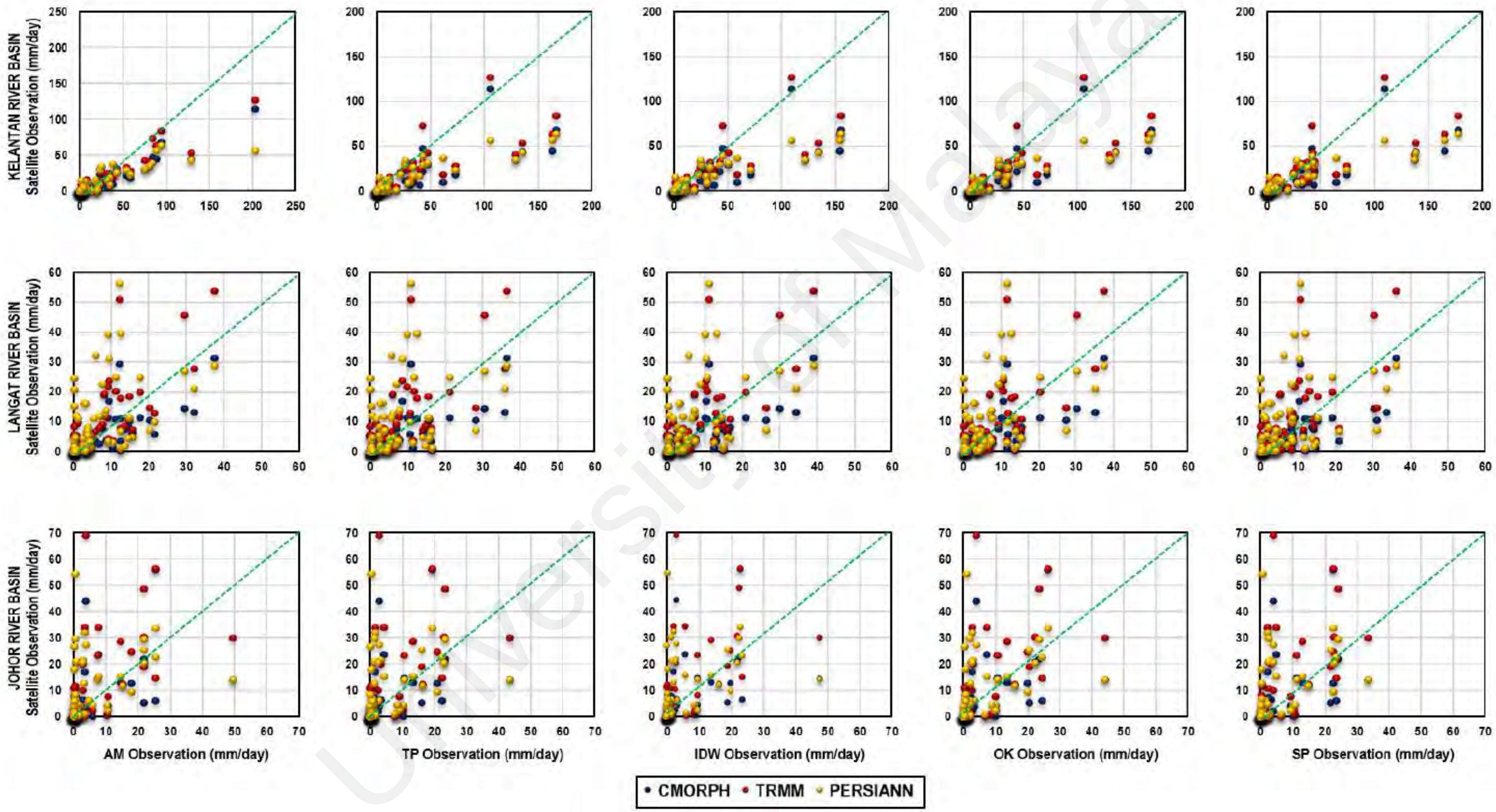

Figure 3.9: Scatter plots comparisons of daily mean precipitation for satellite precipitation products versus rain gauge observation for Kelantan, Langat and Johor river basins.

Table 3.4: Statistical analysis of SPP versus rainfall interpolation methods for the 2014-2015 flood events.

Rainfall Interpolation Method		Kelantan River Basin			Langat River Basin			Johor River Basin		
		CMORPH	**TRMM**	**PERSIANN**	**CMORPH**	**TRMM**	**PERSIANN**	**CMORPH**	**TRMM**	**PERSIANN**
Arithmetic Mean	***R^2***	0.909	0.908	0.754	0.527	0.626	0.196	0.289	0.352	0.150
	CC	0.954	0.953	0.868	0.726	0.791	0.443	0.538	0.593	0.388
	PBias (%)	-52.1	-31.6	-44.9	-29.2	22.0	50.5	9.7	89.9	92.7
	MAE (mm)	11.207	8.413	11.593	3.912	4.301	7.577	4.187	6.177	6.665
	RMSE (mm)	10.898	8.523	12.860	2.978	3.716	5.828	4.635	6.373	6.159
	NRMSE	0.531	0.415	0.626	0.439	0.548	0.860	0.981	1.348	1.303
Thiessen Polygon	***R^2***	0.654	0.691	0.808	0.460	0.552	0.162	0.257	0.332	0.131
	CC	0.809	0.831	0.899	0.678	0.743	0.402	0.507	0.576	0.362
	PBias (%)	-54.3	-34.7	-47.4	-30.4	19.9	47.9	19.3	106.4	109.5
	MAE (mm)	12.339	10.481	12.040	4.216	4.680	7.923	4.170	6.244	7.028
	RMSE (mm)	14.257	12.306	13.780	3.342	3.993	6.049	4.666	6.527	6.206
	NRMSE	0.662	0.571	0.640	0.484	0.579	0.877	1.073	1.501	1.427
Inverse Distance Weighting (IDW)	***R^2***	0.680	0.715	0.816	0.502	0.582	0.176	0.276	0.345	0.143
	CC	0.824	0.846	0.903	0.709	0.763	0.420	0.526	0.588	0.378
	PBias (%)	-53.1	-33.0	-46.0	-31.9	17.4	44.8	11.6	93.2	96.1
	MAE (mm)	11.694	9.976	11.681	4.217	4.487	7.794	4.150	6.131	6.814
	RMSE (mm)	13.333	11.367	12.974	3.219	3.853	5.944	4.651	6.415	6.170
	NRMSE	0.635	0.541	0.618	0.457	0.547	0.843	1.001	1.381	1.328
Ordinary Kriging	***R^2***	0.653	0.689	0.810	0.498	0.583	0.180	0.321	0.382	0.166
	CC	0.808	0.830	0.900	0.706	0.764	0.424	0.567	0.618	0.407
	PBias (%)	-54.6	-35.2	-47.8	-32.2	16.9	44.2	8.0	87.0	89.7
	MAE (mm)	12.527	10.649	12.214	4.238	4.575	7.732	4.021	6.008	6.612
	RMSE (mm)	14.402	12.450	13.918	3.198	3.851	5.906	4.431	6.235	6.005
	NRMSE	0.664	0.574	0.641	0.452	0.544	0.835	0.923	1.298	1.250
Spline	***R^2***	0.651	0.684	0.807	0.450	0.540	0.161	0.308	0.383	0.174
	CC	0.807	0.827	0.898	0.671	0.735	0.401	0.555	0.619	0.417
	PBias (%)	-55.7	-36.8	-49.1	-30.7	19.5	47.4	14.2	97.7	100.6
	MAE (mm)	12.877	11.020	12.598	4.270	4.736	7.899	4.160	5.995	6.697
	RMSE (mm)	15.055	13.095	14.607	3.359	4.040	6.041	4.398	6.301	5.913
	NRMSE	0.677	0.589	0.657	0.485	0.584	0.873	0.968	1.387	1.302

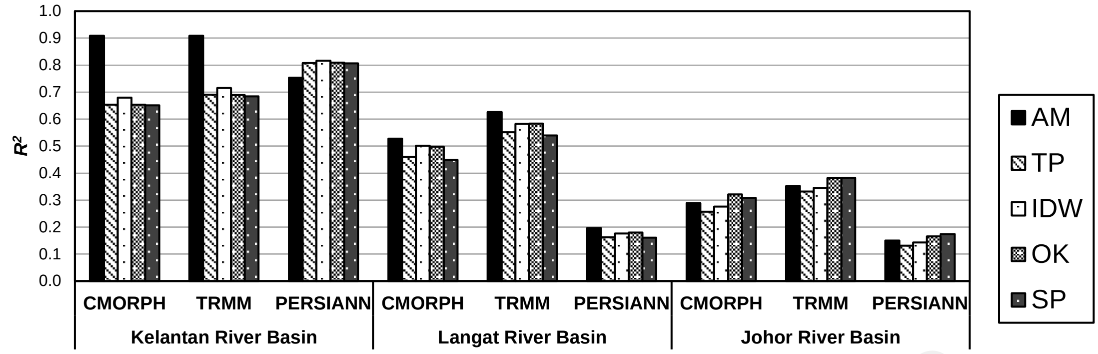

(a)

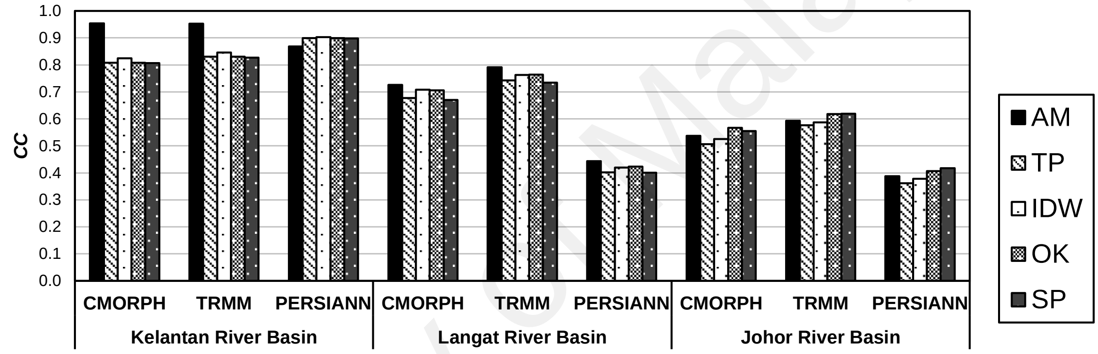

(b)

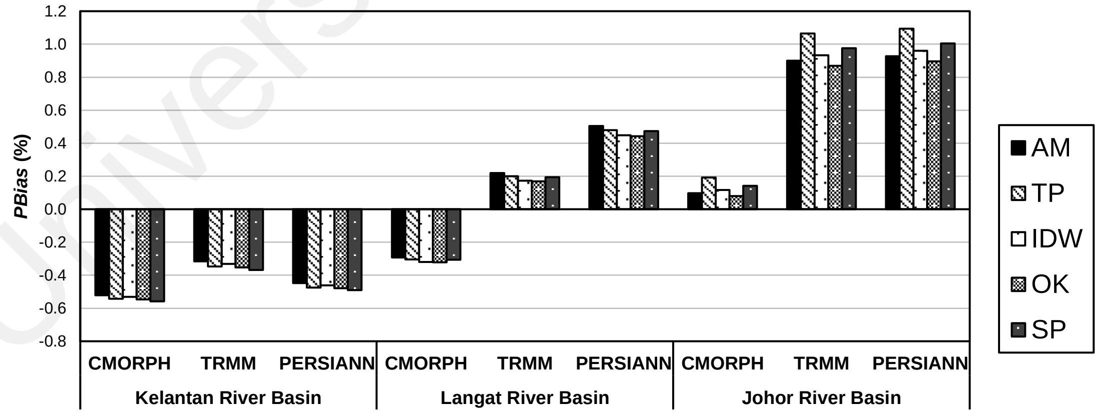

(c)

Figure 3.10: Comparison of the (a) coefficient of determination (*R^2*), (b) coefficient of Pearson Correlation (*CC*), (c) percentage bias (*PBias*), (d) mean absolute error (*MAE*), (e) root mean square error (*RMSE*) and (f) normalized root mean square error (*NRMSE*) for three SPP versus rain gauge observations over Kelantan, Langat and Johor river basins during 2014-2015 flood events.

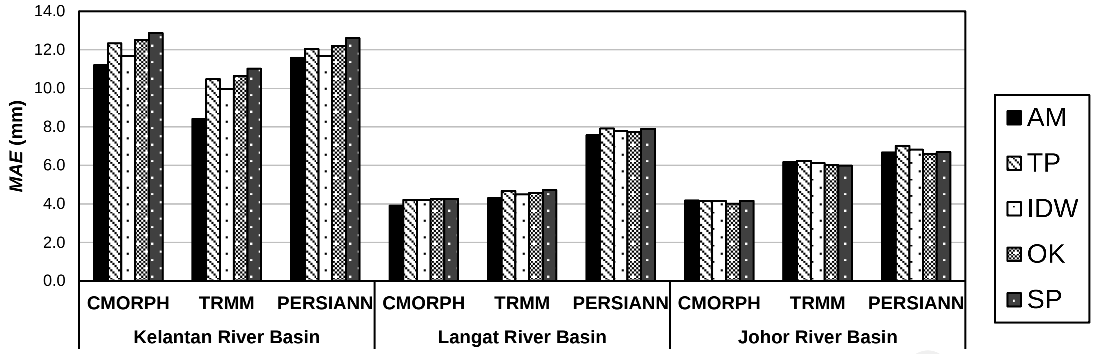

(d)

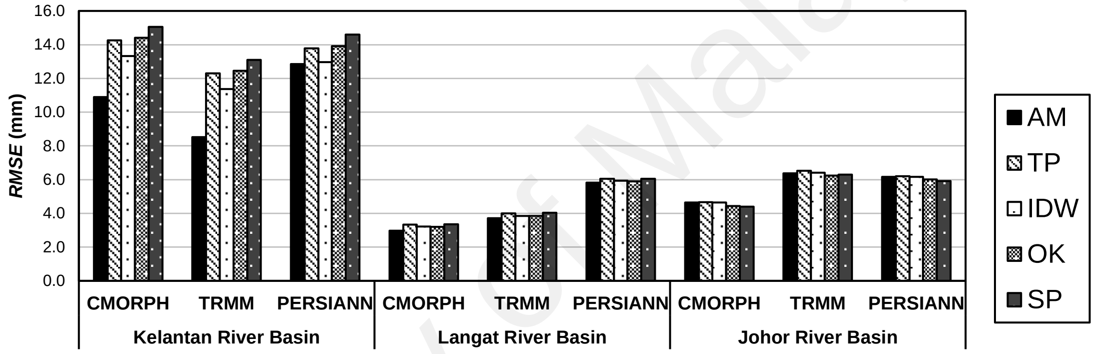

(e)

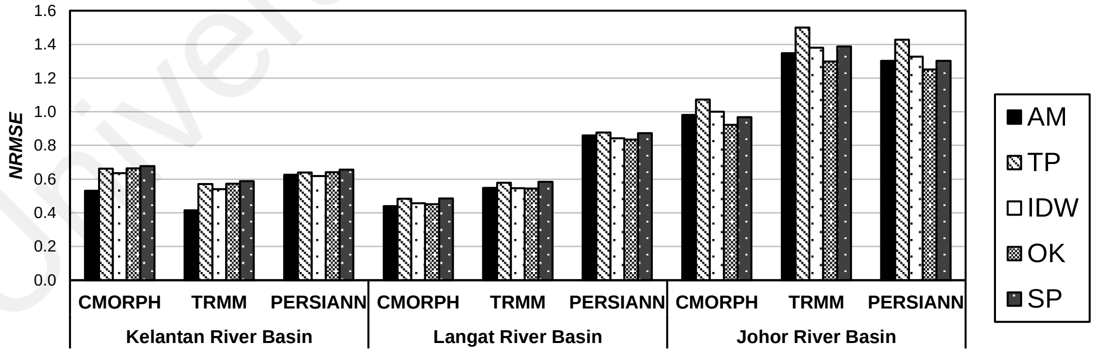

(f)

Figure 3.10, continued

3.6.3 Rain Detection Ability Assessment of SPP

This section discusses the capability of each SPP in detecting the precipitation rate using the categorical evaluation indexes, i.e. *ACC*, *POD*, *FAR*, *CSI* and *HSS*. The result is presented in Figure 3.11 and Table 3.5. This study uses a 1 mm/day rainfall threshold to discriminate whether it is a rainy or no-rain day. It is noticeable that the TRMM and PERSIANN perform better for all the categorical evaluation indexes for all river basins. Nevertheless, the differences in all categorical values for these two SPP are not great compared to CMORPH. For example, TRMM gives the highest *ACC* with value varies from 0.790 – 0.839 for all basins. As for *POD* and *FAR*, the highest is shown by PERSIANN, i.e. *POD* from 0.846 – 0.962 and *FAR* from 0.149 – 0.390. TRMM also exhibits well in *CSI* and *HSS*. As *ACC* and *POD* indexes denote the level of agreement and correctly detected rainfall, it is observed that the Langat river basin has shown a better result based on these two indexes for all SPP. As for the rest of the indexes, i.e. *FAR*, *CSI* and *HSS*, the best is shown by Johor, Langat and Kelantan river basins, respectively. It can be thought that the categorical indexes are unlikely influenced by the geographic location or size of the river basin. These factors are somehow difficult to be determined in this case.

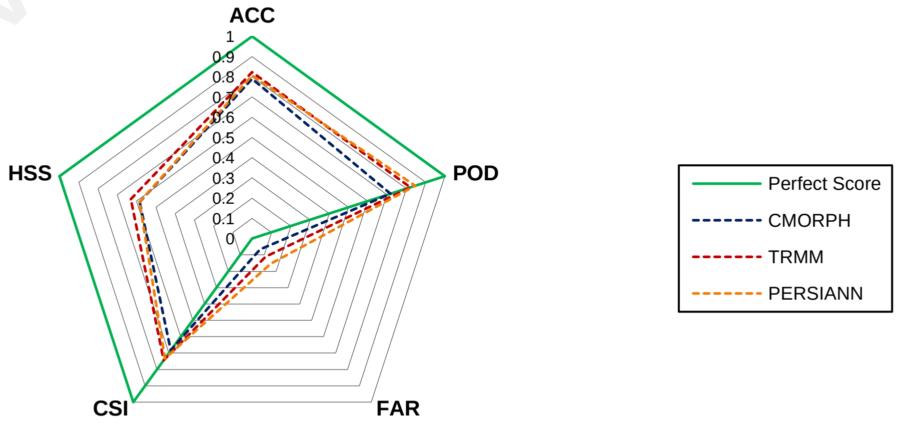

(a) Kelantan river basin

Figure 3.11: Rain Detection Capability of SPP in (a) Kelantan, (b) Langat and (c) Johor river basins

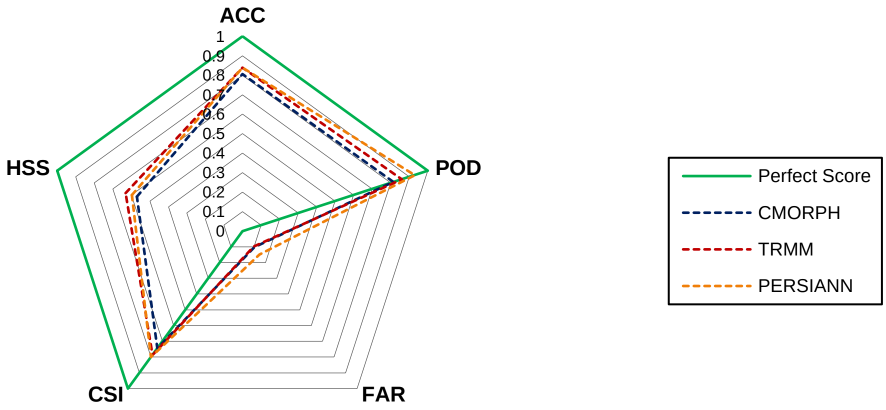

(b) Langat river basin

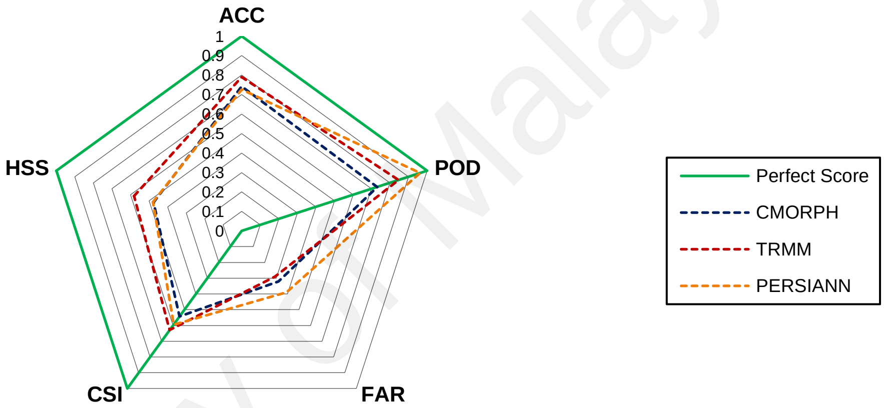

(c) Johor river basin

Figure 3.11, continued

Table 3.5: Overall rain detection capability of each precipitation product

River Basin		CMORPH	TRMM	PERSIANN
	ACC	0.790	0.823	0.806
	POD	0.718	0.821	0.846
Kelantan	***FAR***	0.067	0.111	0.154
	CSI	0.683	0.744	0.733
	HSS	0.584	0.630	0.585
	ACC	0.806	0.839	0.839
	POD	0.814	0.860	0.930
Langat	***FAR***	0.103	0.098	0.149
	CSI	0.745	0.787	0.800
	HSS	0.570	0.631	0.597
	ACC	0.742	0.790	0.726
	POD	0.731	0.846	0.962
Johor	***FAR***	0.321	0.290	0.390
	CSI	0.543	0.629	0.595
	HSS	0.476	0.581	0.479

3.6.4 Capturing Storm Performance of SPP

In this section, the capability of every SPP in capturing storm using the *HSS* categorical index is further demonstrated. The rainfall threshold is increased in order to examine the ability of every SPP to capture the rain. Generally, all SPP perform poorer as the extreme precipitation threshold increases. The *HSS* is decreasing as the storm threshold increases.

In the Kelantan river basin (Figure 3.12), TRMM exhibits the best performance as the *HSS* ranging from 0.4 to 0.9 which implies this satellite precipitation estimation at watershed scale is better than chance performance. For CMORPH and PERSIANN, when the storm threshold is reduced from or equal to 40 mm, the *HSS* values are larger than 0.5 implies that both satellites capable of capturing moderate storms effectively. When the storm threshold is more than or equal to 50 mm, the *HSS* of CMORPH seems unstable. As for PERSIANN, the *HSS* shows zero at storm threshold more than or equal to 70 mm where this satellite precipitation product could not capture extreme storm effectively at watershed scale.

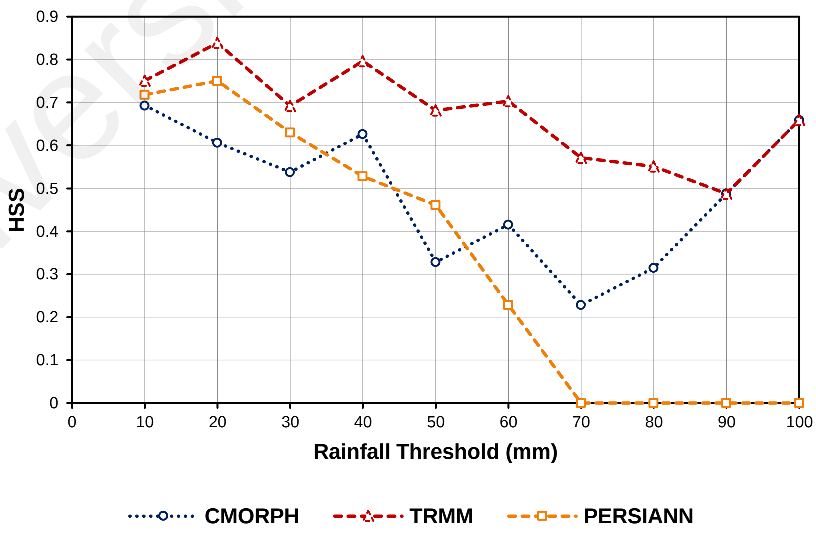

Figure 3.12: The Heidke Skill Score (*HSS*) of three satellite precipitation products (CMORPH, TRMM and PERSIANN) for storm thresholds ranging from 10 mm to 100 mm in Kelantan river basin

For the Langat river basin (Figure 3.13), all three satellites cannot capture heavy storms as in the Kelantan river basin. When the storm threshold is less than or equal to 11 mm, the forecast of TRMM and CMORPH satellites show better than the gauge observations as they show positive *HSS,* ranging from 0.4 to 0.7. However, CMORPH does not perform well when the storm threshold is more than 11 mm where the *HSS* shows less than 0.4. As for TRMM, it does not perform well when the storm threshold is more than 15 mm. PERSIANN does not perform well compared to the other two satellites where the *HSS* shows less than 0.4 when the storm threshold is more than 5 mm, and the results become worse as the storm threshold increases.

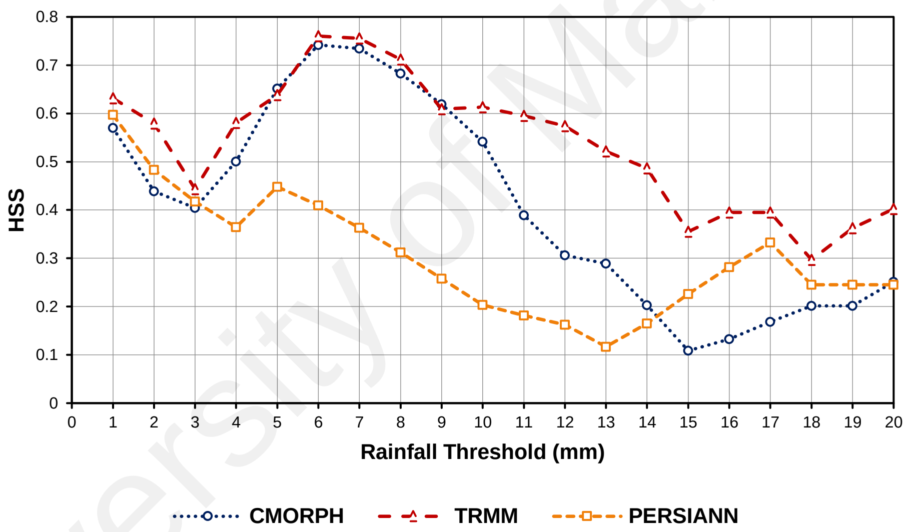

Figure 3.13: The Heidke Skill Score (*HSS*) of three satellite precipitation products (CMORPH, TRMM, and PERSIANN) for storm thresholds ranging from 1 mm to 20 mm in Langat river basin

In Johor river basin (Figure 3.14), all three satellites could not capture the storm as effective as in the Kelantan river basin. Among three satellites, when the storm threshold is less than 20 mm, the *HSS* values are larger than 0.4. For CMORPH, it seems that this product is unstable for the storm threshold of more than 12 mm. As for PERSIANN, the *HSS* is around 0.35 to 0.5, however, the performance is getting worse when the storm threshold more than 20 mm and shows zero at storm threshold more than or equal to 26 mm. The results showed that none of the SPP can be considered ideal for detecting extreme events. Although in the previous section on rainfall detection, TRMM showed lower *POD* compared to PERSIANN product, however, low *POD* of a product cannot be concluded as no rainfall detection. In fact, the product may have detected precipitation, but below the selected rainfall threshold (AghaKouchak *et al.*, 2011).

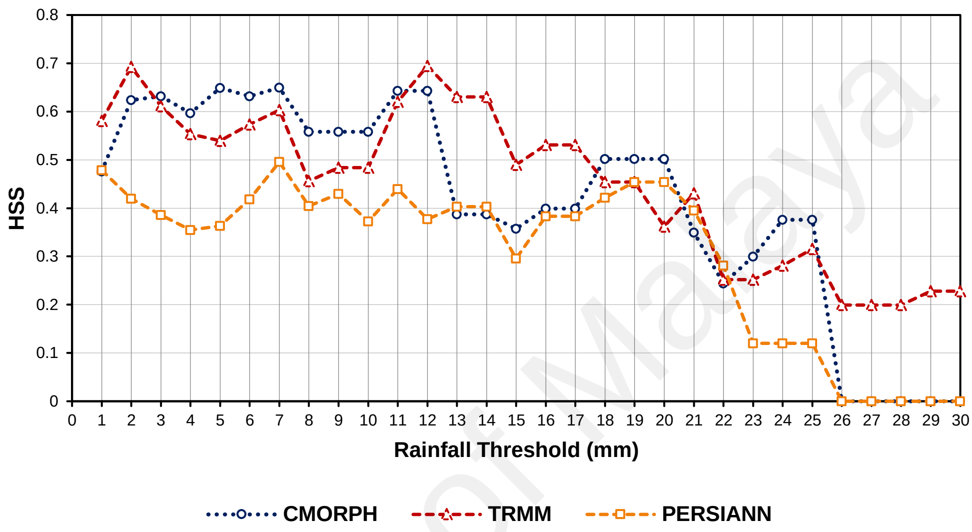

Figure 3.14: The Heidke Skill Score (*HSS*) of three satellite precipitation products (CMORPH, TRMM, and PERSIANN) for storm thresholds ranging from 1 mm to 30 mm in Johor river basin

3.7 Summary

This chapter has presented the outcomes for the first and second objectives of this study, which are validating various spatial interpolation methods to be adopted on the rain gauge network before comparing with the grid-based satellite estimations and evaluating the performance of SPP with reference to the interpolated rain gauge observations during extreme floods at different geographic locations of Peninsular Malaysia.

This study uses daily observed rainfall data with the total number of 62 days and applied several rainfall interpolation methods, i.e. Arithmetic Mean (AM), Thiessen polygon (TP), Inverse Distance Weighting (IDW), Ordinary Kriging (OK) and Spline

(SP) methods to examine the effect of different spatial interpolation methods based on the observed data. The result indicates that the areal precipitation transformed by these interpolation methods give a slight varies in values but overall it is comparable. Even though the AM overestimated the peak rainfall for Kelantan river basin, the output of these five selected rainfall interpolation methods can be adopted on the rain gauge observations before comparing with the gridded SPP estimations.

Based on the verification of the three SPP (CMORPH, TRMM 3B42V7, PERSIANN) during 2014-2015 extreme floods at three study areas (Langat, Kelantan, and Johor river basins), this study found that all three SPP perform better during this extreme event as they show an acceptable accuracy in capturing high rainfall in Kelantan river basin. However, this performance has decreased as monsoon moving away towards the west and south that hit Langat and Johor river basin. About 50 – 60% accuracy is obtained for the Langat and 30 – 40% for the Johor river basin given by the TRMM and CMORPH. Conversely, PERSIANN shows poor accuracy for these two river basins. It is noted that all SPP tend to overestimate or underestimate the actual rainfall. By comparing those three river basins, extreme events in Kelantan river basin are better captured by all SPP compared to the other basins. This might be due to geographic location near to the South China Sea that is directly exposed to heavy rainfall during the northeast monsoon.

The categorical indexes indicate that TRMM has a good level of agreement as denoted by *ACC* whereas PERSIANN shows better performance in detecting rainfall, as denoted by *POD*. Langat river basin is found as the best river basin with the highest *ACC* and *POD* for all SPP. In general, the values of *ACC* and *POD* for all river basins computed by all SPP are relatively quite close. Based on this study, it can conclude that all SPP be able to capture extreme events of heaviest rainfall with acceptable accuracy. As proven by this study, all SPP work well for Kelantan however, as the monsoon moves further away, the TRMM and CMORPH outperform PERSIANN.

Based on the conclusions derived above, it is important to highlight that the spatial and temporal uncertainties may exist when comparing different SPP with the ground observations. Thus, bias-adjustment is suggested in order to improve the reliability of the estimation of SPP.

CHAPTER 4: BIAS ADJUSTMENT OF SATELLITE PRECIPITATION ESTIMATIONS

4.1 Introduction

In the previous chapter, we noted that the available SPP (TRMM 3B42V7, CMORPH and PERSIANN) perform better during the 2014-2015 extreme floods as they show an acceptable accuracy in capturing high rainfall in Kelantan river basin. However, the performance has decreased as monsoon moving away towards the west and south that hit Langat and Johor river basin. In this chapter, we attempt to improve the SPP estimations by adopting bias correction (BC) schemes and produce more accurate prediction, before the data are ready to be input into the hydrologic modeling. This section is unique as studies regarding the BC on satellite estimations in Malaysia appear to be limited. Moreover, in order to evaluate the uncertainty of the BC parameters applied on the SPP rainfall and whether these parameters can be applied in a similar event of different time period (Terink *et al.*, 2010), this chapter has included an addition of four flood events of the same month as 2014-2015 floods (December and January) for sensitivity analysis. It should be noted that evaluation is only implemented in the Langat river basin.

4.2 Review on Bias Correction

Bias correction (BC) or bias adjustment is a model output statistics approach that seeks to use information from biased model outputs (Chen *et al.*, 2013a). The correction usually identifies possible differences between the observed and simulated climate variables, which provide the basis for correcting both control and scenario model runs with a transformation algorithm. However, BC of precipitation is more challenging compared to other climate variables such as temperature due to the fact of spatial/temporal heterogeneity and zero inflation.

In recent years, numerous studies of improving the SPP estimations by BC have been done varies with location, season, topography, climatology, and so on (Abera *et al.*, 2016; Boushaki *et al.*, 2009; Fang *et al.*, 2015; Gumindoga *et al.*, 2016; Habib *et al.*, 2014; Pan *et al.*, 2016; Tesfagiorgis *et al.*, 2011; Valdés-Pineda *et al.*, 2016; Worqlul *et al.*, 2017a). Table 4.1 shows an overview of some BC methods used to correct precipitation data.

Table 4.1: Overview of some BC schemes.

Method	Advantage	Disadvantage	Reference
Linear scaling (LS)	• *Mean-based* • A mean monthly correction factor is applied to the regional climate model (RCM) simulated daily precipitation in a month. It is the simplest bias correction method.	• The daily precipitation sequence is the same as that of the RCM-simulated data (usually too many wet days compared to the observation). • It does not account for the changes in the frequency distribution of precipitation. • No adjustment is made to the temporal structure of daily precipitation occurrence.	Lenderink et al. (2007) Teutschbein and Seibert (2013)
Local intensity scaling (LOCI)	• *Mean-based* • The wet-day frequency is corrected. A mean monthly correction factor is applied to the RCM-simulated daily precipitation in a month.	• It does not account for the different changes in the frequency distribution of precipitation. • No adjustment is made to the temporal structure of daily precipitation occurrence.	Schmidli *et al.* (2006)
Power Transformation (PT)	• *Mean-based* • a precipitation threshold can be introduced a priori to avoid too many drizzle days (i.e., very low but non-zero precipitation). corrects mean and standard deviation • (variance) • events are adjusted non-linearly • variability of corrected data is more consistent with original data	• Adjustment of wet-day frequencies and intensities only to some extent.	Leander and Buishand (2007)

Table 4.1, continued

Method	Advantage	Disadvantage	Reference
Quantile mapping based on an empirical distribution (QME)	• *Distribution-based* • Corrects the RCM-simulated precipitation based on point-wise daily constructed empirical cumulative distribution functions (ecdfs). The frequency of precipitation occurrence is corrected at the same time.	• No adjustment is made to the temporal structure of daily precipitation occurrence.	Jakob Themeßl *et al.* (2011)
Quantile mapping based on a gamma distribution (QMG)	• *Distribution-based* • Corrects the RCM-simulated precipitation based on a gamma distribution. The frequency of precipitation occurrence is corrected using the LOCI method.	• The performance depends on whether the observed and RCM-simulated precipitation follows the gamma distribution (or not). • No adjustment is made to the temporal structure of daily precipitation occurrence.	Piani *et al.* (2010); Teutschbein and Seibert (2012)

The linear scaling (LS) scheme corrects the average precipitation value based on the differences between the rain gauge data and satellite data. However, this method does not correct the standard deviation or variance and all events are adjusted with the same correction factor (Ajaaj *et al.*, 2016; Boushaki *et al.*, 2009; Lenderink *et al.*, 2007; Tesfagiorgis *et al.*, 2011; Teutschbein & Seibert, 2013; Vila *et al.*, 2009). Local Intensity Scaling (LOCI) scheme combines a precipitation threshold with LS (Ajaaj *et al.*, 2016; Schmidli *et al.*, 2006; Teutschbein & Seibert, 2013). This method separately corrects wet-day frequency and wet-day intensity, applied pointwise and individually for each day of the year, and the estimated precipitation is corrected using a scaling factor. However, the output of this method is limited because, as with LS, the standard deviation and variance are not corrected and all events are adjusted using the same correction factor. The Power Transformation (PT) method is a nonlinear correction in an exponential form that combines the correction of the coefficient of variation (CV) with LS. This scheme corrects the mean and variance of the temporal series of estimated precipitation (Leander & Buishand, 2007; Teutschbein & Seibert, 2012, 2013). The coefficient of variation of both daily and multiple-day precipitation amounts depends on the wet-day frequency but this correction does not adjust the frequency of wet days (Leander & Buishand, 2007).

Quantile Mapping (QM) (Ajaaj *et al.*, 2016; Leander & Buishand, 2007; Piani *et al.*, 2010; Teutschbein & Seibert, 2013) also known as the Distribution Mapping adjusts the cumulative distribution of estimated data to the cumulative distribution of rain gauge data using a transfer function. This correction can capture the evolution of the mean and the variability of precipitation while matching all statistical moments. Under this correction method, it can be referring to an empirical distribution or a gamma distribution. Hay *et al.* (2002) applied a gamma transform to correct RCM precipitation data and Leander and Buishand (2007) applied a power transformation, which corrects for the coefficient of variation (CV) and mean of the precipitation values. Hay *et al.* (2002) found that the corrected precipitation data did not contain the day-to-day variability which was presented in the observed data set. Piani *et al.* (2010) validated a statistical BC method based on QM method (with Gamma distribution) and the performance was good for seasonal means, heavy rainfall events and seasonal drought index but not for the daily rainfall events. Lafon *et al.* (2013) compared the performance of LS, PT, QMG and QME methods and found out that mean and standard deviation of daily rainfall can be effectively corrected while the correction of skewness and kurtosis of daily rainfall are sensitive to the choice of BC method and calibration period. Although, gamma-based quantile mapping method provides better results where the variability in rainfall was captured by gamma distribution, the study employed monthly gamma parameters to correct the daily rainfall data. The performance of distribution derived, parametric and nonparametric transformations was compared by Gudmundsson *et al.* (2012) and identified that nonparametric transformations possess good proficiency in the reduction of biases in rainfall simulated by RCM. While assessing hydrological response to climate change, Teutschbein and Seibert (2012) reported that all BC methods improved RCM outputs (rainfall and temperature) and distribution mapping method was found to be superior for hydrological simulation but the corrections employed monthly factors.

Although the correction of climate variables can considerably improve the hydrologic simulations under current climate conditions (Chen *et al.*, 2013b; Teutschbein & Seibert, 2012), there is a major drawback whereby most methods follow the assumption of stationarity of model errors which means that the correction algorithm and its parameterization for current climate conditions are assumed to be valid for a time series of changed future climate conditions. Whether or not this condition is fulfilled for our future climate, it cannot be evaluated directly. This motivated us to address this issue and to test how well different correction schemes perform for conditions that differ from those used for calibration.

4.3 Description of the study area and selected flood events

In this chapter, evaluation is performed on the Langat river basin only, map as shown in Figure 4.1. The description can be referred to Chapter 3 (Section 3.3.1). In addition to the 2014-2015 flood events, another four extreme flood events due to NEM specifically during the month of December to January are added. Table 4.2 shows the details of all five selected flood events. Figure 4.2 shows the daily temporal precipitation of every selected flood event and the inter-correlation of the rain gauge observations between these events was tabulated in Table 4.3. It can be noticed that the rainfall pattern of the selected events was slightly different from each other even though they are of the same monsoon (NEM) and the same months. Figure 4.3 exhibits the frequency distribution of daily precipitation in different intensities to each flood event focused on Langat river basin. It is noticed that Events 2 and 4 are drier compared to the other events whereby more than 50% of the event is no-rain (0 mm/day). Light rainfall (0 – 1 and 1 – 5 mm/day) occurred at less than 20% of every period whereas heavy rainfall (20 – 30 and > 30 mm/day) occurred at about 3 – 8% of the event period.

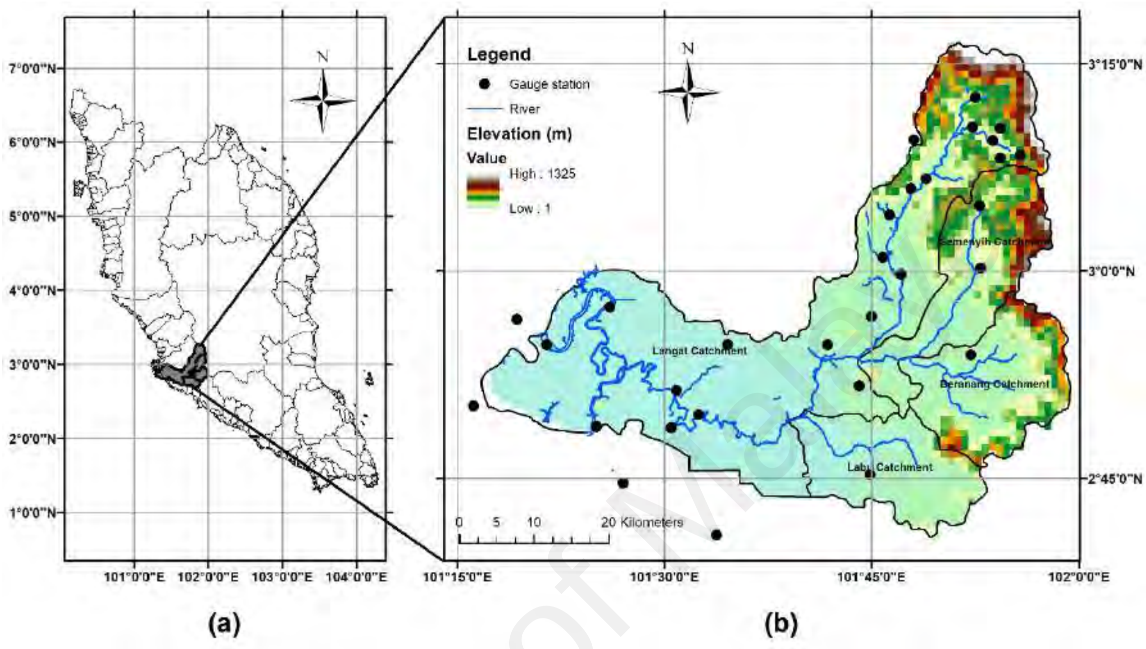

Figure 4.1: (a) Location of study area. (b) Distribution of gauge stations and DEM of the Langat river basin.

Table 4.2: Selected flood events for this study

Event	Rainy Period
1	1 December 2012 – 31 January 2013
2	1 December 2013 – 31 January 2014
3	1 December 2014 – 31 January 2015
4	1 December 2015 – 31 January 2016
5	1 December 2016 – 31 January 2017

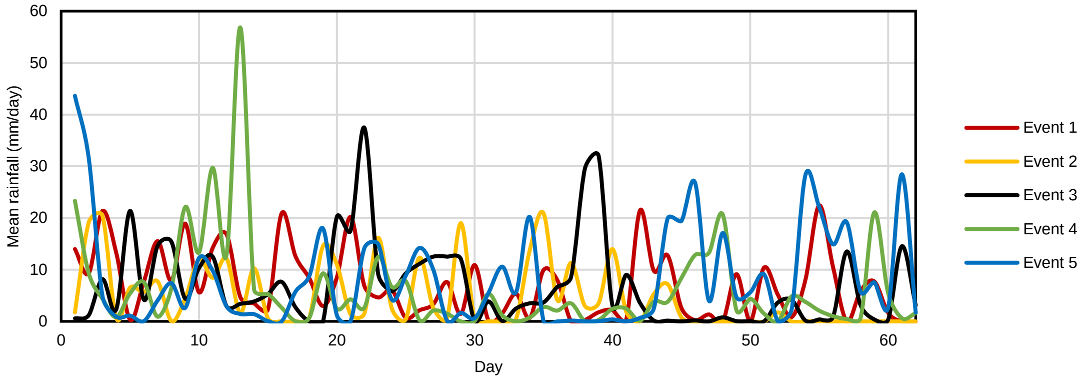

Figure 4.2: Daily mean precipitation series of selected flood events in Langat river basin

Table 4.3: Inter-correlation of rain gauge observations between selected flood events in Langat river basin.

Event	1	2	3	4	5
1		0.061	-0.108	0.047	-0.026
2	0.061		0.092	0.015	0.010
3	-0.108	0.092		-0.158	-0.187
4	0.047	0.015	-0.158		0.151
5	-0.026	0.010	-0.187	0.151	

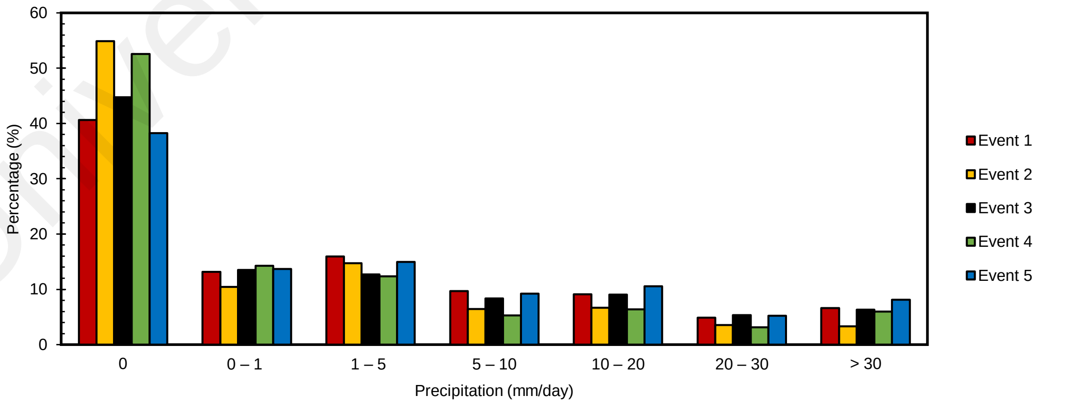

Figure 4.3: Frequency distribution of daily precipitation of selected flood events in Langat river basin.

4.4 Data Acquisition

For rain gauge ground observations, daily rainfall data collected at 28 operating rain gauge stations collected from the Department of Drainage and Irrigation (DID), Malaysia are analyzed (Refer Appendix A1). As for SPP, the same products and respective resolutions presented in Chapter 3 (Section 3.4.2) are utilized for this chapter.

4.5 Bias correction methods

SPP estimates exhibit large systematic and random errors which may cause large uncertainties in hydrologic modeling. Moreover, the models could augment or suppress rainfall biases to the streamflow based on the response mode of the model (Fang *et al.*, 2015; Habib *et al.*, 2014; Segond *et al.*, 2007). Several bias-correction (BC) schemes have been developed to downscale the meteorological variables from any datasets or models, ranging from the simple scaling approach to sophisticated distribution mapping (Teutschbein & Seibert, 2012). However, these schemes have not been investigated in Malaysia. Thus, it is necessary to apply the BC schemes to improve the reliability of the estimation of SPP in Malaysia. In the present study, all SPP are bias-corrected utilizing three BC schemes, i.e. Linear scaling (LS) (Lenderink *et al.*, 2007), Local intensity scaling (LOCI) (Schmidli *et al.*, 2006) and Power transformation (PT) (Leander & Buishand, 2007) methods. In this study, Quantile Mapping, which is known as the best effective correction scheme, was not selected as this scheme is often used to reduce the biases in statistical downscaling of future climate change projections (Jeon *et al.*, 2016) and ignores the correlation between raw ensemble forecasts and observations, thus there is still a large uncertainty in representation of extreme precipitation (Huang *et al.*, 2014; Zhao *et al.*, 2017). More detailed descriptions of the selected methods is presented below.

4.5.1 Linear Scaling (LS)

The LS method aims to perfectly match the monthly mean of corrected estimations with that of observed ones (Lenderink *et al.*, 2007). This method operates with monthly correction values based on the differences between observed and estimated data. The daily satellite precipitation amounts, P are transformed into P^* by multiplying with the monthly scaling factor, s. (Equation 4.1)

$$P^* = s \times P \tag{4.1}$$

The scaling factor is the ratio of the true mean to the mean of biased estimates (Anagnostou *et al.*, 1998). In this case, this study assumed the rain gauge measurement as the true observation and the satellite estimations are the biased estimation as shown by Equation 4.2.

$$s = \frac{\overline{G_i}}{\overline{S_i}} \tag{4.2}$$

where S and G represents satellite/gridded and gauge precipitation, respectively, i is the date of the events, $\bar{S}$ is the monthly average value of S_i and $\bar{G}$ is the monthly average value of G_i.

Unlike other studies (Ajaaj *et al.*, 2016; Schmidli *et al.*, 2006; Teutschbein & Seibert, 2013), this study is focusing on the calculation of the monthly scaling factors. These scaling factors are applied separately for every selected extreme event as the rainfall pattern is not consistent even though they are of the same monsoon (NEM) and the same months.

4.5.2 Local intensity scaling (LOCI)

The LOCI method (Schmidli *et al.*, 2006) corrects the wet-day frequencies and intensities and can effectively improve the raw data which have too many drizzle days (days with little precipitation). It normally involves two steps: firstly, a wet-day threshold for the *m*th month $P_{thres,m}$ is determined from the raw precipitation series to ensure that the threshold exceedance matches the wet-day frequency of the observation; secondly, a scaling factor $c = \frac{\mu(\mathrm{P_{obs,m,d}}|\mathrm{P_{obs,m,d}}>0)}{\mu(\mathrm{P_{raw,m,d}}|\mathrm{P_{raw,m,d}}>\mathrm{P_{thres,m}})}$ is calculated and used to ensure that the mean of the corrected precipitation is equal to that of the observed precipitation:

$$P_{LOCI,m,d} = \begin{cases} 0 & , \ P_{S,m,d} < P_{thres,m} \\ P_{S,m,d} \times c, & \text{otherwise.} \end{cases} \tag{4.3}$$

Similar to LS scheme, the scaling factor is calculated and applied separately for every selected event.

4.5.3 Power transformation (PT)

Shabalova *et al.* (2003) and Leander and Buishand (2007) advocated the PT method because it uses an exponential form to further adjust the standard deviation of precipitation series, P, as shown in Equation (4.4).

$$P^{*} = a \cdot P^{b} \tag{4.4}$$

To implement this method, there are two scaling factors to be calculated, a and b. The b factor is calculated iteratively so that the coefficient of variation (CV) of the satellite daily precipitation time series matches that of the gauged precipitation time series. Next, the a factor is calculated such that the mean of the transformed precipitation values matches that of the gauged precipitation. Finally, these two scaling factors are applied to each uncorrected daily satellite observations corresponding to that month to generate the corrected daily time series.

4.6 Results and Discussions

4.6.1 Evaluation of raw satellite estimates over selected extreme flood events

Before performing the BC schemes, the accuracy of the three selected satellite products (TRMM, CMORPH, and PERSIANN) at Langat river basin for all events is first examined. Table 4.4 shows the summarized result of the raw satellite estimations for Langat river basin. TRMM capable to estimate rainfall reasonably well with *CC* ranging from 0.52 – 0.77 and so does the CMORPH although the poor correlation is shown for Event 2. As for PERSIANN, the estimation is slightly poor compared to TRMM and CMORPH for the first three events but somehow slight improvement is noticeable in Event 4 and 5. Based on the bias, it is found that the raw TRMM and PERSIANN estimations almost overestimate the actual precipitation of every event of the same months (December – January) for about 6 – 60% whereas CMORPH underestimates the actual precipitation by 27 – 51%. Similar results were reported by Tan *et al.* (2015) and Derin and Yilmaz (2014), where CMORPH showed significant precipitation underestimation over Peninsular Malaysia and the western part of Turkey, respectively compared to other SPP. According to Thiemig *et al.* (2012), the significant overestimation and underestimation of the SPP might be due to poor ability in estimating heavy rain (>10 mm/day). Overall, the results found that PERSIANN performs poorly compared to the other two satellites for the selected basin. However, there are some studies that indicated PERSIANN can estimate well the rainfall compared in other regions (Ghajarnia *et al.*, 2015; Kizza *et al.*, 2012). Based on the *NRMSE* and *MAE*, it is noted that CMORPH has the lowest value among those three SPP estimations which implies the CMORPH rainfall estimation is more reliable.

Table 4.4: Statistical Results of Raw Satellite Estimations for the overall Langat river basin

SPP	Event	1	2	3	4	5
TRMM	***CC***	0.54	0.52	0.77	0.66	0.61
	***PBias* (%)**	14.9	54.5	17.6	6.1	-3.1
	NRMSE	1.4	2.5	1.3	1.4	1.2
	***MAE* (mm/day)**	5.4	5.1	5.0	5.4	5.6
CMORPH	***CC***	0.63	0.49	0.63	0.80	0.68
	***PBias* (%)**	-37.9	1.9	-37.6	-51.2	-26.9
	NRMSE	0.8	1.9	1.0	1.1	1.0
	***MAE* (mm/day)**	4.0	4.0	4.3	3.8	4.9
PERSIANN	***CC***	0.30	0.50	0.37	0.56	0.54
	***PBias* (%)**	6.4	61.8	43.9	-15.1	28.7
	NRMSE	1.1	2.4	1.8	1.2	1.2
	***MAE* (mm/day)**	5.6	5.8	7.9	4.5	6.6

4.6.2 Performance evaluation of bias-corrected satellite estimates

4.6.2.1 Rainfall pattern and distribution

Figure 4.4 shows the direct comparison of the daily and accumulated rainfall data of every raw and bias-corrected dataset over every study period at Langat river basin to give a first impression of the data characterization. It is found that LS-corrected rainfall estimates predict the overall gauged rainfall reasonably well but as for LOCI, this method is less effective for the PERSIANN estimations as it exacerbates the overall rainfall over the basin by 40 – 85% overestimation. Nevertheless, this method is seemed suitable in certain events for TRMM and CMORPH estimations. This might due to the rainfall threshold that we set (1 mm) to ensure that the threshold exceedance matches the wet-day frequency of the observation. Here, sensitivity analysis based on the rainfall threshold is recommended as every region has different geographical condition and the rainfall will never be equally distributed. Thus, the rainfall threshold might be varying from region to region. For PT-corrected rainfall estimates, it is noted that this scheme is much better compared to LOCI, the difference in total rainfall compared to the accumulated gauge observations are less than 20% except for PT-corrected PERSIANN estimation in Event 4, whereby the corrected estimation overestimated the total rainfall over basin by 31%.

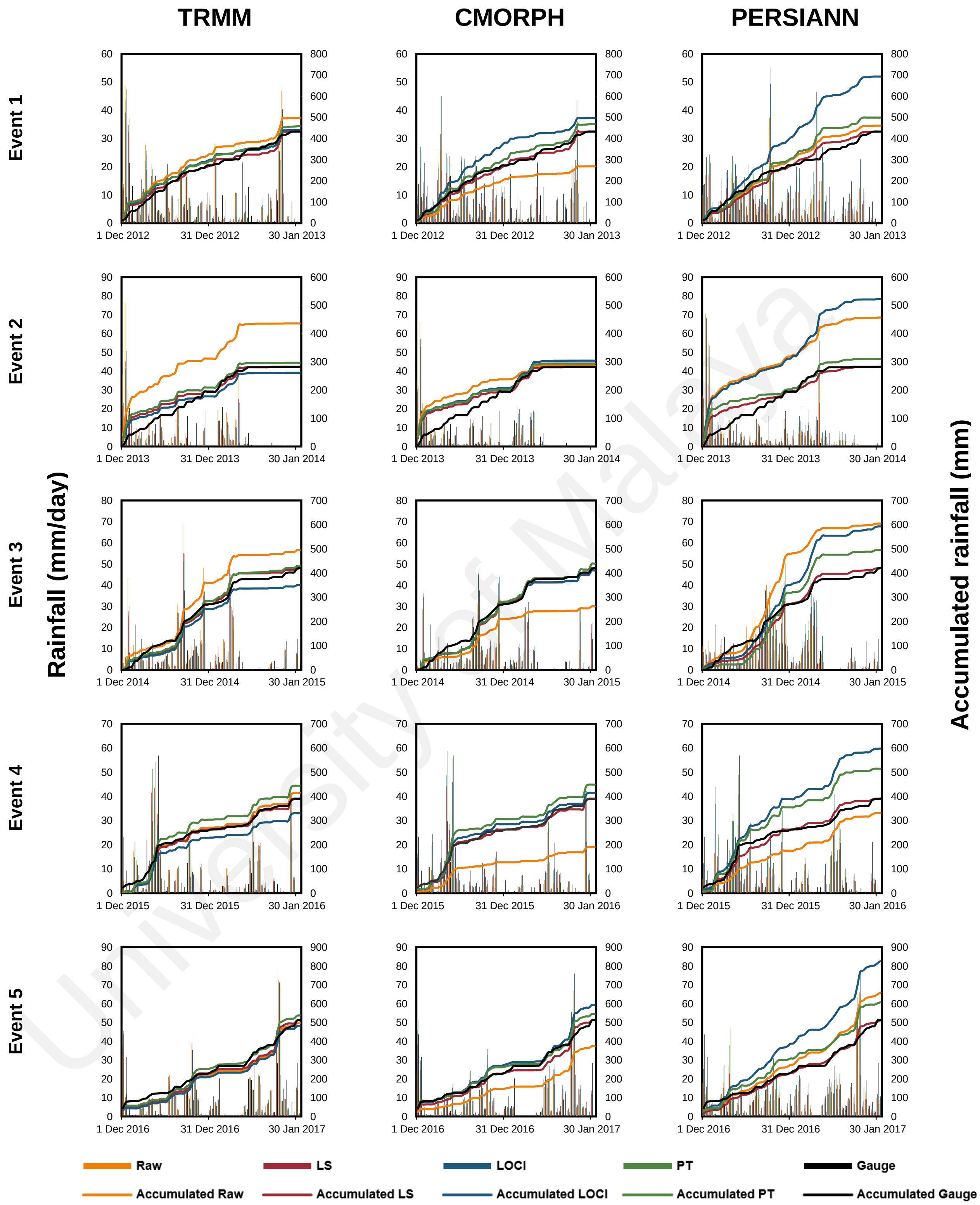

Figure 4.4: Time series of daily rainfall data (mm/day) and daily accumulated rainfall data (mm) of gauge observations, raw and bias-corrected satellite estimations for selected flood events in Langat river basin.

Next, the distribution of the data is evaluated based on the Quantile-Quantile plots (QQ plots) as shown in Figure 4.5 and accompanied by Table 4.5. QQ plot provides a useful comparison of the response of rainfall distribution across various bias-corrected rainfall values. In every QQ plot (Figure 4.5), a 45° reference line is also plotted. If the two sets come from a population with the same distribution, the points should fall approximately along this reference line. The greater the departure from this reference line, the greater the evidence for the conclusion that the two data sets have come from populations with different distributions. Based on Table 4.5, all the BC methods exhibit a significant improvement for TRMM and CMORPH estimations whereas a satisfactory level (0.70 – 0.80) for some selected events are achieved by PERSIANN estimations corrected by LS and LOCI. PT scheme was found to be the best scheme for correcting the distribution of satellite estimations as it adjusted the rainfall data points closer to the reference line with high *NSE* (Nash-Sutcliffe Efficiency) values (> 0.85) in all events.

Table 4.5: Nash-Sutcliffe Efficiency

	Nash-Sutcliffe Efficiency (*NSE*)			
	Raw	LS	LOCI	PT
TRMM				
Event 1	0.96	0.92	0.96	0.99
Event 2	0.78	0.95	0.94	0.98
Event 3	0.94	0.99	0.96	0.99
Event 4	0.62	0.91	0.81	0.97
Event 5	0.93	0.99	0.97	0.99
CMORPH				
Event 1	0.65	0.91	0.97	0.99
Event 2	0.97	0.98	0.98	0.99
Event 3	0.77	0.99	0.98	0.99
Event 4	0.33	0.89	0.87	0.95
Event 5	0.81	0.96	0.97	0.98
PERSIANN				
Event 1	0.74	0.78	0.84	0.97
Event 2	0.84	0.91	0.77	0.99
Event 3	0.86	0.81	0.88	0.94
Event 4	0.35	0.72	0.76	0.88
Event 5	0.80	0.77	0.82	0.95

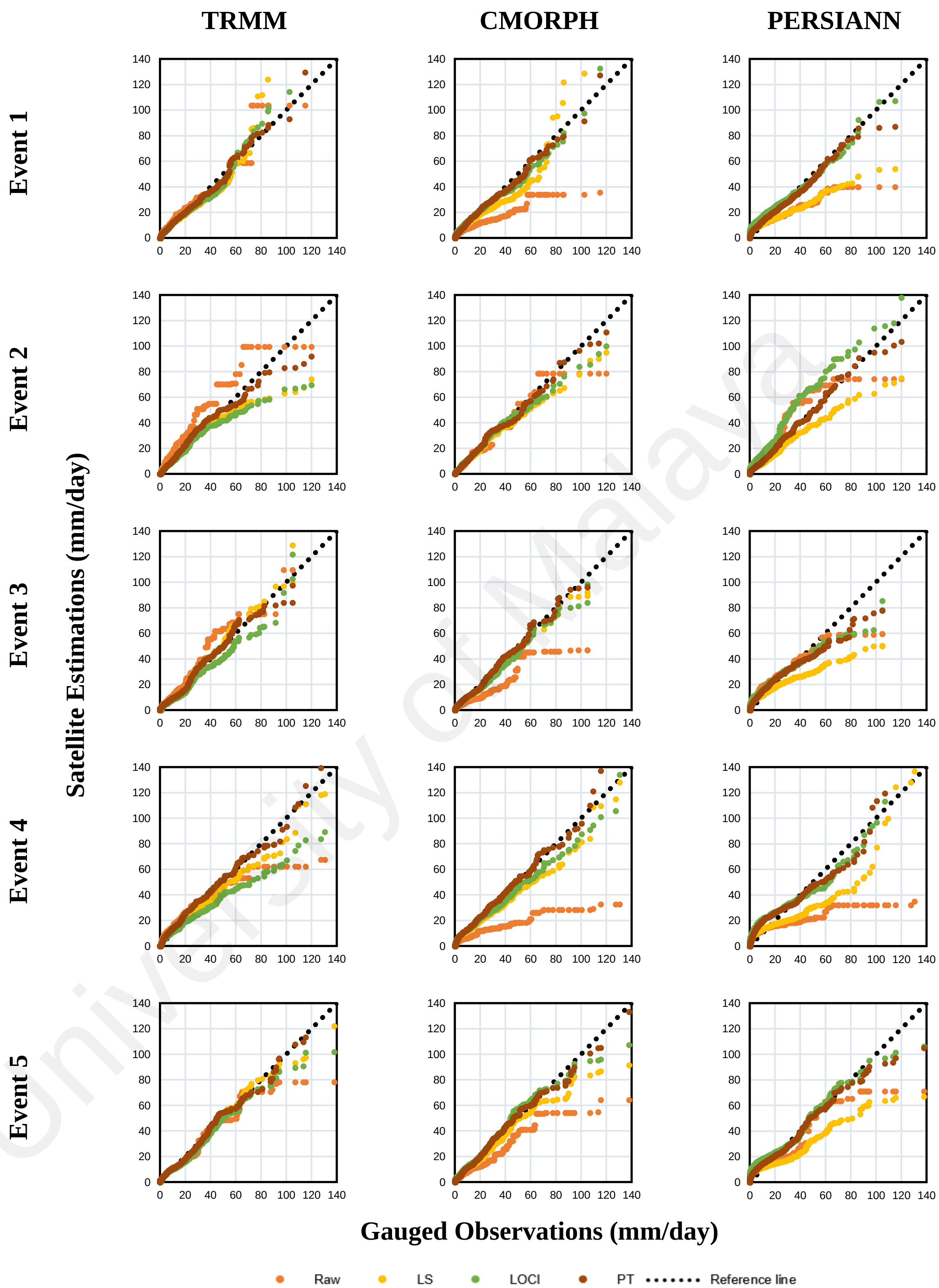

Figure 4.5: Quantile-Quantile plots of raw and corrected satellite estimations versus gauged observations for every flood event in Langat river basin.

4.6.2.2 Statistical performance

In Section 4.5, we described the methods of the BC, that is employed to fit the mean, standard deviation (*SD*) and coefficient of variation (*CV*) for the precipitation data. Figure 4.6 shows several scatter plots for the fitting statistics of all events which imply the observed statistics are plotted versus those of the uncorrected and corrected satellite data. The detailed statistical performances are shown in Table 4.6. Based on the scatter plots, generally, it is observed that LS scheme matches the mean precipitation of every satellite estimation, but it does not correct the biases in *SD* and *CV*. When applying a higher degree BC scheme, such as LOCI and PT schemes, a significant improvement on the *SD* and *CV* were noted as the data points in the scatter plots are almost matches to the gauged observations. PT exhibits greater improvement compared to LOCI. These results are considered as good as the method of BC schemes applied for this study was only intended to correct the aforementioned statistical parameters.

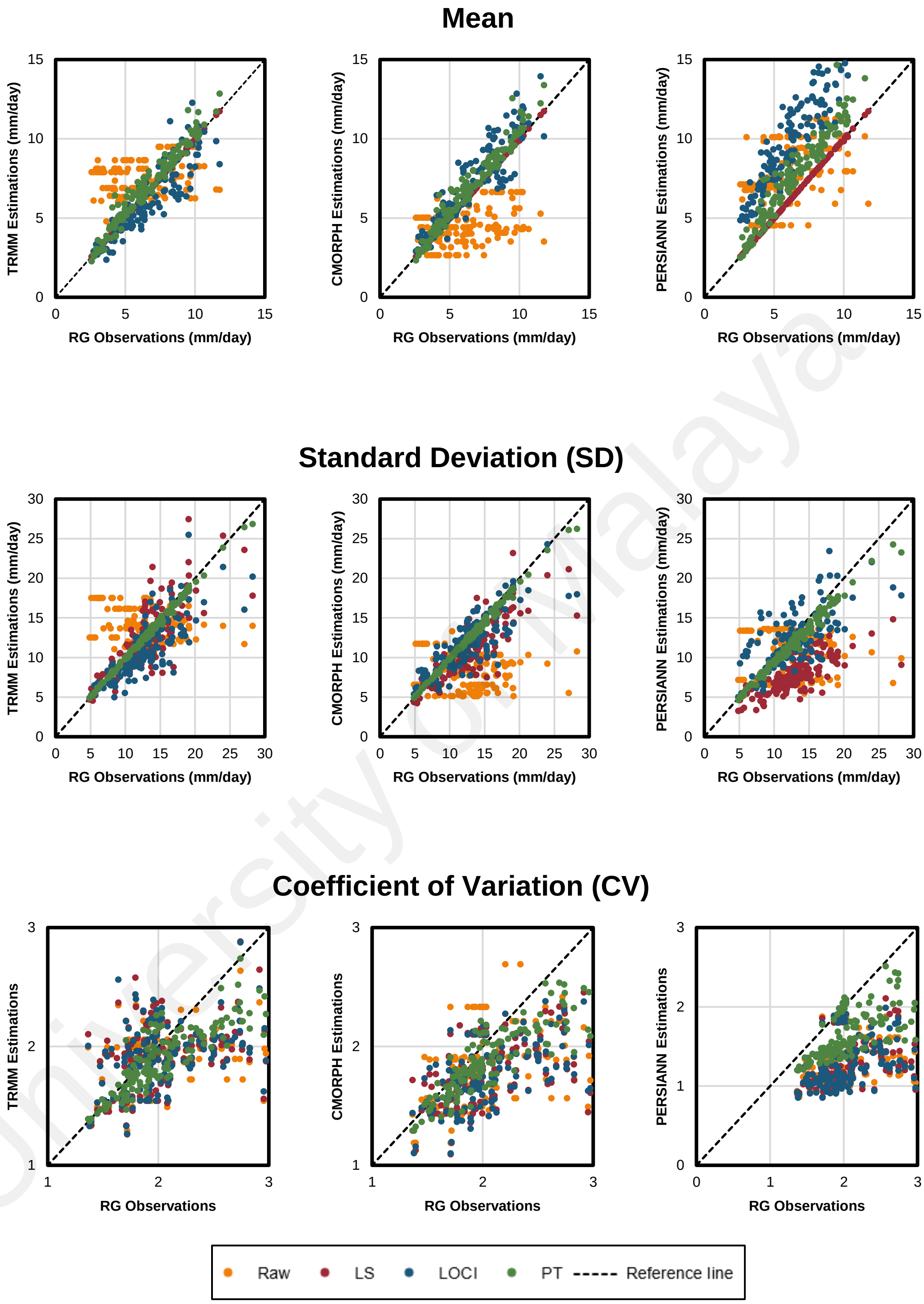

Figure 4.6: Scatter plots of statistics of the rain gauge (RG) precipitation versus raw and corrected satellite precipitation estimations.

Table 4.6: Statistical analysis of original and corrected satellite estimations versus gauged observations at Langat river basin.

SPP	Statistical measures	Mean				SD				CV			
		Raw	LS	LOCI	PT	Raw	LS	LOCI	PT	Raw	LS	LOCI	PT
TRMM	***CC***	0.16	1.00	0.92	0.98	-0.15	0.90	0.87	1.00	0.30	0.36	0.39	0.83
	***PBias* (%)**	14.74	0.01	-8.58	6.54	5.10	-6.85	-15.73	-1.82	-9.21	-7.50	-7.50	-7.84
	***MAE* (mm/day)**	2.11	0.00	0.87	0.50	4.41	2.25	2.59	0.29	0.36	0.35	0.33	0.21
	***RMSE* (mm/day)**	3.06	0.00	1.25	0.78	7.88	3.40	4.51	0.44	0.48	0.45	0.44	0.31
	NRMSE	0.41	0.00	0.21	0.11	0.56	0.27	0.40	0.03	0.25	0.23	0.23	0.16
CMORPH	***CC***	0.15	1.00	0.94	0.99	-0.17	0.93	0.92	1.00	0.34	0.49	0.53	0.84
	***PBias* (%)**	-32.11	-0.02	9.02	7.68	-40.20	-15.22	-8.86	-2.37	-12.97	-15.22	-15.53	-9.26
	***MAE* (mm/day)**	2.50	0.00	0.92	0.55	6.30	2.39	2.05	0.34	0.38	0.37	0.37	0.22
	***RMSE* (mm/day)**	3.60	0.01	1.17	0.82	9.64	3.68	3.62	0.50	0.52	0.50	0.49	0.31
	NRMSE	0.81	0.00	0.16	0.12	1.20	0.32	0.30	0.04	0.29	0.28	0.28	0.17
PERSIANN	***CC***	0.27	1.00	0.94	0.98	-0.16	0.93	0.86	1.00	0.30	0.40	0.39	0.66
	***PBias* (%)**	23.29	-0.03	58.60	19.07	-24.53	-40.46	-5.70	-7.41	-38.93	-39.21	-39.71	-21.72
	***MAE* (mm/day)**	2.42	0.00	3.85	1.26	5.19	5.44	2.55	1.00	0.81	0.82	0.83	0.46
	***RMSE* (mm/day)**	3.40	0.02	4.17	1.64	8.84	6.82	4.06	1.30	0.92	0.92	0.92	0.56
	NRMSE	0.42	0.00	0.40	0.21	0.87	0.85	0.32	0.10	0.73	0.72	0.74	0.34

4.6.3 Variation and sensitivity of parameters

Based on the statistical analysis, the determined parameters or bias factors (*s* for LS scheme, *c* for LOCI scheme as well as *a* and *b* for PT scheme) greatly affecting the corrected daily precipitation value of the extreme flood. However, the statistical analysis does not provide a true answer for the study as hydrological events are subject to great variability and uncertainties. Thus, it is important to evaluate the sensitivity of these parameters based on the selected events of this study. Moreover, it is also important to assess whether these parameters can be applied in a similar event of different time periods (Terink *et al.*, 2010). Figure 4.7 shows the boxplots for every parameter applied throughout the five selected events with the small circles represent the outliers. For LS scheme, the parameter *s* is determined. It is found that most of the rainfall points (for both months of December and January) of TRMM and PERSIANN are multiplied with the parameter *s* around 1.00, which indicates that most of the data points are almost accurate and there is no any significant correction. For CMORPH, most of the parameter *s* are more than 1.00, which means that the actual precipitation is underestimated and thus correction should be applied on the CMORPH data from a dry to a wet condition for every extreme flood event. For LOCI scheme, the parameter *c* was almost in the same range as parameter *s* in LS scheme for TRMM and CMORPH estimations. However, the multiplier is slightly larger for PERSIANN estimation. For PT scheme, there are two parameters, *a* and *b*, which used to correct the mean and the standard deviation or variance of the datasets, respectively. It is noted that the parameter *a* applied on all three estimations varies over every event except for PERSIANN estimation in January. The parameter *a* applied on PERSIANN estimation in January is smaller than 1.00, which means that PERSIANN overestimated the actual rainfall that happened in January over the five flood events.

To address the uncertainty concerning the determined parameters of every scheme, bootstrapping (Tian *et al.*, 2014) is performed for every parameter of the selected BC scheme. Based on the parameters obtained, 1000 random samples are generated and the sampling distribution is visualized using histograms to observe the skewness of the samples. This bootstrapping procedure is repeated for every parameter and every satellite estimation. Figure 4.8 shows one of the histograms for the resampled parameter *s* (bias factor of LS scheme) for January's TRMM estimations. The mean of the original and resampled parameters, as well as the 95% confidence intervals, are shown in Table 4.7. These results can be as a reference for correcting the near-real-time data for further use.

Based on the results, it is noted that the uncertainty ranges of every parameter applied for the month of December are larger compared to that month of January. Thus, careful consideration should be given when improving the satellite rainfall estimations. By comparing the BC scheme, the difference between the original and the resampled mean for the parameter *a* and *b* of PT scheme is much smaller compared to *s* for LS scheme and *c* for LOCI scheme. However, there is still a large uncertainty range for this scheme to be applied in CMORPH (Parameter *b* in January) and PERSIANN estimations (Parameter *a* in January and *b* in December).

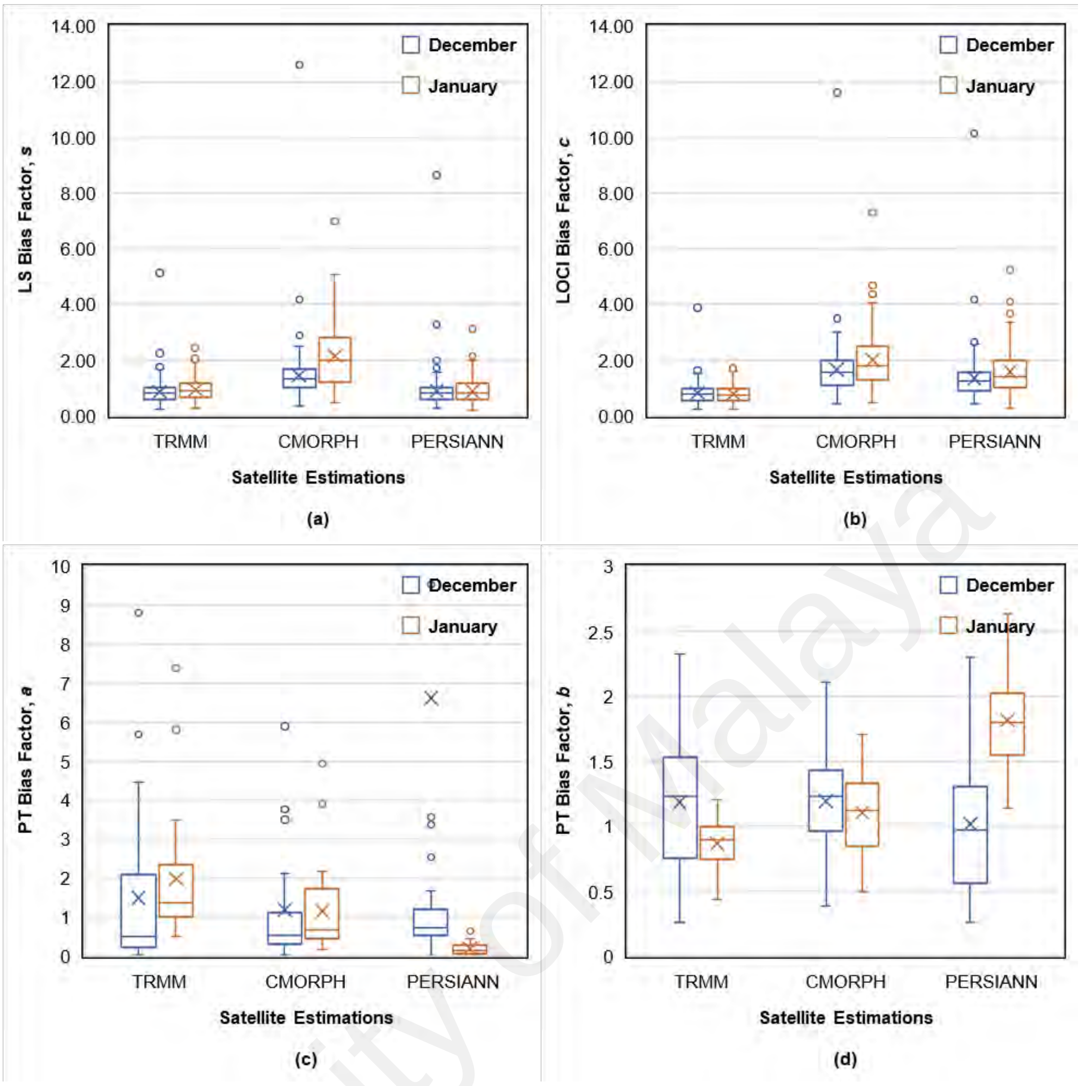

Figure 4.7: Boxplot of the parameters used in BC for every satellite estimation. [(a) Parameter *s* for LS scheme, (b) Parameter *c* for LOCI scheme, (c) Parameters *a* and (d) *b* for PT scheme]

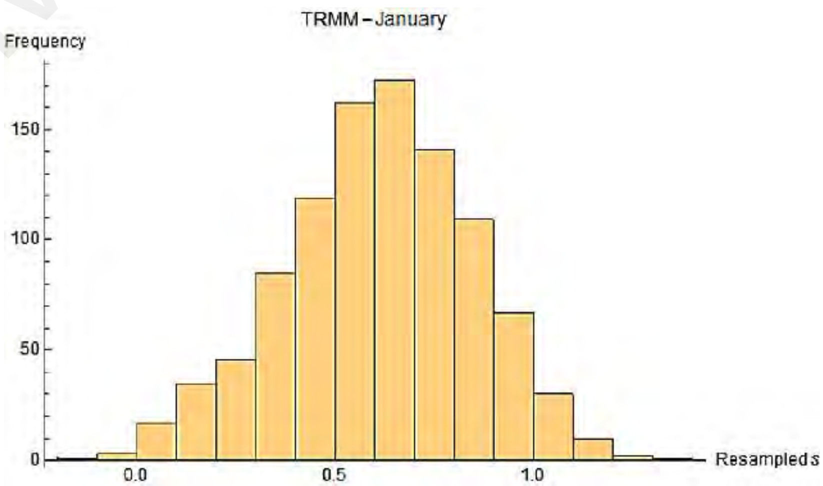

Figure 4.8: Sample histogram of bootstrap values for 1000 random samples.

Table 4.7: The mean, resampled mean and 95% confidence interval (95% CI) for every parameter applied on the SPP.

[For SPP, T- TRMM, C – CMORPH and P – PERSIANN]

Method	Parameter	SPP	December			January		
			Mean	Resampled Mean	95% CI	Mean	Resampled Mean	95% CI
LS	***s***	T	0.86	5.13	[0.38, 5.77]	0.94	2.43	[0.11, 1.04]
		C	1.43	12.62	[0.02, 8.45]	2.15	6.97	[0.53, 1.60]
		P	0.89	8.65	[0.60, 8.98]	0.88	3.11	[0.46, 2.20]
LOCI	***c***	T	0.81	3.88	[0.27, 4.40]	0.78	1.87	[0.36, 1.08]
		C	1.65	11.62	[0.26, 6.62]	2.00	7.29	[0.47, 2.26]
		P	1.34	10.14	[0.41, 6.81]	1.57	5.25	[0.71, 2.11]
PT	***a***	T	1.48	1.82	[0.93, 2.98]	1.97	1.9	[0.65, 3.07]
		C	1.18	1.66	[0.74, 3.04]	1.15	1.68	[0.43, 2.77]
		P	6.62	3.5	[1.55, 5.29]	0.19	1.36	[0.49, 2.26]
	b	T	1.18	0.22	[-0.49, 0.81]	0.86	0.51	[-1.26, 0.26]
		C	1.19	0.12	[-0.49, 0.63]	1.10	-0.09	[-0.75, 0.56]
		P	1.02	-2.56	[-4.17, -0.20]	1.81	0.07	[-0.54, 0.74]

4.7 Summary

Although climatology adjustments or calibrations have been adopted on the algorithm of SPP estimations and improved with inputs of evolving versions, the estimations are still imperfect and their performance varies from region to region, as well as season to season. This chapter presents an application of three BC schemes (LS, LOCI and PT) to improve the accuracy of three satellite estimations (TRMM 3B42 V7, CMORPH, and PERSIANN) at the Langat river basin during the five selected extreme flood events due to NEM specifically in the month of December to January. Studies of BC on satellite estimations in Malaysia are arguably limited and therefore accuracy of this global coverage rainfall data should be assessed according to Malaysia's topography, location, and weather system. The selection of BC methods for this study is considered universal as these methods have been applied in most of the studies. However, due to the rapid evolution of the SPP estimations, as well as changing climate, it is crucial to implement these BC on the latest version of SPP for the extreme events of the Malaysia region.

During the process of BC, we noticed that the parameters or bias factors (*s* for LS scheme, *c* for LOCI scheme as well as *a* and *b* for PT scheme) vary for every flood event even though these floods happened on the same season/ monsoon. Thus, we also evaluate the sensitivity of these parameters to the extreme floods selected and whether these parameters can be applied in a similar event of different time periods.

Based on the findings, all BC schemes are able to improve the satellite estimations. LS-corrected rainfall estimates predict the overall gauged rainfall of the catchment very well. Nevertheless, this method matches well the mean precipitation of every satellite estimation and does not correct the SD and CV of the estimations. For LOCI, in the present study, we set 1 mm as the rainfall threshold to ensure that the threshold exceedance matches the wet-day frequency of the observation. We found that this scheme is suitable for correcting the TRMM and CMORPH estimations in certain flood events but does not suitable for PERSIANN estimations as it overestimated the overall rainfall of the catchment by 40 – 85%. Sensitivity analysis on the setting of the daily rainfall threshold should be carried out. PT scheme offers the best results in this study as it corrects up to the second statistical moment of the frequency distribution such as SD and CV and corrected well the rainfall distribution of satellite estimations.

The outputs of this study will help hydrologists to understand the efficiency and application of satellite estimations data in rainfall-runoff modeling to predict the river discharge in this catchment which may be useful to our water resources management. Also, it is required to devote efforts towards operationalizing the BC algorithms.

CHAPTER 5: PRECISION OF RAW AND BIAS-ADJUSTED SATELLITE PRECIPITATION ESTIMATIONS IN RAINFALL-RUNOFF MODELLING

5.1 Introduction

This chapter presents findings of the final objective, i.e. to simulate rainfall-runoff during 2014-2015 flood events in the Langat river basin based on raw and improved (LS, LOCI and PT) SPP estimations (TRMM, CMORPH, and PERSIANN) that had been discussed in previous chapters. The Hydrological Modelling System (HEC-HMS) is applied to validate the performance of the raw and bias-adjusted SPP that had been discussed in previous chapters with rain gauge model parameters.

5.2 Review on Hydrological Modelling with SPP Estimations

Rainfall data or precipitation is an important input required for water resource management, hydrologic and ecologic modeling, recharge assessment, and irrigation scheduling (Behrangi *et al.*, 2011; Jiang *et al.*, 2018; Mair & Fares, 2010; Su *et al.*, 2008). A plethora of studies estimated the streamflow by using hydrological models with SPP estimations as input. (Dinku *et al.*, 2008; Hong *et al.*, 2006; Hossain & Anagnostou, 2004; Jiang *et al.*, 2018; Li *et al.*, 2018; Nijssen & Lettenmaier, 2004; Worqlul *et al.*, 2017a; Yilmaz *et al.*, 2005).

In China, Tong *et al.* (2014) investigated the streamflow simulation abilities of TRMM, CMORPH, and PERSIANN using the Variable Infiltration Capacity (VIC) hydrologic model in upper Yellow and Yangtze river basins and found that TRMM had comparable performance to the observed data in simulations, whereas the other SPP exhibited little capability for streamflow simulations. In another study, Liu *et al.* (2017) accessed the capability of PERSIANN in the Hydro Informatic Modelling System (HIMS) model for the same rivers as Tong *et al.* (2014). Results concluded that the

PERSIANN-CDR was suitable to simulate reasonably good streamflow in basins of the Tibetan Plateau and also has the potential to be an alternative source of the sparse gauge network for future hydrological and climate change studies. Li *et al.* (2015) simulated TRMM and CMORPH via geomorphology-based hydrological model (GBHM) model for the Yangtze river and concluded that TRMM performed best for annual water budgeting and monthly streamflow simulation. Jiang *et al.* (2012) highlighted that the streamflow simulation results of different precipitation inputs in both spatiotemporal resolutions and accuracy could be somewhat similar through model calibration with each of the input data.

In other regions, Nijssen and Lettenmaier (2004) investigated the effect of satellite-based precipitation sampling error on estimated hydrological fluxes. Using TMPA data, Su *et al.* (2008) investigated the feasibility of TMPA satellite-based precipitation data for hydrologic predictions and concluded that satellite estimates have the potential for hydrologic forecasting particularly with respect to the simulation of seasonal and inter-annual stream-flow variability. Yilmaz *et al.* (2005) investigated the PERSIANN in streamflow forecasting with a lumped hydrologic model (SACramento Soil Moisture Accounting (SAC-SMA) (Burnash, 1995)) over several medium-size basins in the southeastern United States. Results indicated that the accuracy of model simulations depended on the bias in the precipitation estimates and the size of watersheds. Behrangi *et al.* (2011) assessed the effectiveness of five SPP (TRMM-RT, TRMM 3B42 V6, CMORPH, PERSIANN and its adjusted version PERSIANN-adj) using the same model as Yilmaz *et al.* (2005) for streamflow simulation over Illnois river basin and found that these SPP streamflow patterns significantly overestimated over warm months (spring and summer months) and underestimated during cold season. Su *et al.* (2008) investigated the feasibility of TRMM 3B42 Version 6 (V6) for La Plata basin found that the SPP has the potential for hydrologic forecasting but tended to overestimate peak flows. Their extended work (Su *et al.*, 2011) indicated that the relative accuracy and the hydrologic performance of real time-based TRMM (TRMM-RT) streamflow simulations generally improved and suggests considerable potential for hydrologic prediction using purely satellite-derived precipitation estimates in parts of the globe with sparse in-situ observations. Worqlul *et al.* (2017) tested the TRMM 3B42V7 in two semi-distributed hydrological models Hydrologiska Byråns Vattenbalansavdelning (HBV) (Lindström *et al.*, 1997) and Parameter Efficient Distributed (PED) (Steenhuis *et al.*, 2009) for Blue Nile Basin in Ethiopia was not be able to capture the gauged rainfall temporal variation in both watersheds and was not tested further. They suggested that further calibration of the satellite is required before applying. Harris *et al.* (2007) assessed one of the real time products of TRMM (TRMM 3B41RT) for Upper Cumberland River in southeastern Kentucky and indicated that the current level of uncertainty in satellite rainfall warrants caution before institutionalizing its use in operational flood forecasting systems at the basin scale. In order to minimize the model's propensity to produce false prediction of streamflow, they suggested that bias adjustment of satellite rainfall data needs to be identified.

5.3 Methods

5.3.1 Hydrologic Modelling System (HEC-HMS)

HEC-HMS is a hydrologic modeling software developed by the US Army Corps of Engineers Hydrologic Engineering Center (HEC). This physically based and conceptual semi-distributed model is designed to simulate the rainfall-runoff processes in a wide range of geographic areas such as large river basin, water supply, and flood hydrology to small urban and natural watershed runoff. The system encompasses losses, runoff transform, open channel routing, analysis of meteorological data, rainfall-runoff simulation and parameter estimation. HEC-HMS uses separate models to represent each component of the runoff process, including models that compute runoff volume, models of direct runoff, and models of base flow. Each model run combines a basin model, meteorological model and control specifications with run options to obtain results. A schematic diagram for the setup of HEC-HMS for the Langat river basin is shown in Figure 5.1. The selected methods for each component of the runoff process such as runoff depth, direct runoff, base-flow and channel routing in event-based hydrological modeling are discussed in the following section.

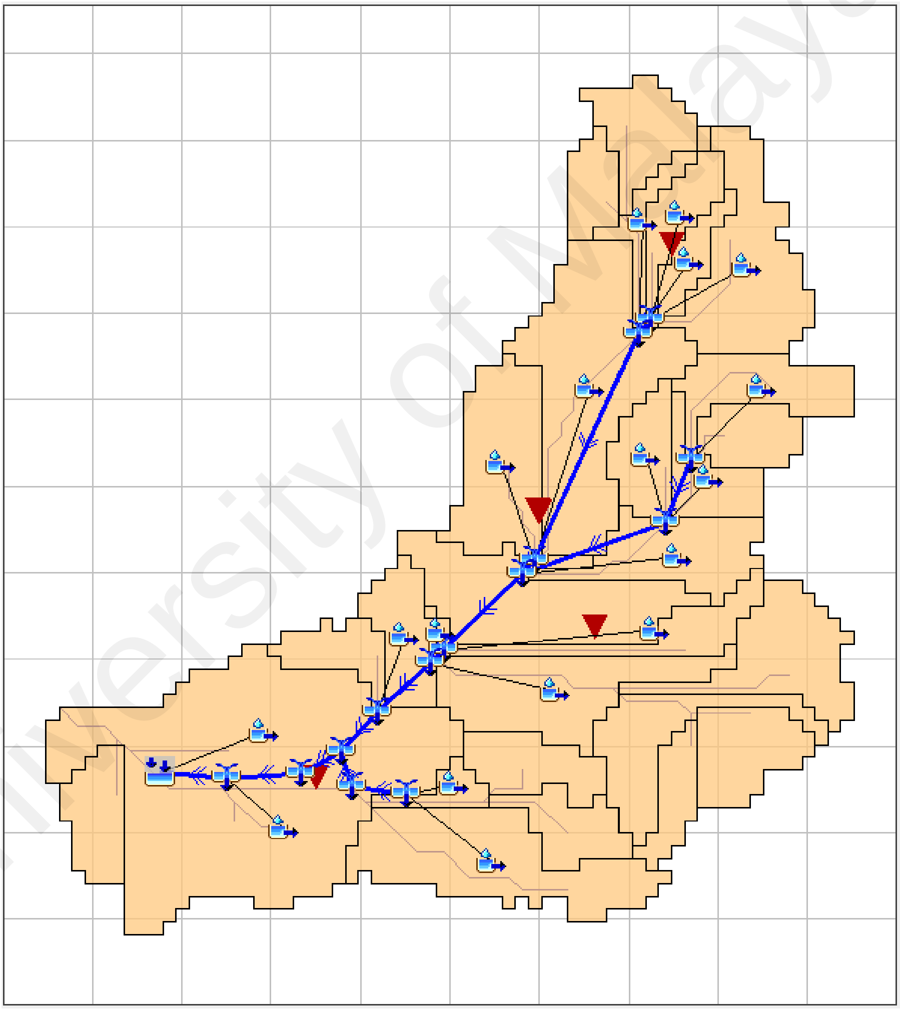

Figure 5.1: Schematic diagram for the setup of HEC-HMS hydrological modeling system.

5.3.2 Soil Conservation Service Curve Number (SCS-CN) method

The SCS-CN loss method is chosen to estimate the accumulated precipitation excess or the runoff of the watershed. This method uses an integration of land use and soil data to determine the runoff curve number, *CN* values of the watershed. The SCS-CN equation is as shown below:

$$Q = \frac{(P - I_a)^2}{(P - I_a) + S} \tag{5.1}$$

where Q = runoff at time t, P =accumulated rainfall depth at time t, I_a = initial abstraction and S = potential maximum retention after runoff begins.

Initial abstraction (I_a) is all losses before runoff begins. This parameter includes water retained in surface depressions, water intercepted by vegetation, evaporation, and infiltration. I_a is highly variable but generally is correlated with soil and cover parameters. Through studies of many small agricultural watersheds, I_a was found to be approximated by the following empirical equation:

$$I_a = 0.2S \tag{5.2}$$

S is known as the potential maximum retention, which can be calculated based on Equation (5.3).

$$S = \frac{25400}{CN} - 254 \text{ (in millimeter)} \tag{5.3}$$

The runoff curve number *CN* in the equation can be estimated based on the hydrological soil group, plant cover, amount of impervious areas, interception, and surface storage of the watershed. The aforementioned parameters can be referred to (Cronshey, 1986). In the case of non-homogenous sub-basins, the *CN* are taken as a weighted value based on different land uses in the study area. Calculation of weighted curve number (*WCN*) is shown by Equation (5.4), where, *WCN* is weighted curve number, A_i is area for *i*th landuse type and CN_i is curve number for *i*th land use type.

$$WCN = \frac{\sum_{i=1}^{i=n} CN_i \cdot A_i}{\sum_{i=1}^{i=n} A_i} \tag{5.4}$$

5.3.3 SCS unit hydrograph method

SCS unit hydrograph is applied for estimating direct runoff. Under this method, the basin lag time (T_{lag}) is the parameter which can be calculated from Equation (5.5).

$$T_{lag} = L^{0.8} \cdot \frac{(S+1)^{0.7}}{1900\sqrt{Y}} \tag{5.5}$$

where *L* is the longest flor path in kilometer, *Y* is the watershed slope in percent and *S* is the potential maximum retention.

5.3.4 Muskingum method

Muskingum method for channel routing is chosen. Under this method, the *X* and *K* parameters must be evaluated. Theoretically, parameter *K* is the time of passing of wave in reach length and parameter *X* is a constant ranging from 0 to 0.5. The parameters can be estimated with the help of observed inflow and outflow hydrographs. Parameter *K* estimated as the interval between similar points on the inflow and outflow hydrographs. Once *K* is estimated, *X* can be estimated by trial and error (USACE-HEC, 2008).

5.3.5 Hydrologic simulation process

This chapter utilizes all rain gauge (RG) observations, raw and bias-adjusted (LS, LOCI and PT-adjusted) SPP datasets starting from 1st December 2014 – 31st January 2015

(62 days) for the flood simulation in Langat river basin. Apart from that, in order to allow the model to reach an "optimal" state, additional RG and SPP data starting from 1st – 30st November 2014 is collected to "warm-up" the model and the same BC processes described in Chapter 4 (Section 4.5) are repeated and produced additional bias-adjusted estimations.

As mentioned in Section 3.5.1, when a limited number of rain gauge (RG) is compared to the satellite products, point-to-grid precipitation is insufficient for the large variability of rain gauge associated to the spatial and temporal resolution of satellite products. Therefore, conversion to a gridded surface from rain gauge data at the same resolution of the satellite data by the interpolation method is applied to overcome the large variability issue (Lo Conti *et al.*, 2014). In Chapter 3, we have compared the trend of mean areal precipitation between five different rainfall interpolation methods for Langat river basin and found that all interpolation methods performed based on RG data exhibit similar pattern with values are quite close across all the methods of any interpolation methods. However, based on the statistical analysis reported in Table 3.4 and Figure 3.10, excluding the result of Arithmetic mean rainfall (as the mean precipitation computed is equally distributed to the whole basin), generally, we noticed that the inverse-distance-weighting (IDW) performed slightly better than other rainfall interpolation results such as Thiessen polygon and Spline in terms of correlation and other statistical indicators such as *NRMSE*. According to Dirks *et al.* (1998), he reported that the inverse-distance-weighting (IDW) method is much accurate and feasible compared to other interpolation methods as it gives consideration to both complexity and calculating time. Therefore, in this case, we adopted the IDW-interpolated RG data to drive the HMS model and optimize the parameter values by comparing the simulated RG streamflow with the observed streamflow gauge station. Finally, the model is then forced by raw and bias-adjusted TRMM, CMORPH and PERSIANN rainfall data are subsequently used to run the model with the RG optimized parameters. Figure 5.2 summarizes the overall hydrologic process simulation for this study.

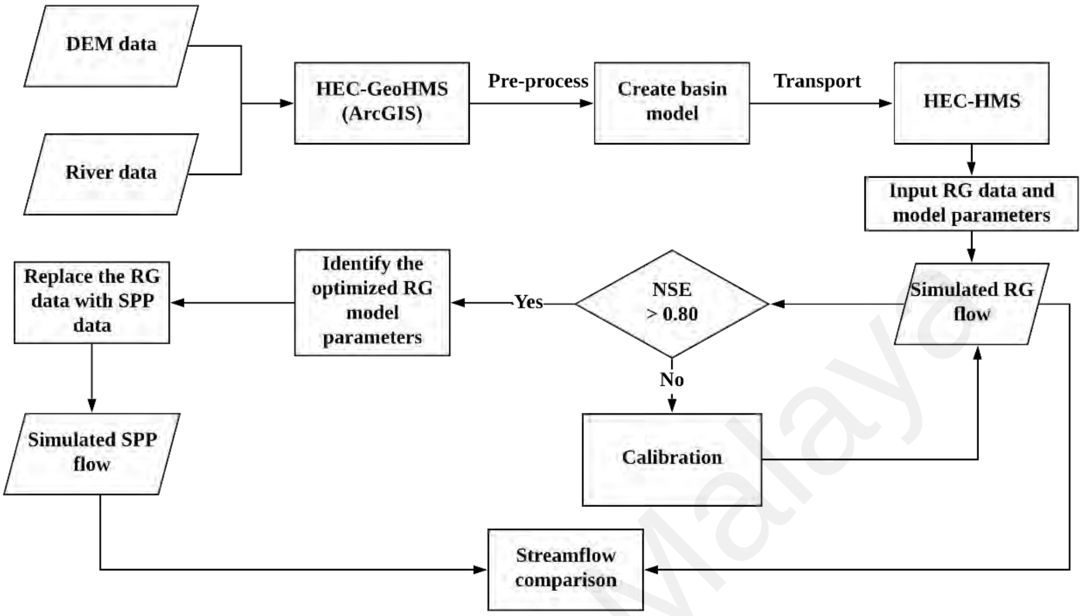

Figure 5.2: Overall hydrologic simulation process

5.3.6 Model Performance Indicators

There is no single model performance indicator that determines the strengths and weaknesses of a particular model. For determining the model performance, five indicators were adopted, including the Nash Sutcliffe Efficiency (*NSE*), percent bias (*PBias*), root mean square error (*RMSE*), mean absolute error (*MAE*) and peak error. *NSE* indicates how well the simulation matches the observation and it ranges between $-\infty$ and 1, with *NSE* =1 meaning a perfect fit. Table 5.1 provides a classification of the performance of *NSE*.

PBias investigates the tendency of over or underestimation of the simulated flow. *RMSE* indicates how closely the modeled discharge predicts the simulated discharge. *MAE* demonstrates the average model prediction error with less sensitivity to large errors.

RMSE and *MAE* values of 0 indicate a perfect fit. Singh *et al.* (2005) state that *RMSE* and *MAE* values less than half the standard deviation of the measured data may be considered low and that either is appropriate for model evaluation. Peak error indicates how close between the peaks of modeled and observed simulations. Equations (5.6) to (5.10) show the aforementioned quantitative evaluations, where Q_o is the mean of observed discharges, and Q_m is modeled discharge. Q_o^t is the observed discharge at time *t*. $Q_{m_{peak}}$ is the modeled peak discharge and $Q_{o_{peak}}$ is the observed peak discharge.

$$NSE = 1 - \frac{\sum_{t=1}^{T}(Q_m^t - Q_o^t)^2}{\sum_{t=1}^{T}(Q_o^t - \overline{Q_o})^2} \quad (5.6)$$

$$PBias = \frac{\sum_{t=1}^{T}(Q_m^t - Q_o^t)}{\sum_{t=1}^{T}(Q_o^t)} \times 100\% \quad (5.7)$$

$$MAE = \frac{\sum_{t=1}^{T}|Q_m^t - Q_o^t|}{n} \quad (5.8)$$

$$RMSE = \sqrt{\frac{\sum_{t=1}^{T}(Q_m^t - Q_o^t)^2}{n}} \quad (5.9)$$

$$\text{Peak Error} = \frac{Q_{m_{peak}} - Q_{o_{peak}}}{Q_{o_{peak}}} \times 100\% \quad (5.10)$$

Table 5.1: Classification of performance of *NSE* of models.

(Moriasi *et al.*, 2007)

NSE	**Classification**
≤ 0.40	Unsatisfactory
0.40 – 0.50	Acceptable
0.50 – 0.65	Satisfactory
0.65 – 0.75	Good
0.75 – 1.00	Very Good

5.4 Results and Discussions

5.4.1 Comparison of SPP rainfall estimates with rain gauge (RG) observations

This section focuses/ recaps on the rainfall comparison at basin scale between raw SPP estimations with IDW-interpolated RG observations for 2014-2015 flood events in Langat river basin that had been discussed in Chapter 3. Apart from that, further comparison with the bias-adjusted SPP estimations were included to observe the effect of bias correction on rainfall datasets at basin scale.

Figure 5.3 shows the comparison of the daily and accumulated rainfall data of every raw and bias-corrected dataset over the focused study period at Langat river basin, accompanied with Table 5.2. Comparing the inverse distance weighting (IDW) interpolated areal rainfall of RG observations with every original SPP estimations, TRMM and PERSIANN overestimated the overall rainfall series by 17.40 and 44.80%, CMORPH underestimated the total rainfall by 31.90%.

In Chapter 4, we had adopted three BC scheme on every SPP. Generally, it was noted that the bias of every SPP was greatly reduced regardless of any BC scheme applied, exceptional for LOCI-TRMM and LOCI-PERSIANN. After performing bias correction on the rainfall datasets, LS-corrected rainfall estimates predict the overall gauged rainfall very well. LOCI-TRMM underestimated the overall areal rainfall by 16.81%, however, compared with other bias-adjusted SPP estimations (including bias-adjusted CMORPH and PERSIANN sets) it obtains the best *MAE* (3.88 mm/day) and *RMSE* (5.97 mm/day). It noted that LOCI was not really suitable for PERSIANN estimations as it exacerbates the overall rainfall over the basin still by about 40% overestimation. However, this method was seemed suitable in certain events for TRMM and CMORPH estimations. This might due to the rainfall threshold that we set (1 mm) to ensure that the threshold exceedance matches the wet-day frequency of the observation.

Table 5.2: Statistical analysis of raw and bias-adjusted SPP versus IDW-interpolated RG observations for the 2014-2015 flood events at Langat river basin

SPP	*CC*	*PBias* (%)	*MAE* (mm/day)	*RMSE* (mm/day)
TRMM	0.76	17.40	4.49	3.85
LS-TRMM	0.81	-0.01	4.10	6.75
LOCI-TRMM	0.79	-16.81	3.88	5.97
PT-TRMM	0.80	-2.10	4.05	6.62
CMORPH	0.71	-31.90	4.22	3.22
LS-CMORPH	0.75	0.00	3.97	6.83
LOCI-CMORPH	0.73	-1.81	3.96	7.00
PT-CMORPH	0.75	4.36	4.12	7.30
PERSIANN	0.42	44.80	7.79	5.94
LS-PERSIANN	0.46	0.00	5.77	8.20
LOCI-PERSIANN	0.48	41.06	7.30	10.38
PT-PERSIANN	0.43	17.77	7.35	10.82

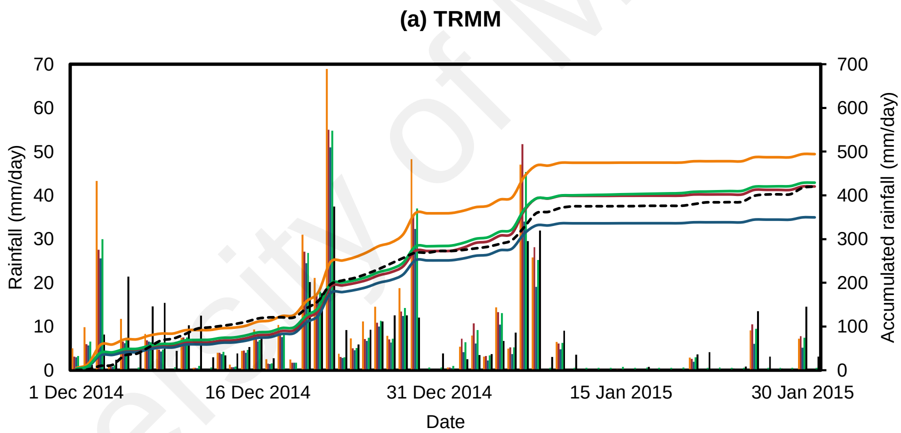

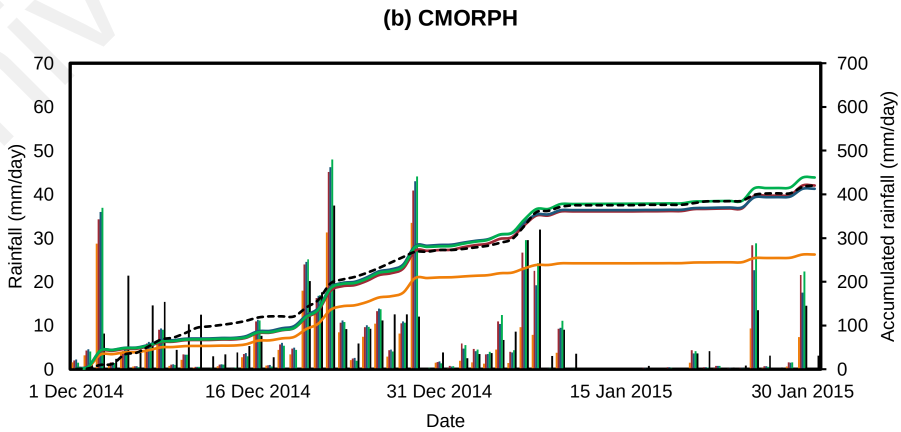

Figure 5.3: Comparison of daily mean precipitation series between interpolated RG observations and selected SPP estimations for 2014-2015 flood events at Langat river basin.

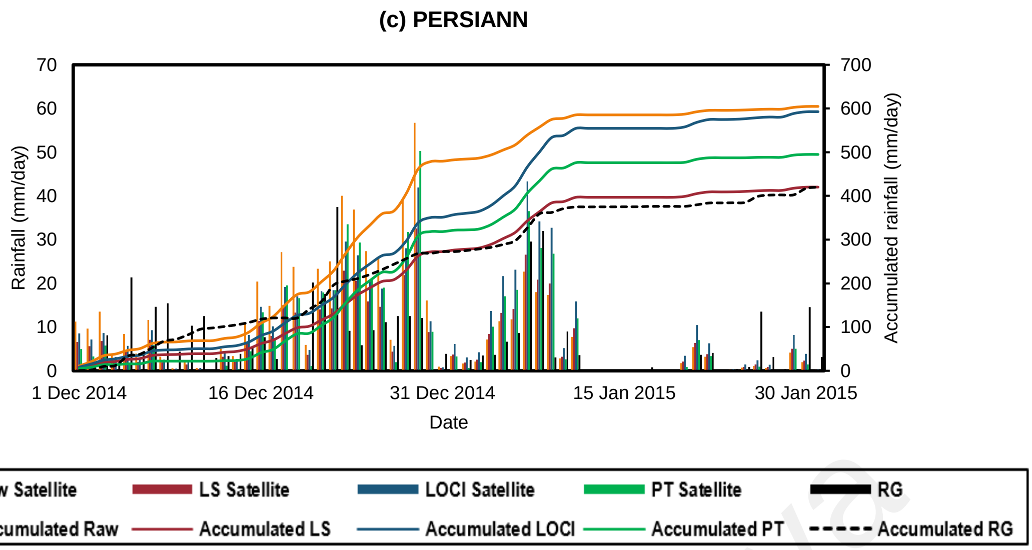

Figure 5.3, continued

5.4.2 Model calibration

In order to assess the runoff predictions obtained from the RG and selected SPP datasets, the daily IDW-interpolated RG rainfall data was first used to drive the HEC-HMS model and optimize the parameter values by comparing the simulated RG streamflow with the observed streamflow gauge station. The objective of the model calibration is to match the RG simulated flow with the observed streamflow from DID and maximize the Nash Sutcliffe Efficiency (*NSE*) (at least 0.8). Among the parameters selected to calibrate the model including the Curve Number (*CN*), Muskingum factor *K* and *X*. As HEC-HMS is an event-based model, we divided the study period into five sub-events, namely Sub-Event A, B, C, D, and E, and the simulation ran and calibrated separately. The optimized parameters of every sub-event are listed in Table 5.3 and Figure 5.4 shows the comparison of simulated and calibrated runoff hydrograph, accompanied by Table 5.4 showing the model performance before and after calibration. It is observed that the optimized parameter in the HEC-HMS model of every sub-event gave values of different runoff hydrograph parameters close to the observed streamflow than that before optimization, with *NSE* ranging from 0.81 – 0.93. From Figure 5.4, sub-event B is the peak event of the overall study period. The statistical analysis of this sub-event gave values of *MAE* and *RMSE* of 96.9 m^3/s and 106.7 m^3/s, respectively. After the optimized values are considered, the performances of *MAE* and *RMSE* have improved to 33.5 m^3/s and 38.9 m^3/s, respectively. A similar case is noted for all other events, the statistical analysis reveals that the optimized model parameters listed in Table 5.3 should be considered in the model to simulate the runoff hydrograph.

Table 5.3: Optimized model parameter sets of HEC-HMS model

Sub-Event	A	B	C	D	E
Start Date	1 Nov 2014	20 Nov 2014	1 Dec 2014	20 Dec 2014	5 Jan 2015
End Date	19 Nov 2014	30 Nov 2014	19 Dec 2014	4 Jan 2015	20 Jan 2015
Imperviousness (%)	9.90%	9.90%	9.90%	9.90%	9.90%
Lag time (minutes)	18.37	18.37	18.37	18.37	18.37
CN	80	90	80	90	90
Initial Abstraction	17.23	17.23	17.23	17.23	17.23
Muskingum K	1	1.5	2	2	1
Muskingum X	0.2	0.1	0.1	0.1	0.2

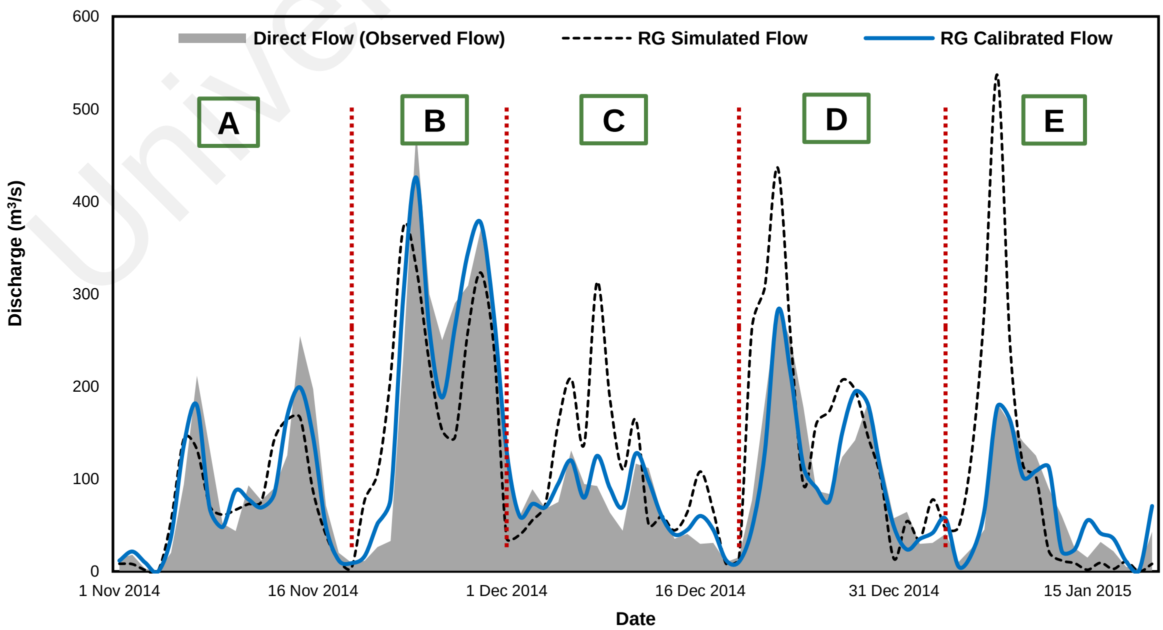

Figure 5.4: Comparison of runoff hydrograph for 2014-2015 flood events

Table 5.4: Calibration result for every sub-event

Sub Event	A	B	C	D	E
Initial Date	1 Nov 2014	20 Nov 2014	1 Dec 2014	20 Dec 2014	5 Jan 2015
End Date	19 Nov 2014	31 Nov 2014	19 Dec 2014	4 Jan 2015	20 Jan 2015
Nash-Sutcliffe (*NSE*)					
Simulated RG	0.60	0.45	-3.25	-0.21	-3.03
Calibrated RG	0.83	0.93	0.81	0.83	0.87
MAE **(m^3/s)**					
Simulated RG	33.2	96.9	54.1	63.6	68.3
Calibrated RG	22.5	33.5	12.4	23.5	15.8
RMSE **(m^3/s)**					
Simulated RG	46.0	106.7	75.2	82.6	114.9
Calibrated RG	30.6	38.9	16.1	30.7	20.6
Peak Discharge (m^3/s)					
Observed SF	254.6	476.4	130.7	286	182
Simulated RG	166.1	371.9	312.5	436.4	537
Calibrated RG	198.9	425.8	130	282	177.5
Peak Error (%)					
Simulated RG	34.8	21.9	139.1	52.6	195.1
Calibrated RG	21.9	10.6	0.5	1.4	2.5

5.4.3 Model Validation using Raw and Bias-adjusted SPP Rainfall Datasets

As discussed in the previous section, the RG precipitation data was first used to derive the HEC-HMS model and optimize parameters against observed streamflow at the outlet. The model was then forced by raw and bias-adjusted TRMM, CMORPH and PERSIANN rainfall data are subsequently used to run the model with the same parameter values listed in Table 5.3 and the simulated runoff by the selected SPP is computed. Figure 5.5 shows the comparison of hydrograph for every raw and bias-adjusted SPP estimation simulated flow. The statistical performance of each raw and bias-adjusted TRMM, CMORPH and PERSIANN simulated flows are presented in Tables 5.5, 5.6 and 5.7, respectively.

5.4.3.1 Simulation of streamflow with raw SPP estimations

Generally, with the rain gauge optimized parameters, the streamflow simulations from all three original SPP do not show comparable results with the RG-calibrated streamflow. The simulations of the raw TRMM and PERSIANN overestimated the overall streamflow series by 23.5% and 19.9% respectively due to their systematic overestimation of precipitation that has been identified in the previous section. On the other hand, CMORPH simulation flow shows an underestimation of 45.6%. Practically, CMORPH performed well compared to TRMM and PERSIANN as it shows the lowest *RMSE* and *MAE* among three SPP simulated flows. This result is consistent with Bitew and Gebremichael (2011). However, referring to Figure 5.5(a) and Table 5.5, it is noted that the original TRMM predicted the peak event (sub-event B) well, with *NSE* = 0.45, *MAE* = 75.1 m^3/s and *RMSE* = 95.7 m^3/s. The other two SPP (CMORPH and PERSIANN) (Tables 5.6 and 5.7) did not predict well the peak streamflow, as negative *NSE* and larger *MAE* and *RMSE* values are shown.

Comparing with other studies, TRMM rainfall had been shown to perform well in certain regions (Javanmard *et al.*, 2010; Moazami *et al.*, 2016; Ochoa *et al.*, 2014; Tian & Peters-Lidard, 2007). However, there are also some regions that do not reflect the performance of TRMM in hydrological simulation (Dinku *et al.*, 2008; Haile *et al.*, 2013). Haile *et al.* (2013) identified that the latest version of TRMM was improved (or bias-adjusted) based on the data from GPCC (Zulkafli *et al.*, 2014), instead of based on rain gauge data. The distribution of the GPCC and the number of stations per grid is scarce and therefore further adjustment has to be done to use TRMM 3B42 rainfall products. On the other hand, the results obtained for PERSIANN streamflow are consistent as Miao *et al.* (2015) conducted a similar study over China. Liu *et al.* (2017) indicated that the PERSIANN-CDR rainfall product has good potential to be a reliable dataset and an alternative information source of a limited gauge network for conducting long-term hydrological and climate studies on the Tibetan Plateau, China.

5.4.3.2 Simulation of streamflow with Bias-adjusted SPP estimations

The performance of the simulated flow using bias-adjusted SPP indicated an improved performance for all three SPP. Based on the above analysis for every SPP, it is found that the BC schemes be able to improve the streamflow simulation especially on the peak events of the study period.

For TRMM simulated flows, as shown in Table 5.5, it is noted that LOCI-corrected TRMM estimations (LOCI-TRMM) was found to be the best estimations compared to LS-TRMM and PT-TRMM, whereby the *NSE*, *MAE*, and *RMSE* had improved from -0.27 to 0.43, 70.1 to 49.8 m^3/s and 101.8 to 68.0 m^3/s, respectively. Based on Figure 5.5(a), this estimation (LOCI-TRMM) has matched the two highest peaks of the overall study period, i.e. in sub-event B (20th November 2014 – 31st November 2014) and sub-event D (20th December 2014 – 4th January 2015).

For CMORPH simulated flows (Figure 5.5(b) and Table 5.6), the bias-adjusted simulated flows are improved equally regardless of any bias correction scheme. Simulation of bias-adjusted CMORPH rainfall estimate using the RG optimized parameters performs well with *NSE* around 0.30 – 0.40, as for the peak event (sub-event B) the *NSE* is ranging from 0.45 – 0.50. However, unlike the bias-adjusted TRMM, all three bias-adjusted CMORPH estimations deteriorate the intermediate simulation flow in sub-event C and D. PERSIANN flows exhibit lowest improvement regardless of which bias correction scheme was adopted on the rainfall estimations (Figure 5.5(c) and Table 5.7). However, it is surprising that the performance of LOCI-PERSIANN indicated a great improvement for sub-event B with NSE = 0.70, MAE = 70.3 m^3/s and $RMSE$ = 57.7 m^3/s.

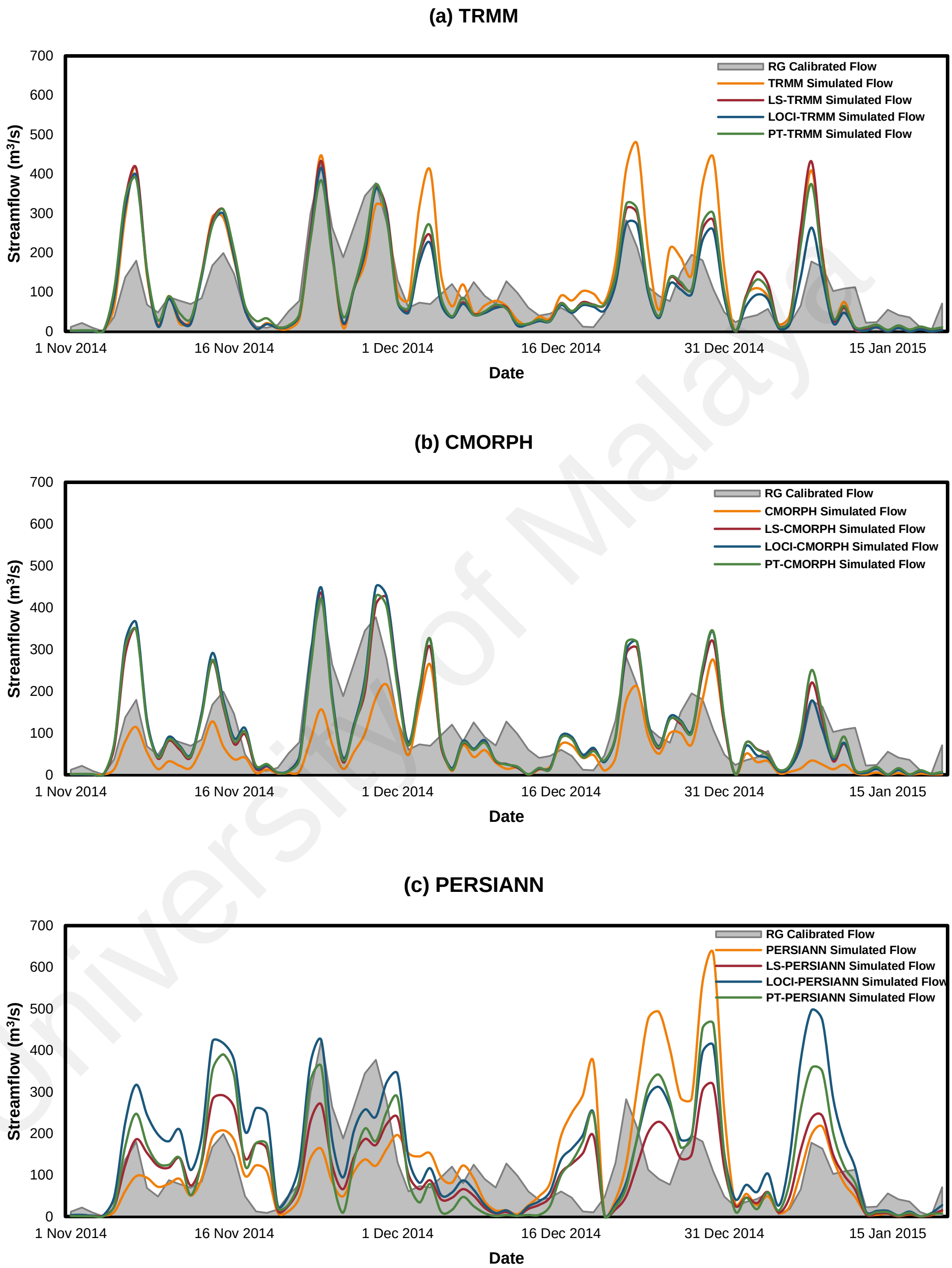

Figure 5.5: Comparison of raw and bias-adjusted (a) TRMM, (b) CMORPH and (c) PERSIANN simulated flow and RG calibrated flow for 2014-2015 flood events at Langat river basin.

Table 5.5: Statistical result for raw and bias-corrected TRMM streamflow

Sub Event	A	B	C	D	E	Overall
Nash-Sutcliffe (*NSE*)						
TRMM	-0.67	0.45	-8.35	-2.46	-1.39	-0.27
LS-TRMM	-0.98	0.55	-2.60	0.04	-1.91	0.21
LOCI-TRMM	-0.66	0.54	-2.17	0.39	0.02	0.43
PT-TRMM	-0.81	0.59	-3.05	-0.05	-0.90	0.28
***MAE* (m^3/s)**						
TRMM	52.6	75.1	69.5	102.3	55.7	70.1
LS-TRMM	57.8	63.6	50.0	57.8	59.3	57.0
LOCI-TRMM	54.1	65.1	48.6	44.0	41.5	49.8
PT-TRMM	57.0	62.9	50.2	59.2	49.0	55.0
***RMSE* (m^3/s)**						
TRMM	79.6	95.7	107.1	134.9	82.6	101.8
LS-TRMM	86.7	86.7	66.5	71.2	91.1	80.4
LOCI-TRMM	79.4	87.3	62.4	56.6	53.0	68.0
PT-TRMM	82.8	82.6	70.5	74.3	73.6	76.6

Table 5.6: Statistical result for raw and bias-corrected CMORPH streamflow

Sub Event	A	B	C	D	E	Overall
Nash-Sutcliffe (*NSE*)						
CMORPH	0.30	-0.84	-3.12	0.11	-0.77	0.03
LS-CMORPH	-0.11	0.45	-4.44	0.06	0.35	0.37
LOCI-CMORPH	-0.39	0.50	-4.87	-0.12	0.37	0.31
PT-CMORPH	-0.19	0.49	-4.73	-0.15	0.35	0.33
***MAE* (m^3/s)**						
CMORPH	37.8	153.8	52.9	49.9	54.6	62.8
LS-CMORPH	44.1	77.0	62.0	50.1	32.3	51.6
LOCI-CMORPH	47.0	75.2	62.8	53.1	29.9	52.3
PT-CMORPH	45.0	76.4	61.0	54.9	31.7	52.3
***RMSE* (m^3/s)**						
CMORPH	51.4	175.5	71.1	68.3	71.0	88.9
LS-CMORPH	64.8	95.8	81.8	70.4	42.9	71.7
LOCI-CMORPH	72.7	91.6	84.9	76.6	42.2	74.7
PT-CMORPH	67.2	92.5	83.9	77.9	42.9	73.7

Table 5.7: Statistical result for raw and bias-corrected PERSIANN streamflow

Sub Event	A	B	C	D	E	Overall
Nash-Sutcliffe (*NSE*)						
PERSIANN	0.42	-0.60	-12.93	-10.05	0.55	-1.45
LS-PERSIANN	-0.58	0.19	-4.29	-1.19	0.30	0.08
LOCI-PERSIANN	-4.91	0.70	-7.77	-2.82	-6.70	-1.06
PT-PERSIANN	-1.75	0.25	-7.11	-3.90	-1.78	-0.62
***MAE* (m^3/s)**						
PERSIANN	47.1	163.7	130.8	241.2	35.7	141.1
LS-PERSIANN	77.4	116.6	80.6	107.3	44.8	86.3
LOCI-PERSIANN	149.7	70.3	103.8	141.8	148.3	129.5
PT-PERSIANN	102.1	111.8	99.8	160.6	89.0	114.6
***RMSE* (m^3/s)**						
PERSIANN	34.0	141.3	94.4	178.4	29.8	90.4
LS-PERSIANN	58.0	96.3	65.4	81.7	36.7	65.4
LOCI-PERSIANN	121.8	57.7	80.2	108.2	95.3	95.4
PT-PERSIANN	77.5	87.2	82.3	114.4	61.7	84.1

The effect of bias correction of rainfall data on the simulation flow was also evaluated using the daily flow duration curves to assess the ability in simulating different ranges of streamflow and its probability of occurrence. The flow duration curves for streamflow simulated with RG, raw and bias-adjusted rainfall were plotted as shown in Figure 5.6.

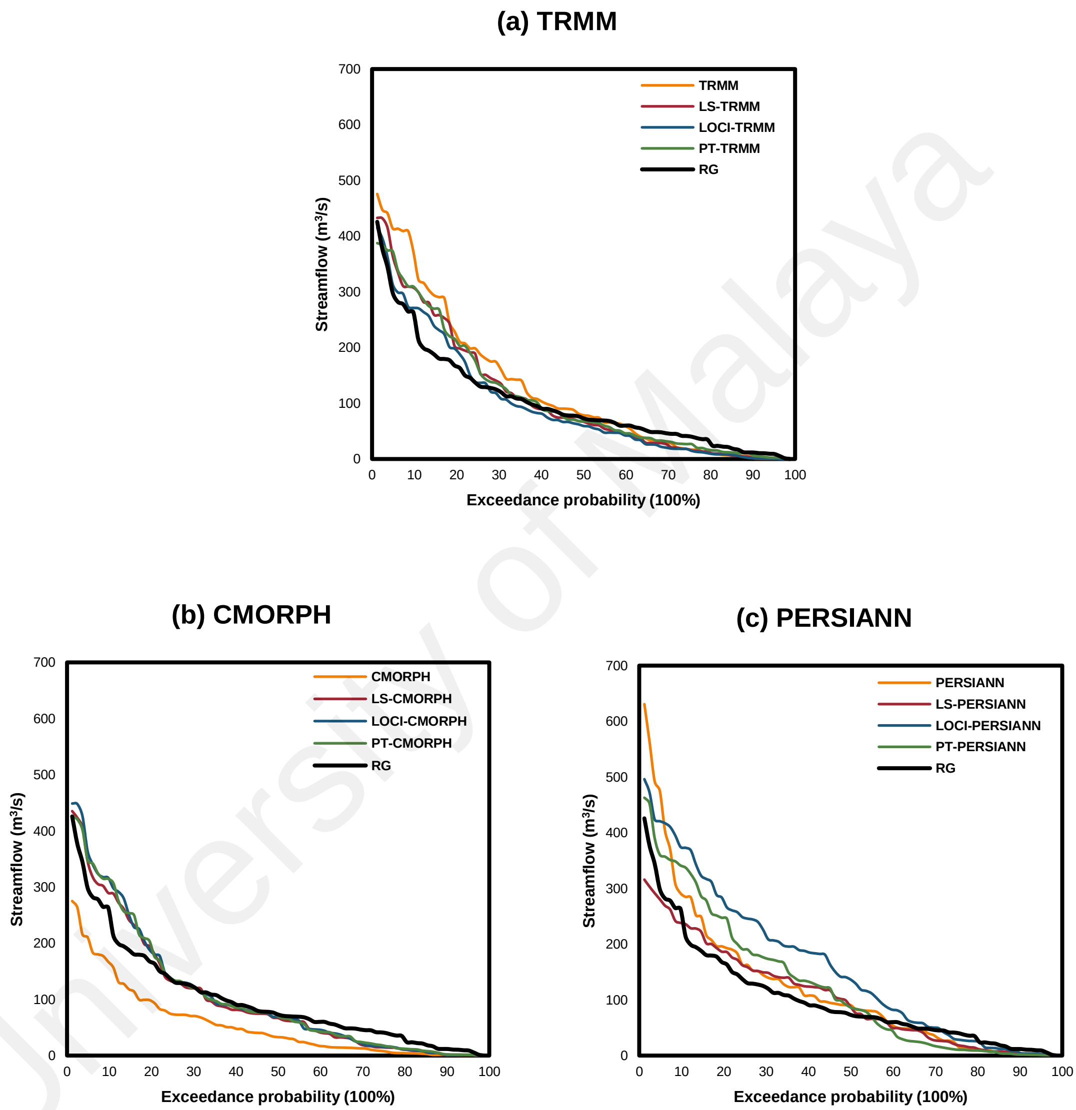

Figure 5.6: Flow duration curves of raw and bias-adjusted SPP simulated flows.

Based on the flow duration curves of original TRMM and its bias-adjusted data sets plotted (Figure 5.6a), it is observed that the streamflow simulated using LOCI-TRMM data followed closely the RG flow distribution even though there is a tendency of overestimating the streamflow at the range of 150 – 250 m^3/s. This overestimation of streamflow could be due to the inaccurate simulation in the wet day frequencies during bias correction (Smitha *et al.*, 2018).

For CMORPH (Figure 5.6b), the streamflow distribution simulated with the LS, LOCI and PT methods are almost similar. This proven that the streamflow analysis is correct. Based on Figure 5.6(b), all bias-adjusted CMORPH streamflow indicate an overestimation at high stream flows (more than 200 m^3/s). As for PERSIANN (Figure 5.6c), the LOCI and PT-PERSIANN streamflow distribution are deteriorated whereby the tendency of overestimation of streamflow is higher compared to the original PERSIANN distribution. In this case, LS-PERSIANN is the best among the three bias-adjusted PERSIANN data.

Based on the general result, there is room for improvement in order to adopt these bias-adjusted SPP estimations for flood prediction. Li *et al.* (2018) commented that the calibrated parameters of the model have a tendency to be affected by the correlations between model parameters and observed data. Thus, it is recommended to the use all raw and bias-adjusted SPP as the forcing inputs to recalibrate the HEC-HMS model and then for validation as in the same periods aimed at examining the influence of satellite precipitation datasets uncertainty on streamflow simulations. Apart from that, we may examine the difference between the RG optimized model parameters and all raw and bias-adjusted SPP optimized model parameters.

5.5 Summary

Accurate and reliable precipitation data are the basis for hydro-climatological studies. SPP estimations have provide alternative precipitation data for regions with sparse rain gauge measurements. Despite the continuing great efforts to develop fine resolution SPP, the errors of SPP estimates cannot be removed completely because the characteristics of the retrieval errors vary in different climatic regions, seasons, and surface conditions (Sorooshian *et al.*, 2011). In this chapter, we investigated the capability of raw and bias-adjusted SPP estimations with rain gauge model parameters in the HEC-HMS model for the 2014-2015 flood events in Langat river basin.

Comparing the three original SPP estimations (TRMM, CMORPH, and PERSIANN) simulated flow with RG optimized parameters, the simulations of the raw TRMM and PERSIANN overestimated the overall streamflow series and CMORPH simulation flow show an underestimation of 45.6%. TRMM had the potential to predict the peak streamflow although CMORPH shows the best performance in general.

Next, we simulate the rainfall-runoff by replacing with the bias-adjusted SPP estimations. Precipitation correction methods have more significant influence during the high rainfall event especially LOCI-adjusted TRMM. For PERSIANN-simulated flow, the BC schemes able to improve the discharge simulation but only to a certain extent. Based on the general result, it is indicated that the current level of uncertainty in SPP estimations is still imperfect before institutionalizing its use in operational flood forecasting systems at the basin scale. As the calibrated parameters are affected by correlations between model parameters and observed data. To avoid the calibration effects of different datasets, cross-validation of different datasets is required.

CHAPTER 6: CONCLUSIONS AND RECOMMENDATIONS

6.1 Introduction

Reliable precipitation is critical in any climatic analysis as well as for the verification of climate model simulations. SPP have provided an alternative for precipitation measures due to its large-scale approach. Although climatology adjustments or calibrations have been adopted on the algorithm of SPP estimations and improved with inputs of evolving versions, the current estimations are still imperfect and their performance varies from region to region, and probably season to season. The verification of SPP, bias-adjustment, and application of the rainfall estimates into hydrological modeling for extreme floods happened in Malaysia's river basin are the main aspects of this research and the conclusions are drawn according to the objectives.

6.2 Verification of Spatial Interpolation Methods of Rain Gauge Network

In order to examine the spatial distribution of satellite precipitation products, daily observed rainfall data are obtained representing the three different river basins, i.e. Kelantan, Langat and Johor river basin situated at the northern, western and southern part of Peninsular Malaysia. Several spatial interpolation methods, i.e. AM, TP, IDW, OK and SP methods are evaluated to examine the effect of different spatial interpolation methods on the observed data before comparing it with the grid-based SPP estimations. The result indicates that the areal precipitations transformed by these interpolation methods give a slight varies in values but overall it is comparable. Even though the AM-estimated peak rainfall for the Kelantan river basin is too far away from other methods, the output of these five selected rainfall interpolation methods can be adopted on the rain gauge observations before comparing with the gridded SPP estimations.

6.3 Validation of SPP at Different Geographic Location of Peninsular Malaysia

For the next objective, the performance of satellite precipitation products (SPP) during extreme floods at three different geographic locations of selected river basins in Peninsular Malaysia is investigated with the interpolated rain gauge observations as a reference. For this objective, the following conclusions are drawn.

- All SPP are able to capture extreme events of heaviest rainfall with acceptable accuracy.
- Comparing among those three river basins, extreme events in the Kelantan river basin is better captured by all SPP compared to the other basins. This might be due to its geographic location of which near to the South China Sea so that it is directly exposed to heavy rainfall during the northeast monsoon.
- The performance has decreased as monsoon moving away towards the west and south that hit Langat and Johor river basin.
- The categorical indexes indicate that TRMM showed the best performance in terms of accuracy whereas PERSIANN had higher capability in detecting rainfall.
- During the flood events, all SPP show slightly better accuracy and rain detection capability in Langat river basin compared with the other two basins.

6.4 Evaluation of Bias-Adjusted SPP Estimations

For the third objective of this research, an application of three BC schemes (LS, LOCI and PT) was presented to improve the accuracy of three satellite estimations (TRMM 3B42 V7, CMORPH and PERSIANN) at Langat river basin during five different extreme flood events due to NEM specifically during the month of December to January. This section is unique as studies regarding the BC on SPP estimations in Malaysia appear to be limited. Based on the findings, the following conclusion are drawn.

- LS-corrected rainfall estimates predict the overall gauged rainfall of the catchment very well. Nevertheless, this method matches well the mean precipitation of every satellite estimation and does not correct the SD and CV of the estimations.
- For LOCI, in the present study, we set 1 mm as the rainfall threshold to ensure that the threshold exceedance matches the wet-day frequency of the observation. We found that this scheme is suitable for correcting the TRMM and CMORPH estimations in certain flood events but does not suitable for PERSIANN estimations as it overestimated the overall rainfall of the catchment by 40 – 85%.
- PT scheme offers the best results in this study as it corrects up to the second statistical moment of the frequency distribution such as SD and CV and corrected well the rainfall distribution of satellite estimations.

6.5 Rainfall-runoff using Raw and Bias-Adjusted SPP Estimations

For the final objective of this research, the raw and bias-adjusted SPP were applied in the HEC-HMS with the rain gauge optimized parameters for the 2014-2015 flood events in Langat river basin. The following conclusion are drawn.

- The original TRMM and PERSIANN simulated flow overestimated the overall streamflow series and CMORPH simulation flow show an underestimation. TRMM had the potential to predict the peak streamflow although CMORPH shows the best performance in general.

- The bias adjustment of precipitation has significant influence during the high rainfall event especially LOCI-adjusted TRMM. For PERSIANN-simulated flow, the BC schemes able to improve the discharge simulation but only to a certain extent.
- Based on the general result, we indicated that the current level of uncertainty in SPP estimations are still imperfect before institutionalizing its use in operational flood forecasting systems at the basin scale as the calibrated parameters were affected by correlations between model parameters and observed data. To avoid the calibration effects of different datasets, cross-validation of different datasets is required.

6.6 Recommendations and Future Perspectives

This research reveals that the current SPP need to be improved over the Malaysia region, particularly during extreme events happened. Based on the conclusions derived above, it is important to highlight that the spatial and temporal uncertainties may exist when comparing different SPP with the ground observations. Although bias-adjustments were done on all three SPP, there is room for improving these bias-adjusted SPP. Therefore, it is required to devote efforts towards operationalizing the bias correction algorithms.

Apart from that, the current verification has been conducted using limited data. Further verification may be conducted with additional data and products and using finer temporal and spatial scales for the utility of SPP in flood forecasting. Also, the bias-adjustment technique could be further explored as additional data becomes available. Longer sets of concurrent data between the SPP and rain gauge observation may provide a better estimate of bias correction which could be applied for improved flood forecasting.

REFERENCES

Abdulkareem, J. H., Pradhan, B., Sulaiman, W. N. A., & Jamil, N. R. (2018). Review of studies on hydrological modelling in Malaysia. *Modeling Earth Systems and Environment, 4*(4), 1577-1605. doi:10.1007/s40808-018-0509-y

Abera, W., Brocca, L., & Rigon, R. (2016). Comparative evaluation of different satellite rainfall estimation products and bias correction in the Upper Blue Nile (UBN) basin. *Atmospheric Research, 178-179*(Supplement C), 471-483. doi:10.1016/j.atmosres.2016.04.017

AghaKouchak, A., Behrangi, A., Sorooshian, S., Hsu, K., & Amitai, E. (2011). Evaluation of satellite-retrieved extreme precipitation rates across the central United States. *Journal of Geophysical Research: Atmospheres, 116*(D2). doi:10.1029/2010JD014741

Ajaaj, A. A., Mishra, A. K., & Khan, A. A. (2016). Comparison of BIAS correction techniques for GPCC rainfall data in semi-arid climate. *Stochastic Environmental Research and Risk Assessment, 30*(6), 1659-1675. doi:10.1007/s00477-015-1155-9

Akasah, Z. A., & Doraisamy, S. V. (2015). 2014 Malaysia flood: Impacts & factors contributing towards the restoration of damages. *Journal of Scientific Research and Development, 2*(14), 53-59.

Akbari, A., Othman, F., & Abu Samah, A. (2011). Probing on suitability of TRMM data to explain spatio-temporal pattern of severe storms in tropic region. *Hydrology and Earth System Sciences Discussions, 8*(5), 9435-9468. doi:10.5194/hessd-8-9435-2011

Alazzy, A. A., Lu, H., Chen, R., Ali, A. B., Zhu, Y., & Su, J. (2017). Evaluation of Satellite Precipitation Products and Their Potential Influence on Hydrological Modeling over the Ganzi River Basin of the Tibetan Plateau. *Advances in Meteorology, 2017*, 23. doi:10.1155/2017/3695285

Anagnostou, E. N., Krajewski, W. F., Seo, D.-J., & Johnson, E. R. (1998). Mean-Field Rainfall Bias Studies for WSR-88D. *Journal of Hydrologic Engineering, 3*(3), 149-159. doi:10.1061/(ASCE)1084-0699(1998)3:3(149)

Anagnostou, E. N., Maggioni, V., Nikolopoulos, E. I., Meskele, T., Hossain, F., & Papadopoulos, A. (2010). Benchmarking high-resolution global satellite rainfall products to radar and rain-gauge rainfall estimates. *IEEE Transactions on Geoscience and Remote Sensing, 48*(4), 1667-1683.

Anctil, F., Lauzon, N., Andréassian, V., Oudin, L., & Perrin, C. (2006). Improvement of rainfall-runoff forecasts through mean areal rainfall optimization. *Journal of Hydrology, 328*(3–4), 717-725. doi:10.1016/j.jhydrol.2006.01.016

Bajracharya, S. R., Palash, W., Shrestha, M. S., Khadgi, V. R., Duo, C., Das, P. J., & Dorji, C. (2015). Systematic Evaluation of Satellite-Based Rainfall Products over the Brahmaputra Basin for Hydrological Applications. *Advances in Meteorology, 2015*, 17. doi:10.1155/2015/398687

Behrangi, A., Khakbaz, B., Jaw, T. C., AghaKouchak, A., Hsu, K., & Sorooshian, S. (2011). Hydrologic evaluation of satellite precipitation products over a mid-size basin. *Journal of Hydrology, 397*(3–4), 225-237. doi:10.1016/j.jhydrol.2010.11.043

Bennartz, R., & Petty, G. W. (2001). The sensitivity of microwave remote sensing observations of precipitation to ice particle size distributions. *Journal of Applied Meteorology*, *40*(3), 345-364.

Bitew, M., & Gebremichael, M. (2011). Assessment of satellite rainfall products for streamflow simulation in medium watersheds of the Ethiopian highlands. *Hydrology and Earth System Sciences, 15*(4), 1147-1155.

Boushaki, F. I., Hsu, K.-L., Sorooshian, S., Park, G.-H., Mahani, S., & Shi, W. (2009). Bias Adjustment of Satellite Precipitation Estimation Using Ground-Based Measurement: A Case Study Evaluation over the Southwestern United States. *Journal of Hydrometeorology, 10*(5), 1231-1242. doi:10.1175/2009jhm1099.1

Burnash, R. (1995). The NWS river forecast system-catchment modeling. *Computer models of watershed hydrology, 188*, 311-366.

Buytaert, W., Celleri, R., Willems, P., Bièvre, B. D., & Wyseure, G. (2006). Spatial and temporal rainfall variability in mountainous areas: A case study from the south Ecuadorian Andes. *Journal of Hydrology, 329*(3–4), 413-421. doi:10.1016/j.jhydrol.2006.02.031

Chang, A. T., & Chiu, L. S. (1999). Nonsystematic errors of monthly oceanic rainfall derived from SSM/I. *Monthly weather review*, *127*(7), 1630-1638.

Chen, J., Brissette, F. P., Chaumont, D., & Braun, M. (2013a). Finding appropriate bias correction methods in downscaling precipitation for hydrologic impact studies over North America. *Water Resources Research, 49*(7), 4187-4205. doi:10.1002/wrcr.20331

Chen, J., Brissette, F. P., Chaumont, D., & Braun, M. (2013b). Performance and uncertainty evaluation of empirical downscaling methods in quantifying the climate change impacts on hydrology over two North American river basins. *Journal of Hydrology, 479*(Supplement C), 200-214. doi:10.1016/j.jhydrol.2012.11.062

Chen, S., Liu, H., You, Y., Mullens, E., Hu, J., Yuan, Y., . . . Hong, Y. (2014). Evaluation of High-Resolution Precipitation Estimates from Satellites during July 2012 Beijing Flood Event Using Dense Rain Gauge Observations. *PLOS ONE, 9*(4), e89681. doi:10.1371/journal.pone.0089681

Ciabatta, L., Brocca, L., Massari, C., Moramarco, T., Gabellani, S., Puca, S., & Wagner, W. (2016). Rainfall-runoff modelling by using SM2RAIN-derived and state-of-the-art satellite rainfall products over Italy. *International Journal of Applied Earth Observation and Geoinformation, 48*, 163-173. doi:10.1016/j.jag.2015.10.004

The Climate Data Guide: GPCC: Global Precipitation Climatology Centre. Retrieved from https://climatedataguide.ucar.edu/climate-data/gpcc-global-precipitation-climatology-Center

Collischonn, B., Collischonn, W., & Tucci, C. E. M. (2008). Daily hydrological modeling in the Amazon basin using TRMM rainfall estimates. *Journal of Hydrology, 360*(1–4), 207-216. doi:10.1016/j.jhydrol.2008.07.032

Creutin, J. D., & Obled, C. (1982). Objective analyses and mapping techniques for rainfall fields: An objective comparison. *Water Resources Research, 18*(2), 413-431. doi:10.1029/WR018i002p00413

Cronshey, R. (1986). *Urban hydrology for small watersheds*. Retrieved from

Cruz, F., Narisma, G., Villafuerte Ii, M., Chua, K. C., & Olaguera, L. (2013). A climatological analysis of the southwest monsoon rainfall in the Philippines. *Atmospheric research, 122*, 609-616.

Dale, W. L. (1974). The rainfall of Malaya, Part II. *The climate of west Malaysia and Singapore*, 145.

de Coning, E. (2013). Optimizing Satellite-Based Precipitation Estimation for Nowcasting of Rainfall and Flash Flood Events over the South African Domain. *Remote Sensing, 5*(11), 5702-5724. Retrieved from http://www.mdpi.com/2072-4292/5/11/5702

Derin, Y., & Yilmaz, K. K. (2014). Evaluation of Multiple Satellite-Based Precipitation Products over Complex Topography. *Journal of Hydrometeorology, 15*(4), 1498-1516. doi:10.1175/jhm-d-13-0191.1

Devia, G. K., Ganasri, B. P., & Dwarakish, G. S. (2015). A Review on Hydrological Models. *Aquatic Procedia, 4*, 1001-1007. doi:10.1016/j.aqpro.2015.02.126

Di Piazza, A., Conti, F. L., Noto, L. V., Viola, F., & La Loggia, G. (2011). Comparative analysis of different techniques for spatial interpolation of rainfall data to create a serially complete monthly time series of precipitation for Sicily, Italy. *International Journal of Applied Earth Observation and Geoinformation, 13*(3), 396-408. doi:10.1016/j.jag.2011.01.005

Diederich, M., Ryzhkov, A., Simmer, C., Zhang, P., & Trömel, S. (2015). Use of Specific Attenuation for Rainfall Measurement at X-Band Radar Wavelengths. Part II: Rainfall Estimates and Comparison with Rain Gauges. *Journal of Hydrometeorology, 16*(2), 503-516. doi:10.1175/jhm-d-14-0067.1

Dinku, T., Ceccato, P., Grover‐Kopec, E., Lemma, M., Connor, S. J., & Ropelewski, C. F. (2007). Validation of satellite rainfall products over East Africa's complex topography. *International journal of remote sensing, 28*(7), 1503-1526. doi:10.1080/01431160600954688

Dinku, T., Chidzambwa, S., Ceccato, P., Connor, S. J., & Ropelewski, C. F. (2008). Validation of high‐resolution satellite rainfall products over complex terrain. *International journal of remote sensing, 29*(14), 4097-4110. doi:10.1080/01431160701772526

Dinku, T., Connor, S. J., Ceccato, P., Gebremichael, M., & Hossaim, F. (2010). *Satellite rainfall applications for surface hydrology* (Vol. null).

Dinku, T., Ruiz, F., Connor, S. J., & Ceccato, P. (2009). Validation and Intercomparison of Satellite Rainfall Estimates over Colombia. *Journal of Applied Meteorology and Climatology, 49*(5), 1004-1014. doi:10.1175/2009JAMC2260.1

Dirks, K. N., Hay, J. E., Stow, C. D., & Harris, D. (1998). High-resolution studies of rainfall on Norfolk Island: Part II: Interpolation of rainfall data. *Journal of Hydrology, 208*(3), 187-193. doi:10.1016/S0022-1694(98)00155-3

Easterling, D. R., Diaz, H. F., Douglas, A. V., Hogg, W. D., Kunkel, K. E., Rogers, J. C., & Wilkinson, J. F. (1999). Long-term Observations for Monitoring Extremes in the Americas. *Climatic Change, 42*(1), 285-308. doi:10.1023/a:1005484820026

Easton, Z., Fuka, D., White, E., Collick, A., Biruk Ashagre, B., McCartney, M., . . . Steenhuis, T. (2010). A multi basin SWAT model analysis of runoff and sedimentation in the Blue Nile, Ethiopia. *Hydrology and Earth System Sciences, 14*(10), 1827-1841.

Ebert, E. E., Janowiak, J. E., & Kidd, C. (2007). Comparison of near-real-time precipitation estimates from satellite observations and numerical models. *Bulletin of the American Meteorological Society, 88*(1), 47-64.

Falck, A. S., Maggioni, V., Tomasella, J., Vila, D. A., & Diniz, F. L. (2015). Propagation of satellite precipitation uncertainties through a distributed hydrologic model: A case study in the Tocantins–Araguaia basin in Brazil. *Journal of Hydrology, 527*, 943-957.

Fang, G. H., Yang, J., Chen, Y. N., & Zammit, C. (2015). Comparing bias correction methods in downscaling meteorological variables for a hydrologic impact study in an arid area in China. *Hydrol. Earth Syst. Sci., 19*(6), 2547-2559. doi:10.5194/hess-19-2547-2015

Faurès, J.-M., Goodrich, D. C., Woolhiser, D. A., & Sorooshian, S. (1995). Impact of small-scale spatial rainfall variability on runoff modeling. *Journal of Hydrology, 173*(1), 309-326. doi:10.1016/0022-1694(95)02704-S

Franke, R. (1982). Smooth interpolation of scattered data by local thin plate splines. *Computers & Mathematics with Applications, 8*(4), 273-281. doi:10.1016/0898-1221(82)90009-8

Gado, T. A., Hsu, K., & Sorooshian, S. (2017). Rainfall frequency analysis for ungauged sites using satellite precipitation products. *Journal of Hydrology, 554*, 646-655. doi:10.1016/j.jhydrol.2017.09.043

Gao, H., Tang, Q., Shi, X., Zhu, C., Bohn, T., Su, F., . . . Wood, E. (2010). Water budget record from Variable Infiltration Capacity (VIC) model.

Ghajarnia, N., Liaghat, A., & Daneshkar Arasteh, P. (2015). Comparison and evaluation of high resolution precipitation estimation products in Urmia Basin-Iran. *Atmospheric Research, 158-159*(Supplement C), 50-65. doi:10.1016/j.atmosres.2015.02.010

Ghaju, S., & Alfredsen, K. (2012). Evaluation of Satellite Based Precipitations and Their Applicability for Rainfall Runoff Modelling in Narayani Basin of Nepal. *Journal of Hydrology and Meteorology, 8*(1), 22-31.

Ghulami, M., Babel, M. S., & Singh Shrestha, M. (2017). Evaluation of gridded precipitation datasets for the Kabul Basin, Afghanistan. *International journal of remote sensing, 38*(11), 3317-3332.

Golding, B. W. (2009). Uncertainty propagation in a London flood simulation. *Journal of Flood Risk Management, 2*(1), 2-15. doi:10.1111/j.1753-318X.2008.01014.x

Gottschalck, J., Meng, J., Rodell, M., & Houser, P. (2005). Analysis of Multiple Precipitation Products and Preliminary Assessment of Their Impact on Global Land Data Assimilation System Land Surface States. *Journal of Hydrometeorology, 6*(5), 573-598. doi:10.1175/jhm437.1

Grillakis, M., Tsanis, I., & Koutroulis, A. (2010). Application of the HBV hydrological model in a flash flood case in Slovenia. *Natural Hazards and Earth System Sciences, 10*(12), 2713-2725.

Groisman, P. Y., & Legates, D. R. (1994). The Accuracy of United States Precipitation Data. *Bulletin of the American Meteorological Society, 75*(2), 215-227. doi:10.1175/1520-0477(1994)075<0215:taousp>2.0.co;2

Gu, H.-h., Yu, Z.-b., Yang, C.-g., Ju, Q., Lu, B.-h., & Liang, C. (2010). Hydrological assessment of TRMM rainfall data over Yangtze River Basin. *Water Science and Engineering, 3*(4), 418-430. doi:10.3882/j.issn.1674-2370.2010.04.005

Gudmundsson, L., Bremnes, J., Haugen, J., & Skaugen, T. E. (2012). Downscaling RCM precipitation to the station scale using quantile mapping--a comparison of methods. *Hydrology & Earth System Sciences Discussions, 9*(5).

Gumindoga, W., Rientjes, T. H. M., Haile, A. T., Makurira, H., & Reggiani, P. (2016). Bias correction schemes for CMORPH satellite rainfall estimates in the Zambezi River Basin. *Hydrol. Earth Syst. Sci. Discuss., 2016*, 1-36. doi:10.5194/hess-2016-33

Guo, H., Bao, A., Ndayisaba, F., Liu, T., Kurban, A., & De Maeyer, P. (2017). Systematical Evaluation of Satellite Precipitation Estimates Over Central Asia Using an Improved Error‐Component Procedure. *Journal of Geophysical Research: Atmospheres, 122*(20), 10,906-910,927.

Habib, E., Haile, A., Sazib, N., Zhang, Y., & Rientjes, T. (2014). Effect of Bias Correction of Satellite-Rainfall Estimates on Runoff Simulations at the Source of the Upper Blue Nile. *Remote Sensing, 6*(7), 6688. Retrieved from http://www.mdpi.com/2072-4292/6/7/6688

Habib, E., Haile, A. T., Tian, Y., & Joyce, R. J. (2012). Evaluation of the High-Resolution CMORPH Satellite Rainfall Product Using Dense Rain Gauge Observations and Radar-Based Estimates. *Journal of Hydrometeorology, 13*(6), 1784-1798. doi:10.1175/jhm-d-12-017.1

Haile, A. T., Habib, E., Elsaadani, M., & Rientjes, T. (2013). Inter-comparison of satellite rainfall products for representing rainfall diurnal cycle over the Nile basin. *International Journal of Applied Earth Observation and Geoinformation, 21*, 230-240. doi:10.1016/j.jag.2012.08.012

Halwatura, D., & Najim, M. M. M. (2013). Application of the HEC-HMS model for runoff simulation in a tropical catchment. *Environmental Modelling & Software, 46*, 155-162. doi:10.1016/j.envsoft.2013.03.006

Harris, A., Rahman, S., Hossain, F., Yarborough, L., Bagtzoglou, A., & Easson, G. (2007). Satellite-based Flood Modeling Using TRMM-based Rainfall Products. *Sensors, 7*(12), 3416. Retrieved from http://www.mdpi.com/1424-8220/7/12/3416

Hay, L. E., Clark, M. P., Wilby, R. L., Jr., W. J. G., Leavesley, G. H., Pan, Z., . . . Takle, E. S. (2002). Use of Regional Climate Model Output for Hydrologic Simulations. *Journal of Hydrometeorology, 3*(5), 571-590. doi:10.1175/1525-7541(2002)003<0571:uorcmo>2.0.co;2

Hirpa, F. A., Gebremichael, M., & Hopson, T. (2010). Evaluation of high-resolution satellite precipitation products over very complex terrain in Ethiopia. *Journal of Applied Meteorology and Climatology, 49*(5), 1044-1051.

Hong, Y., Gochis, D., Cheng, J.-t., Hsu, K.-l., & Sorooshian, S. (2007). Evaluation of PERSIANN-CCS rainfall measurement using the NAME event rain gauge network. *Journal of Hydrometeorology, 8*(3), 469-482.

Hong, Y., Hsu, K. l., Moradkhani, H., & Sorooshian, S. (2006). Uncertainty quantification of satellite precipitation estimation and Monte Carlo assessment of the error propagation into hydrologic response. *Water Resources Research, 42*(8).

Hossain, F., & Anagnostou, E. N. (2004). Assessment of current passive‐microwave‐ and infrared‐based satellite rainfall remote sensing for flood prediction. *Journal of Geophysical Research: Atmospheres, 109*(D7).

Hou, A. Y., Kakar, R. K., Neeck, S., Azarbarzin, A. A., Kummerow, C. D., Kojima, M., . . . Iguchi, T. (2014). The global precipitation measurement mission. *Bulletin of the American Meteorological Society, 95*(5), 701-722.

Hsu, K.-l., Gao, X., Sorooshian, S., & Gupta, H. V. (1997). Precipitation Estimation from Remotely Sensed Information Using Artificial Neural Networks. *Journal of Applied Meteorology, 36*(9), 1176-1190. doi:10.1175/1520-0450(1997)036<1176:pefrsi>2.0.co;2

Huang, G., & Yan, Z. (1999). The East Asian summer monsoon circulation anomaly index and its interannual variations. *Chinese Science Bulletin, 44*(14), 1325-1329.

Huang, S., Krysanova, V., & Hattermann, F. F. (2014). Does bias correction increase reliability of flood projections under climate change? A case study of large rivers in Germany. *International Journal of Climatology, 34*(14), 3780-3800. doi:10.1002/joc.3945

Huff, F. A. (1970). Spatial distribution of rainfall rates. *Water Resources Research, 6*(1), 254-260. doi:10.1029/WR006i001p00254

Huffman, G., Bolvin, D., Braithwaite, D., Hsu, K., Joyce, R., & Xie, P. (2015). Integrated multi-satellite retrievals for GPM (IMERG), version 4.4. *NASA's Precipitation Processing Center*.

Huffman, G. J., Bolvin, D. T., Nelkin, E. J., Wolff, D. B., Adler, R. F., Gu, G., . . . Stocker, E. F. (2007). The TRMM Multisatellite Precipitation Analysis (TMPA): Quasi-Global, Multiyear, Combined-Sensor Precipitation Estimates at Fine Scales. *Journal of Hydrometeorology, 8*(1), 38-55. doi:10.1175/jhm560.1

Hughes, D. A. (2006). Comparison of satellite rainfall data with observations from gauging station networks. *Journal of Hydrology, 327*(3–4), 399-410. doi:10.1016/j.jhydrol.2005.11.041

Hutchinson, M. F. (1995). Interpolating mean rainfall using thin plate smoothing splines. *International Journal of Geographical Information Systems, 9*(4), 385-403. doi:10.1080/02693799508902045

Jakob Themeßl, M., Gobiet, A., & Leuprecht, A. (2011). Empirical-statistical downscaling and error correction of daily precipitation from regional climate models. *International Journal of Climatology, 31*(10), 1530-1544. doi:10.1002/joc.2168

Javanmard, S., Yatagai, A., Nodzu, M. I., BodaghJamali, J., & Kawamoto, H. (2010). Comparing high-resolution gridded precipitation data with satellite rainfall estimates of TRMM_3B42 over Iran. *Adv. Geosci., 25*, 119-125. doi:10.5194/adgeo-25-119-2010

Jeon, S., Paciorek, C. J., & Wehner, M. F. (2016). Quantile-based bias correction and uncertainty quantification of extreme event attribution statements. *Weather and Climate Extremes, 12*, 24-32. doi:10.1016/j.wace.2016.02.001

Jiang, Q., Li, W., Wen, J., Qiu, C., Sun, W., Fang, Q., . . . Tan, J. (2018). Accuracy Evaluation of Two High-Resolution Satellite-Based Rainfall Products: TRMM 3B42V7 and CMORPH in Shanghai. *Water, 10*(1), 40. Retrieved from http://www.mdpi.com/2073-4441/10/1/40

Jiang, S., Ren, L., Hong, Y., Yong, B., Yang, X., Yuan, F., & Ma, M. (2012). Comprehensive evaluation of multi-satellite precipitation products with a dense rain gauge network and optimally merging their simulated hydrological flows using the Bayesian model averaging method. *Journal of Hydrology, 452–453*, 213-225. doi:10.1016/j.jhydrol.2012.05.055

Jiang, S., Ren, L., Yong, B., Hong, Y., Yang, X., & Yuan, F. (2016). Evaluation of latest TMPA and CMORPH precipitation products with independent rain gauge observation networks over high-latitude and low-latitude basins in China. *Chinese Geographical Science, 26*(4), 439-455. doi:10.1007/s11769-016-0818-x

Joyce, R. J., Janowiak, J. E., Arkin, P. A., & Xie, P. (2004). CMORPH: A Method that Produces Global Precipitation Estimates from Passive Microwave and Infrared Data at High Spatial and Temporal Resolution. *Journal of Hydrometeorology, 5*(3), 487-503. doi:10.1175/1525-7541(2004)005<0487:camtpg>2.0.co;2

Khan, S. I., Hong, Y., Wang, J., Yilmaz, K. K., Gourley, J. J., Adler, R. F., . . . Irwin, D. (2011). Satellite remote sensing and hydrologic modeling for flood inundation mapping in Lake Victoria Basin: Implications for hydrologic prediction in ungauged basins. *IEEE Transactions on Geoscience and Remote Sensing, 49*(1), 85-95.

Kidd, C., Becker, A., Huffman, G. J., Muller, C. L., Joe, P., Skofronick-Jackson, G., & Kirschbaum, D. B. (2017). So, how much of the Earth's surface is covered by rain gauges? *Bulletin of the American Meteorological Society, 98*(1), 69-78.

Kidd, C., & Huffman, G. (2011). Global precipitation measurement. *Meteorological Applications, 18*(3), 334-353. doi:10.1002/met.284

Kidd, C., & Levizzani, V. (2011). Status of satellite precipitation retrievals. *Hydrol. Earth Syst. Sci., 15*(4), 1109-1116. doi:10.5194/hess-15-1109-2011

Kilaru, S., Goud, B. K., & Rao, V. K. (2013). Crustal structure of the western Indian shield: model based on regional gravity and magnetic data. *Geoscience Frontiers, 4*(6), 717-728.

Kizza, M., Westerberg, I., Rodhe, A., & Ntale, H. K. (2012). Estimating areal rainfall over Lake Victoria and its basin using ground-based and satellite data. *Journal of Hydrology, 464-465*(Supplement C), 401-411. doi:10.1016/j.jhydrol.2012.07.024

Krajewski, W. F., & Smith, J. A. (2002). Radar hydrology: rainfall estimation. *Advances in Water Resources, 25*(8–12), 1387-1394. doi:10.1016/S0309-1708(02)00062-3

Kubota, T., Shige, S., Hashizume, H., Aonashi, K., Takahashi, N., Seto, S., . . . Okamoto, K. (2007). Global Precipitation Map Using Satellite-Borne Microwave Radiometers by the GSMaP Project: Production and Validation. *IEEE Transactions on Geoscience and Remote Sensing, 45*(7), 2259-2275. doi:10.1109/TGRS.2007.895337

Kubota, T., Ushio, T., Shige, S., Kida, S., Kachi, M., & Okamoto, K. i. (2009). Verification of high-resolution satellite-based rainfall estimates around Japan using a gauge-calibrated ground-radar dataset. *Journal of the Meteorological Society of Japan. Ser. II, 87*, 203-222.

Kummerow, C. (1998). Beamfilling errors in passive microwave rainfall retrievals. *Journal of Applied Meteorology, 37*(4), 356-370.

Lafon, T., Dadson, S., Buys, G., & Prudhomme, C. (2013). Bias correction of daily precipitation simulated by a regional climate model: a comparison of methods. *International Journal of Climatology, 33*(6), 1367-1381. doi:10.1002/joc.3518

Lambrigtsen, B. H., Brown, S. T., Dinardo, S. J., Gaier, T. C., Kangaslahti, P. P., Tanner, A. B., . . . Rogacki, S. (2006). *GeoSTAR: a microwave sounder for geostationary applications* (Vol. 6361): SPIE.

Leander, R., & Buishand, T. A. (2007). Resampling of regional climate model output for the simulation of extreme river flows. *Journal of Hydrology, 332*(3), 487-496. doi:10.1016/j.jhydrol.2006.08.006

Lenderink, G., Buishand, A., & van Deursen, W. (2007). Estimates of future discharges of the river Rhine using two scenario methodologies: direct versus delta approach. *Hydrol. Earth Syst. Sci., 11*(3), 1145-1159. doi:10.5194/hess-11-1145-2007

Levizzani, V., Bauer, P., & Turk, F. J. (2007). *Measuring precipitation from space: EURAINSAT and the future* (Vol. 28): Springer Science & Business Media.

Li, D., Christakos, G., Ding, X., & Wu, J. (2018). Adequacy of TRMM satellite rainfall data in driving the SWAT modeling of Tiaoxi catchment (Taihu lake basin, China). *Journal of Hydrology, 556*, 1139-1152. doi:10.1016/j.jhydrol.2017.01.006

Li, D., Ding, X., & Wu, J. (2015). Simulating the regional water balance through hydrological model based on TRMM satellite rainfall data. *Hydrology and Earth System Sciences Discussions, 12*(2), 2497-2525.

Lindström, G., Johansson, B., Persson, M., Gardelin, M., & Bergström, S. (1997). Development and test of the distributed HBV-96 hydrological model. *Journal of Hydrology, 201*(1-4), 272-288.

Liu, J., Duan, Z., & Zhu, A. (2012). Evaluation of TRMM 3B42 Precipitation Product using Rain Gauge Data in Meichuan Watershed, Poyang Lake Basin, China. *Journal of Resources and Ecology, 3*(4), 359-366. doi:10.5814/j.issn.1674-764x.2012.04.009

Liu, X., Yang, T., Hsu, K., Liu, C., & Sorooshian, S. (2017). Evaluating the streamflow simulation capability of PERSIANN-CDR daily rainfall products in two river basins on the Tibetan Plateau. *Hydrol. Earth Syst. Sci., 21*(1), 169-181. doi:10.5194/hess-21-169-2017

Lo Conti, F., Hsu, K.-L., Noto, L. V., & Sorooshian, S. (2014). Evaluation and comparison of satellite precipitation estimates with reference to a local area in the Mediterranean Sea. *Atmospheric Research, 138*, 189-204. doi:10.1016/j.atmosres.2013.11.011

Luo, M., Liu, T., Meng, F., Duan, Y., Huang, Y., Frankl, A., & De Maeyer, P. (2017). Proportional coefficient method applied to TRMM rainfall data: case study of hydrological simulations of the Hotan River Basin (China). *Journal of Water and Climate Change, 8*(3), jwc2017080. doi:10.2166/wcc.2017.080

Ly, S., Charles, C., & Degre, A. (2011). Geostatistical interpolation of daily rainfall at catchment scale: The use of several variogram models in the Ourthe and Ambleve catchments, Belgium. *HESS, 15*(7), 2259-2274.

Ly, S., Charles, C., & Degré, A. (2013). Different methods for spatial interpolation of rainfall data for operational hydrology and hydrological modeling at watershed scale. A review. *Biotechnologie, Agronomie, Société et Environnement, 17*(2), 392-406.

Maggioni, V., & Massari, C. (2018). On the performance of satellite precipitation products in riverine flood modeling: A review. *Journal of Hydrology, 558*, 214-224. doi:10.1016/j.jhydrol.2018.01.039

Maggioni, V., Meyers, P. C., & Robinson, M. D. (2016). A review of merged high-resolution satellite precipitation product accuracy during the Tropical Rainfall Measuring Mission (TRMM) era. *Journal of Hydrometeorology, 17*(4), 1101-1117.

Mair, A., & Fares, A. (2010). Comparison of rainfall interpolation methods in a mountainous region of a tropical island. *Journal of Hydrologic Engineering, 16*(4), 371-383.

Mashingia, F., Mtalo, F., & Bruen, M. (2014). Validation of remotely sensed rainfall over major climatic regions in Northeast Tanzania. *Physics and Chemistry of the Earth, Parts A/B/C, 67–69*, 55-63. doi:10.1016/j.pce.2013.09.013

Massari, C., Crow, W., & Brocca, L. (2017). An assessment of the performance of global rainfall estimates without ground-based observations. *Hydrology and Earth System Sciences, 21*(9), 4347-4361.

Miao, C., Ashouri, H., Hsu, K.-L., Sorooshian, S., & Duan, Q. (2015). Evaluation of the PERSIANN-CDR Daily Rainfall Estimates in Capturing the Behavior of Extreme Precipitation Events over China. *Journal of Hydrometeorology, 16*(3), 1387-1396. doi:10.1175/jhm-d-14-0174.1

Michelson, D. B., & Koistinen, J. (2000). Gauge-Radar network adjustment for the baltic sea experiment. *Physics and Chemistry of the Earth, Part B: Hydrology, Oceans and Atmosphere, 25*(10), 915-920. doi:10.1016/S1464-1909(00)00125-8

Mishra, D., & Kumar, M. R. (2014). Proterozoic orogenic belts and rifting of Indian cratons: geophysical constraints. *Geoscience Frontiers, 5*(1), 25-41.

Mitáš, L., & Mitášová, H. (1988). General variational approach to the interpolation problem. *Computers & Mathematics with Applications, 16*(12), 983-992. doi:10.1016/0898-1221(88)90255-6

Moazami, S., Golian, S., Hong, Y., Sheng, C., & Kavianpour, M. R. (2016). Comprehensive evaluation of four high-resolution satellite precipitation products under diverse climate conditions in Iran. *Hydrological Sciences Journal, 61*(2), 420-440. doi:10.1080/02626667.2014.987675

Moazami, S., Golian, S., Kavianpour, M. R., & Hong, Y. (2013). Comparison of PERSIANN and V7 TRMM Multi-satellite Precipitation Analysis (TMPA) products with rain gauge data over Iran. *International journal of remote sensing, 34*(22), 8156-8171. doi:10.1080/01431161.2013.833360

Moriasi, D. N., Arnold, J. G., Van Liew, M. W., Bingner, R. L., Harmel, R. D., & Veith, T. L. (2007). Model Evaluation Guidelines for Systematic Quantification of Accuracy in Watershed Simulations. *Transactions of the ASABE, 50*(3), 885-900. doi:10.13031/2013.23153

Morin, E., Goodrich, D. C., Maddox, R. A., Gao, X., Gupta, H. V., & Sorooshian, S. (2006). Spatial patterns in thunderstorm rainfall events and their coupling with watershed hydrological response. *Advances in Water Resources, 29*(6), 843-860. doi:10.1016/j.advwatres.2005.07.014

Nijssen, B., & Lettenmaier, D. P. (2004). Effect of precipitation sampling error on simulated hydrological fluxes and states: Anticipating the Global Precipitation Measurement satellites. *Journal of Geophysical Research: Atmospheres, 109*(D2).

Nikolopoulos, E. I., Anagnostou, E. N., & Hossain, F. (2010). Error propagation of satellite-rainfall in flood prediction applications over complex terrain: A case study in northeastern Italy. In *Satellite Rainfall Applications for Surface Hydrology* (pp. 215-227): Springer.

NOAA. (2012). Arctic Oscillation. Retrieved from http://www.ncdc.noaa.gov/teleconnections/ao/

Ochoa, A., Pineda, L., Crespo, P., & Willems, P. (2014). Evaluation of TRMM 3B42 precipitation estimates and WRF retrospective precipitation simulation over the Pacific–Andean region of Ecuador and Peru. *Hydrology and Earth System Sciences, 18*(8), 3179-3193.

OSS. (2013). Open Source Systems Science Solutions. Artic Oscillation. Retrieved from http://ossfoundation.us/projects/environment/global-warming/arctic-oscillation-ao

Pakoksung, K., & Takagi, M. (2016). Effect of satellite based rainfall products on river basin responses of runoff simulation on flood event. *Modeling Earth Systems and Environment, 2*(3), 143. doi:10.1007/s40808-016-0200-0

Pan, M., Li, H., & Wood, E. (2010). Assessing the skill of satellite‐based precipitation estimates in hydrologic applications. *Water Resources Research, 46*(9).

Pan, X., Yang, D., Li, Y., Barr, A., Helgason, W., Hayashi, M., . . . Janowicz, R. J. (2016). Bias corrections of precipitation measurements across experimental sites in different ecoclimatic regions of western Canada. *The Cryosphere, 10*(5), 2347-2360. doi:10.5194/tc-10-2347-2016

Park, D., & Markus, M. (2014). Analysis of a changing hydrologic flood regime using the Variable Infiltration Capacity model. *Journal of Hydrology, 515*, 267-280.

Pereira Filho, A. J., Carbone, R. E., Janowiak, J. E., Arkin, P., Joyce, R., Hallak, R., & Ramos, C. G. M. (2010). Satellite Rainfall Estimates Over South America – Possible Applicability to the Water Management of Large Watersheds. *JAWRA Journal of the American Water Resources Association, 46*(2), 344-360. doi:10.1111/j.1752-1688.2009.00406.x

Piani, C., Weedon, G. P., Best, M., Gomes, S. M., Viterbo, P., Hagemann, S., & Haerter, J. O. (2010). Statistical bias correction of global simulated daily precipitation and temperature for the application of hydrological models. *Journal of Hydrology, 395*(3), 199-215. doi:10.1016/j.jhydrol.2010.10.024

Porter, S. C. (2001). Chinese loess record of monsoon climate during the last glacial–interglacial cycle. *Earth-Science Reviews, 54*(1), 115-128. doi:10.1016/S0012-8252(01)00043-5

Qi, W., Zhang, C., Fu, G., Sweetapple, C., & Zhou, H. (2016). Evaluation of global fine-resolution precipitation products and their uncertainty quantification in ensemble discharge simulations. *Hydrology and Earth System Sciences, 20*(2), 903-920.

Reuter, M., Kern, A. K., Harzhauser, M., Kroh, A., & Piller, W. E. (2013). Global warming and South Indian monsoon rainfall—lessons from the Mid-Miocene. *Gondwana Research, 23*(3), 1172-1177.

Rodríguez-Iturbe, I., & Mejía, J. M. (1974). The design of rainfall networks in time and space. *Water Resources Research, 10*(4), 713-728. doi:10.1029/WR010i004p00713

Schilling, W., & Fuchs, L. (1986). Errors in Stormwater Modeling—A Quantitative Assessment. *Journal of Hydraulic Engineering, 112*(2), 111-123. doi:doi:10.1061/(ASCE)0733-9429(1986)112:2(111)

Schmidli, J., Frei, C., & Vidale, P. L. (2006). Downscaling from GCM precipitation: a benchmark for dynamical and statistical downscaling methods. *International Journal of Climatology, 26*(5), 679-689. doi:doi:10.1002/joc.1287

Scofield, R. A., & Kuligowski, R. J. (2003). Status and Outlook of Operational Satellite Precipitation Algorithms for Extreme-Precipitation Events. *Weather and Forecasting, 18*(6), 1037-1051. doi:10.1175/1520-0434(2003)018<1037:saooos>2.0.co;2

Segond, M.-L., Wheater, H. S., & Onof, C. (2007). The significance of spatial rainfall representation for flood runoff estimation: A numerical evaluation based on the Lee catchment, UK. *Journal of Hydrology, 347*(1), 116-131. doi:10.1016/j.jhydrol.2007.09.040

Semire, F. A., Mohd-Mokhtar, R., Ismail, W., Mohamad, N., & Mandeep, J. S. (2012). Ground validation of space-borne satellite rainfall products in Malaysia. *Advances in Space Research, 50*(9), 1241-1249. doi:10.1016/j.asr.2012.06.031

Serrat ‐ Capdevila, A., Valdes, J. B., & Stakhiv, E. Z. (2014). Water management applications for satellite precipitation products: Synthesis and recommendations. *JAWRA Journal of the American Water Resources Association, 50*(2), 509-525.

Serreze, M. C., & Barry, R. G. (2010). Climate Change. *R.G. Barry, R.J. Chorley (Eds.), Atmosphere, Weather and Climate, Routledge, Oxon*.

Seyyedi, H., Anagnostou, E. N., Beighley, E., & McCollum, J. (2014). Satellite-driven downscaling of global reanalysis precipitation products for hydrological applications. *HESS, 18*(12), 5077-5091. doi:10.5194/hess-18-5077-2014

Shabalova, M. V., van Deursen, W. P. A., & Buishand, T. A. (2003). Assessing future discharge of the river Rhine using regional climate model integrations and a hydrological model. *Climate Research, 23*(3), 233-246. Retrieved from http://www.jstor.org/stable/24868350

Shaw, E. M., & Lynn, P. P. (1972). Areal Rainfall Evaluation using Two Surface Fitting Techniques *Hydrological Sciences Bulletin, 17*(4), 419-433. doi:10.1080/02626667209493855

Sinclair, S., & Pegram, G. (2005). Combining radar and rain gauge rainfall estimates using conditional merging. *Atmospheric Science Letters, 6*(1), 19-22. doi:10.1002/asl.85

Singh, J., Knapp, H. V., Arnold, J. G., & Demissie, M. (2005). HYDROLOGICAL MODELING OF THE IROQUOIS RIVER WATERSHED USING HSPF AND SWAT1. *JAWRA Journal of the American Water Resources Association, 41*(2), 343-360. doi:10.1111/j.1752-1688.2005.tb03740.x

Smith, J. A., Baeck, M. L., Meierdiercks, K. L., Miller, A. J., & Krajewski, W. F. (2007). Radar rainfall estimation for flash flood forecasting in small urban watersheds.

Advances in Water Resources, 30(10), 2087-2097. doi:10.1016/j.advwatres.2006.09.007

Smitha, P. S., Narasimhan, B., Sudheer, K. P., & Annamalai, H. (2018). An improved bias correction method of daily rainfall data using a sliding window technique for climate change impact assessment. *Journal of Hydrology, 556,* 100-118. doi:10.1016/j.jhydrol.2017.11.010

SOEST. (2013). University of Hawaii. Prediction of Asian summer monsoon rainfall and tropical storm activity close at hand. Retrieved from www.sciencedaily.com/releases/2013/01/130123101613.htm

Sohn, B. J., Han, H.-J., & Seo, E.-K. (2010). Validation of Satellite-Based High-Resolution Rainfall Products over the Korean Peninsula Using Data from a Dense Rain Gauge Network. *Journal of Applied Meteorology and Climatology, 49*(4), 701-714. doi:10.1175/2009jamc2266.1

Sorooshian, S., AghaKouchak, A., Arkin, P., Eylander, J., Foufoula-Georgiou, E., Harmon, R., . . . Skahill, B. (2011). Advanced concepts on remote sensing of precipitation at multiple scales. *Bulletin of the American Meteorological Society, 92*(10), 1353-1357.

Sorooshian, S., Hsu, K.-L., Gao, X., Gupta, H. V., Imam, B., & Braithwaite, D. (2000). Evaluation of PERSIANN System Satellite–Based Estimates of Tropical Rainfall. *Bulletin of the American Meteorological Society, 81*(9), 2035-2046. doi:10.1175/1520-0477(2000)081<2035:eopsse>2.3.co;2

Sow, K. S., Juneng, L., Tangang, F. T., Hussin, A. G., & Mahmud, M. (2011). Numerical simulation of a severe late afternoon thunderstorm over Peninsular Malaysia. *Atmospheric Research, 99*(2), 248-262. doi:10.1016/j.atmosres.2010.10.014

Stampoulis, D., & Anagnostou, E. N. (2012). Evaluation of global satellite rainfall products over continental Europe. *Journal of Hydrometeorology, 13*(2), 588-603.

Steenhuis, T. S., Collick, A. S., Easton, Z. M., Leggesse, E. S., Bayabil, H. K., White, E. D., . . . Ahmed, A. A. (2009). Predicting discharge and sediment for the Abay (Blue Nile) with a simple model. *Hydrological Processes: An International Journal, 23*(26), 3728-3737.

Steiner, M., & Smith, J. A. (2000). Reflectivity, Rain Rate, and Kinetic Energy Flux Relationships Based on Raindrop Spectra. *Journal of Applied Meteorology, 39*(11), 1923-1940. doi:10.1175/1520-0450(2000)039<1923:Rrrake>2.0.Co;2

Strangeways, I. (2004). Improving precipitation measurement. *International Journal of Climatology, 24*(11), 1443-1460. doi:10.1002/joc.1075

Su, F., Gao, H., Huffman, G. J., & Lettenmaier, D. P. (2011). Potential utility of the real-time TMPA-RT precipitation estimates in streamflow prediction. *Journal of Hydrometeorology, 12*(3), 444-455.

Su, F., Hong, Y., & Lettenmaier, D. P. (2008). Evaluation of TRMM Multisatellite Precipitation Analysis (TMPA) and Its Utility in Hydrologic Prediction in the La Plata Basin. *Journal of Hydrometeorology, 9*(4), 622-640. doi:10.1175/2007jhm944.1

Suhaila, J., Deni, S. M., Zin, W. Z. W., & Jemain, A. A. (2010). Trends in peninsular Malaysia rainfall data during the southwest monsoon and northeast monsoon seasons: 1975–2004. *Sains Malaysiana*, *39*(4), 533-542.

Tait, A., Henderson, R., Turner, R., & Zheng, X. (2006). Thin plate smoothing spline interpolation of daily rainfall for New Zealand using a climatological rainfall surface. *International Journal of Climatology, 26*(14), 2097-2115. doi:10.1002/joc.1350

Tan, M. L., Ibrahim, A. L., Duan, Z., Cracknell, A. P., & Chaplot, V. (2015). Evaluation of six high-resolution satellite and ground-based precipitation products over Malaysia. *Remote Sensing, 7*(2), 1504-1528.

Tangang, F. T., Juneng, L., & Ahmad, S. (2007). Trend and interannual variability of temperature in Malaysia: 1961–2002. *Theoretical and Applied Climatology, 89*(3), 127-141. doi:10.1007/s00704-006-0263-3

Tangang, F. T., Juneng, L., Salimun, E., Sei, K., & Halimatun, M. (2012). Climate change and variability over Malaysia: gaps in science and research information. *Sains Malaysiana, 41*(11), 1355-1366.

Tao, T., Chocat, B., Liu, S. & Xin, K. . (2009). Uncertainty Analysis of Interpolation Methods in Rainfall Spatial Distribution¨CA Case of Small Catchment in Lyon. *Journal of Environmental Protection, Vol.01No.01*, 9. Retrieved from http://www.scirp.org/journal/PaperInformation.aspx?PaperID=808

Tapiador, F. J., Turk, F. J., Petersen, W., Hou, A. Y., García-Ortega, E., Machado, L. A. T., . . . de Castro, M. (2012). Global precipitation measurement: Methods, datasets and applications. *Atmospheric Research, 104–105*, 70-97. doi:10.1016/j.atmosres.2011.10.021

Terink, W., Hurkmans, R. T. W. L., Torfs, P. J. J. F., & Uijlenhoet, R. (2010). Evaluation of a bias correction method applied to downscaled precipitation and temperature reanalysis for the Rhine basin. *Hydrology and Earth System Sciences, 14*(4), 687-703. Retrieved from http://edepot.wur.nl/148601

Tesfagiorgis, K., Mahani, S. E., Krakauer, N. Y., & Khanbilvardi, R. (2011). Bias correction of satellite rainfall estimates using a radar-gauge product – a case study in Oklahoma (USA). *Hydrol. Earth Syst. Sci., 15*(8), 2631-2647. doi:10.5194/hess-15-2631-2011

Teutschbein, C., & Seibert, J. (2012). Bias correction of regional climate model simulations for hydrological climate-change impact studies: Review and evaluation of different methods. *Journal of Hydrology, 456-457*(Supplement C), 12-29. doi:10.1016/j.jhydrol.2012.05.052

Teutschbein, C., & Seibert, J. (2013). Is bias correction of regional climate model (RCM) simulations possible for non-stationary conditions? *Hydrol. Earth Syst. Sci., 17*(12), 5061-5077. doi:10.5194/hess-17-5061-2013

Thiemig, V., Rojas, R., Zambrano-Bigiarini, M., Levizzani, V., & Roo, A. D. (2012). Validation of Satellite-Based Precipitation Products over Sparsely Gauged African River Basins. *Journal of Hydrometeorology, 13*(6), 1760-1783. doi:10.1175/jhm-d-12-032.1

Thiessen, A. H. (1911). Precipitation averages for large areas. *Monthly Weather Review, 39*(7), 1082-1089. doi:10.1175/1520-0493(1911)39<1082b:PAFLA>2.0.CO;2

Tian, W., Song, J., Li, Z., & de Wilde, P. (2014). Bootstrap techniques for sensitivity analysis and model selection in building thermal performance analysis. *Applied Energy, 135*, 320-328. doi:10.1016/j.apenergy.2014.08.110

Tian, Y., & Peters-Lidard, C. D. (2007). Systematic anomalies over inland water bodies in satellite-based precipitation estimates. *Geophysical Research Letters, 34*(14). doi:10.1029/2007GL030787

Tian, Y., & Peters-Lidard, C. D. (2010). A global map of uncertainties in satellite-based precipitation measurements. *Geophysical Research Letters, 37*. doi:10.1029/2010GL046008

Tian, Y., Peters-Lidard, C. D., Eylander, J. B., Joyce, R. J., Huffman, G. J., Adler, R. F., . . . Zeng, J. (2009). Component analysis of errors in satellite-based precipitation estimates. *Journal of Geophysical Research: Atmospheres, 114*(D24). doi:10.1029/2009JD011949

Tong, K., Su, F., Yang, D., Zhang, L., & Hao, Z. (2014). Tibetan Plateau precipitation as depicted by gauge observations, reanalyses and satellite retrievals. *International Journal of Climatology, 34*(2), 265-285.

Tramblay, Y., Thiemig, V., Dezetter, A., & Hanich, L. (2016). Evaluation of satellite-based rainfall products for hydrological modelling in Morocco. *Hydrological Sciences Journal, 61*(14), 2509-2519. doi:10.1080/02626667.2016.1154149

Tuo, Y., Duan, Z., Disse, M., & Chiogna, G. (2016). Evaluation of precipitation input for SWAT modeling in Alpine catchment: A case study in the Adige river basin (Italy). *Science of The Total Environment, 573*, 66-82. doi:10.1016/j.scitotenv.2016.08.034

Turk, F. J., Rohaly, G. D., Hawkins, J., Smith, E. A., Marzano, F., Mugnai, A., & Levizzani, V. (2000). Meteorological applications of precipitation estimation from combined SSM/I, TRMM and infrared geostationary satellite data. In (pp. 353-363).

USACE-HEC. (2008). Hydrologic Modeling System (HEC-HMS) Application Guide In: US Army Corps of Engineers, Hydrologic Engineering Center, Davis, Calif.

Valdés-Pineda, R., Demaría, E. M. C., Valdés, J. B., Wi, S., & Serrat-Capdevilla, A. (2016). Bias correction of daily satellite-based rainfall estimates for hydrologic forecasting in the Upper Zambezi, Africa. *Hydrol. Earth Syst. Sci. Discuss., 2016*, 1-28. doi:10.5194/hess-2016-473

Varikoden, H., Samah, A. A., & Babu, C. A. (2010). Spatial and temporal characteristics of rain intensity in the peninsular Malaysia using TRMM rain rate. *Journal of Hydrology, 387*(3–4), 312-319. doi:10.1016/j.jhydrol.2010.04.023

Vieux, B. E., & Bedient, P. B. (1998). Estimation of Rainfall for Flood Prediction from WSR-88D Reflectivity: A Case Study, 17–18 October 1994. *Weather and Forecasting, 13*(2), 407-415. doi:10.1175/1520-0434(1998)013<0407:Eorffp>2.0.Co;2

Vila, D. A., Goncalves, L. G. G. d., Toll, D. L., & Rozante, J. R. (2009). Statistical Evaluation of Combined Daily Gauge Observations and Rainfall Satellite Estimates over Continental South America. *Journal of Hydrometeorology, 10*(2), 533-543. doi:10.1175/2008jhm1048.1

Villarini, G., Krajewski, W. F., & Smith, J. A. (2009). New paradigm for statistical validation of satellite precipitation estimates: Application to a large sample of the TMPA 0.25° 3-hourly estimates over Oklahoma. *Journal of Geophysical Research: Atmospheres, 114*(D12). doi:10.1029/2008JD011475

Villarini, G., Mandapaka, P. V., Krajewski, W. F., & Moore, R. J. (2008). Rainfall and sampling uncertainties: A rain gauge perspective. *Journal of Geophysical Research: Atmospheres*, *113*(D11).

Vu, T. T., Li, L., & Jun, K. S. (2018). Evaluation of Multi-Satellite Precipitation Products for Streamflow Simulations: A Case Study for the Han River Basin in the Korean Peninsula, East Asia. *Water, 10*(5), 642. Retrieved from http://www.mdpi.com/2073-4441/10/5/642

Wagner, P. D., Fiener, P., Wilken, F., Kumar, S., & Schneider, K. (2012). Comparison and evaluation of spatial interpolation schemes for daily rainfall in data scarce regions. *Journal of Hydrology, 464–465,* 388-400. doi:10.1016/j.jhydrol.2012.07.026

Wang, B., Xiang, B., & Lee, J.-Y. (2013). Subtropical high predictability establishes a promising way for monsoon and tropical storm predictions. *Proceedings of the National Academy of Sciences, 110*(8), 2718-2722.

Wang, L., Li, J., Lu, H., Gu, Z., Rioual, P., Hao, Q., . . . Xu, B. (2012). The East Asian winter monsoon over the last 15,000 years: its links to high-latitudes and tropical climate systems and complex correlation to the summer monsoon. *Quaternary Science Reviews*, *32*, 131-142.

Wang, W., Lu, H., Yang, D., Sothea, K., Jiao, Y., Gao, B., . . . Pang, Z. (2016). Modelling Hydrologic Processes in the Mekong River Basin Using a Distributed Model Driven by Satellite Precipitation and Rain Gauge Observations. *PLOS ONE, 11*(3), e0152229. doi:10.1371/journal.pone.0152229

Wang, Z., Chen, J., Lai, C., Zhong, R., Chen, X., & Yu, H. (2018). Hydrologic assessment of the TMPA 3B42-V7 product in a typical alpine and gorge region: the Lancang River basin, China. *Hydrology Research, 49*(6), 2002-2015. doi:10.2166/nh.2018.024

WMO. (2008). World Meteorological Organization Chapter 14: Observation of present and past weather; state of the ground. *Guide to Meteorological Instruments and Methods of Observation. WMO: Geneva*, I.14–17.

Worqlul, A. W., Ayana, E. K., Maathuis, B. H. P., MacAlister, C., Philpot, W. D., Osorio Leyton, J. M., & Steenhuis, T. S. (2017a). Performance of bias corrected MPEG rainfall estimate for rainfall-runoff simulation in the upper Blue Nile Basin, Ethiopia. *Journal of Hydrology*. doi:10.1016/j.jhydrol.2017.01.058

Worqlul, A. W., Yen, H., Collick, A. S., Tilahun, S. A., Langan, S., & Steenhuis, T. S. (2017b). Evaluation of CFSR, TMPA 3B42 and ground-based rainfall data as input for hydrological models, in data-scarce regions: The upper Blue Nile Basin, Ethiopia. *CATENA*, *152*, 242-251. doi:10.1016/j.catena.2017.01.019

Xu, H., Xu, C.-Y., Chen, H., Zhang, Z., & Li, L. (2013). Assessing the influence of rain gauge density and distribution on hydrological model performance in a humid region of China. *Journal of Hydrology*, *505*, 1-12. doi:10.1016/j.jhydrol.2013.09.004

Xue, X., Hong, Y., Limaye, A. S., Gourley, J. J., Huffman, G. J., Khan, S. I., . . . Chen, S. (2013). Statistical and hydrological evaluation of TRMM-based Multi-satellite Precipitation Analysis over the Wangchu Basin of Bhutan: Are the latest satellite precipitation products 3B42V7 ready for use in ungauged basins? *Journal of Hydrology*, *499*, 91-99.

Yilmaz, K. K., Hogue, T. S., Hsu, K.-l., Sorooshian, S., Gupta, H. V., & Wagener, T. (2005). Intercomparison of Rain Gauge, Radar, and Satellite-Based Precipitation Estimates with Emphasis on Hydrologic Forecasting. *Journal of Hydrometeorology*, *6*(4), 497-517. doi:10.1175/jhm431.1

Zhang, X., & Srinivasan, R. (2009). GIS-Based Spatial Precipitation Estimation: A Comparison of Geostatistical Approaches1. *JAWRA Journal of the American Water Resources Association*, *45*(4), 894-906. doi:10.1111/j.1752-1688.2009.00335.x

Zhao, T., Bennett, J. C., Wang, Q. J., Schepen, A., Wood, A. W., Robertson, D. E., & Ramos, M.-H. (2017). How Suitable is Quantile Mapping For Postprocessing GCM Precipitation Forecasts? *Journal of Climate*, *30*(9), 3185-3196. doi:10.1175/jcli-d-16-0652.1

Zhou, T., Yu, R., Zhang, J., Drange, H., Cassou, C., Deser, C., . . . Keenlyside, N. (2009). Why the western Pacific subtropical high has extended westward since the late 1970s. *Journal of Climate*, *22*(8), 2199-2215.

Zulkafli, Z., Buytaert, W., Onof, C., Manz, B., Tarnavsky, E., Lavado, W., & Guyot, J.-L. (2014). A Comparative Performance Analysis of TRMM 3B42 (TMPA) Versions 6 and 7 for Hydrological Applications over Andean–Amazon River Basins. *Journal of Hydrometeorology*, *15*(2), 581-592. doi:10.1175/jhm-d-13-094.1

LIST OF PUBLICATIONS AND PAPERS PRESENTED

Journal Article

Soo, E. Z. X., Wan Jaafar, W. Z., Lai, S. H., Islam, T., Srivastava, P. (2018). Evaluation of Satellite Precipitation Products for Extreme Flood Events: Case Study in Peninsular Malaysia. *Journal of Water and Climate Change*, *10* (4): 871–892. doi:10.2166/wcc.2018.159 **(ISI-indexed, IF=1.009)**

Soo, E. Z. X., Wan Jaafar, W. Z., Lai, S. H., Othman, F., Elshafie, A., Islam, T., Srivastava, P., Othman Hadi, H. S. (2019). Evaluation of Bias Adjusted Satellite Precipitation Estimations for Extreme Flood Events in Langat River Basin, Malaysia. *Hydrology Research*. **(ISI-indexed, IF=2.475)**

Soo, E. Z. X., Wan Jaafar, W. Z., Lai, S. H., Othman, F., Elshafie, A., Islam, T., Srivastava, P., Othman Hadi, H. S. (2019). Precision of Raw and Bias-adjusted Satellite Precipitation Estimations (GPM-IMERG, TRMM, CMORPH and PERSIANN) over Extreme Flood Events：Case Study in Langat River Basin, Malaysia. *Journal of Water and Climate Change*. **(ISI-indexed, IF=1.009)**

Conference Paper

Wan Jaafar, W. Z., **Soo, E. Z. X.**, Lai, S. H., Islam, T. & Srivastava, P. (2017). Performance of satellite precipitation products for 2014-2015 extreme flood events. Proceedings of the 37th IAHR World Congress.